Atmospheric Chemistry in the Outer Solar System: from 40 K to 4000 K

Thesis by

James Richard Lyons

In Partial Fullfillment of the Requirements

for the Degree of

Doctor of Philosophy

California Institute of Technology

Pasadena, California

1996

(Defended 27 September, 1995)

To my parents.

Acknowledgements

This has been an interesting trip down the road from JPL. My advisor, Yuk Yung, made the trip possible by taking an interest in the scientific musings of a (then) electrical engineer. His enthusiasm and willingness to collaborate made the pursuit of scientific understanding very enjoyable, and convinced me of the correctness of coming to Caltech for graduate work. Once here, Yuk provided an environment in which I could pursue my research in directions that I thought most appropriate. Inevitably this led to a few moments of friction, but I will always be grateful to him for providing such an environment.

Many of the faculty contributed to my scientific and personal growth while I was at Caltech. Andy Ingersoll and I collaborated on a model for the interannual variability of Martian dust storms, which was for me a very interesting experience. In addition, Andy provided sage advice on more than one occasion, proved to be a formidable tennis (and table tennis) partner, and supplied those wonderful Thanksgiving dinners with his friends and family. Bruce Murray has generously offered his counsel and wisdom on career-related topics, things historical, and on the big picture. Also, he, Suzanne and Jonathan extended their hospitality to me during my visit to ISAS, and during a very pleasant Thanksgiving dinner (outdoors!). Dewey Muhleman let me tag along on an observing run at OVRO, and lent me his ear at a crucial time. Thanks for listening, Dewey. For the highest level of teaching that I encountered at Caltech, I thank Dave Stevenson. For the opportunity to sink slowly into waist-deep mud, I again thank Dave. Actually, the two

Stevenson hikes that I went on (Paria Canyon and Mt. Whitney) were fabulous trips, both very memorable. I thank Yuk and Shau May for several enjoyable parties and dinners. I also thank the following faculty members: Joe Kirschvink for fascinating conversations and for allowing me to tinker in his lab, Clair Patterson for his honesty and enthusiasm, and Don Helmberger for Saturday morning football. Finally, I must thank Tom Ahrens for supporting my attendance at the Baltimore SL9 meeting, and for giving me the opportunity to pursue the more energetic side of planetary science. I would also like to thank my defense committee (Peter, Dave, Andy, Dewey and Yuk) for reading the thesis.

The kinetics computer program was a crucial tool I employed in each chapter of my thesis, and I always found the code to be amenable to whatever alterations I required. I thank Mark Allen for having the foresight to design a flexible code.

My fellow students contributed in many ways to the quality of academic life at Caltech. First and foremost I thank Hari Nair for answering numerous computer questions over the years, for generously sharing his plotting and interpolation routines, for a visit to The Tonight Show and, of course, for the Tick. I thank my officemates Hari, Dave and Ash for superior camaraderie. I must acknowledge Markarius Gurwellius as the epitome of DPS roommates: Mark, may you never be wanting for a Black & Tan. I thank Eric for ably captaining our soccer team, and the guys in seismo for enjoyable football games.

Thanks also to Kay and Irma for all of their assistance over the past several years, and to Mike Black for prompt help with computer woes.

Finally, I thank N. B. for many things, not the least of which are her insights into Lawrence.

Abstract

This thesis consists of four papers on the general subject of atmospheric chemistry in the outer solar system. Although all are reducing environments, the atmospheres differ widely in the ranges of temperature and pressure they encompass. Individual abstracts are given below.

Photochemistry of the Atmosphere and Ionosphere of Triton

A one-dimensional photochemical model of the atmosphere and ionosphere of Triton was constructed to evaluate the significance of CO and CO_2, detected as surface ices (Cruikshank et al. 1993), to the gas phase chemistry. For a CO mixing ratio of 10^{-4}, consistent with the observed fraction of CO ice, the model yields several interesting results. Gas phase production of CO_2 is slow, but may, with the help of heterogeneous reactions on aerosols, be capable of producing a detectable layer of CO_2 ice over the age of the solar system; however, we consider this unlikely. Atomic nitrogen, produced in the ionosphere, diffuses to the lower atmosphere and recombines to form N_2 in a cycle in which C acts as a catalyst. In a model with solar radiation only, the model predicts N densities a factor of two smaller than reported by Krasnopolsky et al. (1993). Atomic carbon is produced in the ionosphere primarily by dissociative recombination of CO^+. For an assumed rate coefficient for charge exchange from N_2^+ and CO^+ to C of 1×10^{-10} cm^3 sec^{-1}, Triton's ionosphere is dominated by C^+ and can be accounted for entirely by solar radiation. For a rate coefficient 10 times smaller, magnetospheric electron precipitation is needed to account for the observed electron density, but C^+ is still the principal ion. Electron precipitation is necessary to explain the observed N abundances. Measurements of the rate coefficients for ion-molecule reactions involving neutral C are needed.

Metal Ions in the Atmosphere of Neptune

Microwave propagation experiments performed with Voyager 2 at Neptune revealed sharp layers of electrons with densities ~ 10^4 cm^{-3} in Neptune's lower ionosphere. These layers are reminiscent of terrestrial sporadic-E layers, and , when taken together with data from the other giant planets, confirm the importance of the magnetic field in layer formation. A photochemical model which incorporates species produced by meteoroid ablation predicts that Mg^+ is the most likely metal comprising the layers, although laboratory data on the kinetics of metallic atoms and ions in reducing environments are lacking. The metal chemistry discussed here is directly relevant to the abundant metals observed at the impact site of the G fragment of Comet Shoemaker-Levy 9 on Jupiter.

Meteoroidal Influx into the Upper Atmospheres of Uranus and Neptune

Results from a recent analysis of meteoroid ablation rates in the atmosphere of Neptune have been coupled with photochemical models of the upper atmospheres of Neptune and Uranus to yield estimates of stratospheric water profiles as a function of meteoroid influx. Because water has never been detected in the upper atmospheres of the giant planets, the tangential column opacities of the model water profiles were compared with UV absorption measurements made by Voyager to determine maximum water influxes. For Uranus an upper limit is obtained which is consistent with an Oort-family particle population, but not with a large population of planet-family dust particles. For Neptune the model water profile is strongly dependent on the still uncertain eddy coefficient, making it difficult to rule out a large planet-family of IDP's. However, an IDP population sufficiently large to account for the CO observed in Neptune's atmosphere can be ruled out.

A Chemical Kinetics Model for the Comet Impact with Jupiter

A chemical kinetics code was developed for gas phase species comprised of the elements H,C,N,O,S and Si. The code is valid at high temperatures and for H-dominated compositions. The kinetics model was tested by running it to steady state equilibrium and comparing the results with a thermochemical model. Model runs for pressure-temperature histories relevant to the comet Shoemaker-Levy 9 impacts with Jupiter were made for C>O and C<O compositions and for a variety of temperatures. Results indicate that the plume gas must have C>O, in agreement with Zahnle et al. (1995), implying a greater than 50:1 mix of Jupiter gas to vaporized comet.

Table of Contents

List of Figures

Paper I:

Paper II:

List of Tables

Paper I:

Paper III:

Paper IV:

PAPER I

Photochemistry of the Atmosphere and Ionosphere of Triton

James R. Lyons, Yuk L. Yung

Division of Geological and Planetary Sciences

California Institute of Technology

Pasadena, California 91125

and

Mark Allen[1]

Earth and Space Sciences Division, Jet Propulsion Laboratory

California Institute of Technology

4800 Oak Grove Drive

Pasadena, California 91109

Submitted to Icarus

[1]Also , with the Division of Geological and Planetary Sciences, California Institute of Technology, Pasadena, California 91125.

Abstract

The recent detection (Cruikshank et al.,1993) of CO and CO_2 ices on the surface of Triton has important implications for the photochemistry of Triton's atmosphere. Results of a detailed photochemical model of Triton's atmosphere and ionosphere are presented for a CO mixing ratio of 10^{-4}. The model is one-dimensional, has 55 neutral and ion species and 211 reactions, and includes molecular, eddy, and ambipolar diffusion. Specific model calculations include the condensation rates of supersaturated species, atomic nitrogen profiles, and ion and electron profiles. As with earlier models, our model predicts that in the lower atmosphere the condensation of C_2H_4 and other hydrocarbons should produce a detectable layer of ice in about 10^6 years, for present Triton conditions. The lack of detection of any hydrocarbon ices suggests that either the ices are rapidly modified by radiation, or that our understanding of the photochemistry at these low temperatures is incomplete. Gas-phase production of CO_2 is slow but may be able to produce a detectable layer of CO_2 ice over the age of the solar system. Heterogeneous reactions on the surface of aerosol particles may contribute to the formation of CO_2 and scavenging of H may contribute to the hydrogenation of hydrocarbons on the aerosols. Atomic nitrogen, produced in the ionosphere, diffuses to the lower atmosphere where three-body reactions become important. The recombination of nitrogen atoms is found to occur principally via a cycle in which C acts as a catalyst, forming the species CNN during three-body reaction with N_2. The model predicts N densities about a factor of two lower than determined by Krasnopolsky et al. (1993). Atomic carbon is produced in the

ionosphere primarily by the dissociative recombination of CO^+. For an assumed rate coefficient for charge exchange from N_2^+ and CO^+ to C of 1×10^{-10} $cm^{-3}sec^{-1}$, Triton's ionosphere is dominated by C^+ and can be accounted for entirely by solar radiation. Thus, a large flux of precipitating magnetospheric electrons to Triton's upper atmosphere is not necessary to explain Triton's ionosphere. Much of the neutral and ion chemistry involving atomic carbon is very uncertain. Measurement of the rates of several key ion reactions would place an important constraint on the ratio of solar to magnetospheric energy input to Triton's upper atmosphere.

1. Introduction

There are only a few measurements of Triton's atmosphere available. The Voyager ultraviolet spectrometer (UVS) obtained data (Broadfoot et al., 1989) on both EUV emissions and on EUV absorption during Voyager's encounter with Triton. Evidence for H Lyman α and N_2 and N^+ emissions was seen in the airglow data. The EUV absorption measurments, obtained during a solar occultation experiment, yielded the scale height and N_2 number density in the upper atmosphere and the CH_4 scale height and number density in the lower atmosphere. A radio propagation experiment employing the spacecraft telemetry system made measurements (Tyler et al., 1989) of the electron and neutral number densities at two points along Triton's limb as Voyager was occulted by Triton as seen from Earth. The electron data provide an important constraint on ionospheric chemistry and on the energy input to the upper atmosphere, while the number density yields an estimate of the atmospheric number density at the ground. Voyager's infrared spectrometer (Conrath et al., 1989) was unable to measure IR emissions from the atmosphere because of the low temperature and pressure, but was able to determine that the surface temperature was about 38 K, confirming the suggestion of Trafton (1984) that Triton's atmosphere would be in vapor pressure equilibrium with surface ices. The most recent additional data on Triton's atmosphere has come from ground-based reflectance measurements by Cruikshank et al. (1991, 1993) of Triton's surface. Their results confirm that N_2 is the principal ice constituent on the surface and that CH_4 is present in trace quantities, but they also show that CO and CO_2 are present on the surface. The low

volatility of CO_2 precludes it from having a significant atmospheric mixing ratio, but CO is nearly as volatile as N_2 and so is likely to be an important constituent in the atmosphere. Voyager measurements (Broadfoot et al., 1989) were only able to place an upper limit of 1% on the CO mixing ratio in the upper atmosphere. Recently, more complete analyses of the Voyager UVS data have revealed new information about Triton's atmosphere. Herbert and Sandel (1991) showed that CH_4 is probably saturated in the atmosphere, whereas earlier measurements had indicated undersaturated CH_4. This may have important implications for the nature of the ice mixture on Triton's surface. Krasnopolsky et al. (1993) were able to extract densities for atomic nitrogen from the UVS occultation data by noting the absorption change due to the N ionization continuum. These data provide a much needed constraint on the chemistry and physics of the upper atmosphere.

Several groups have developed one-dimensional photochemical models of Triton's atmosphere. Strobel et al. (1991a) discussed the photochemical processing of CH_4 to produce higher hydrocarbons which then condense out contributing to the formation of a photochemical haze. In modeling the ionosphere, Strobel et al. (1991b), Majeed et al. (1991), Ip (1991), Delitsky et al. (1991), and Yung and Lyons (1991) all proposed N^+ as the principal ion present, formed as a result of electron impact ionization resulting from precipitating magnetospheric electrons. The electrons encounter Triton's atmosphere as a result of curvature drift as they travel along the curved field lines of Neptune's magnetic field draped over Triton (Strobel et al., 1991b). Lyons et al. (1992) developed a photochemical model that included carbon and odd-N chemistry. This model predicted

the existence of atomic carbon in the atmosphere and C^+ as the principal ion in the ionosphere, the latter formed as a result of solar ionization only. However, this model pushed the (unknown) rate constants to their maximum possible values; it also did not include CO. Delitsky et al. (1992) pointed out the importance of ion chemistry involving CO as a source of C to the upper atmosphere, and hence the formation of C^+. This is also discussed by Summers and Strobel (1992). A key difference among the models is whether the ionosphere results from solar radiation, in which case C^+ is the dominant ion, or whether the ionosphere is formed by electron impact processes, for which N^+ is the dominant ion. In the latter scenario, Triton's ionosphere would peak as Triton passed through Neptune's magnetic equatorial plane and then rapidly decay before the next equatorial crossing eight hours later.

Several papers have discussed the thermal structure of Triton's atmosphere. Yelle et al. (1991) showed that the temperature gradient in Triton's atmosphere implies a downward energy flux from the ionosphere of 1.1×10^{-3} erg cm^{-2} sec^{-1}. Stevens et al. (1992) determined the heating efficiencies of solar EUV and electron impact and estimated that an orbitally-averaged energy flux of electrons of about twice the solar EUV energy flux was necessary to explain Triton's thermospheric temperature. They also considered rotational cooling by CO and placed an upper limit of 2×10^{-4} on the CO mixing ratio. Krasnopolsky (1993) found that rotational cooling does not imply an upper limit to the CO abundance.

This paper will concentrate exclusively on neutral and ion atmospheric chemistry, with particular emphasis on evaluating the role of CO. No attempt is made to explain

Triton's somewhat elevated thermospheric temperature. Rather, we will identify the key photochemical processes present in Triton's atmosphere and try to determine which kinetics measurements are most needed to clarify the chemistry. In this vein, the neutral and ion chemistry of atomic carbon will be shown below to be especially important. The paper is organized as follows: section 2 gives details of the photochemical model; section 3 describes the formation and loss of condensible species; section 4 describes factors affecting the atomic nitrogen profile; section 5 presents important ionospheric species and reactions; section 6 gives a summary and conclusions and suggests key chemical reactions for further laboratory study.

2. The photochemical model

The photochemical model developed for Triton's atmosphere is one-dimensional and includes the effects of molecular, ambipolar and eddy diffusion in the vertical direction. The model includes 55 neutral and ion species and 211 reactions. The equation of mass continuity, coupled with diffusive transport, was solved for each species, with chemical loss and production providing the coupling between species (Allen et al., 1981). Boundary conditions were applied at the top of the atmosphere to simulate thermal escape. Mixing ratios for the parent species CH_4 and CO were defined at the surface; the N_2 profile was held constant. Table 1 lists the boundary conditions for selected species in the model. The escape altitude was taken to be 870 km; the model has 58 vertical levels with a spacing of ⅓ of a scale height. Because the rates of several important

TABLE 1

BOUNDARY CONDITIONS FOR SELECTED SPECIES IN THE PHOTOCHEMICAL MODEL.

Species	Lower Boundary[a]	Upper Boundary[c]
H	$v = -.075$[b]	$v = 3.0 \times 10^{4}$
H_2	$\phi = 0.0$	$v = 1.4 \times 10^{4}$
C	$v = -.075$	$v = 9.8$
CH_4	$f = 1.7 \times 10^{-4}$	$v = 0.0$
C_2H_4	$v = -.075$	$v = 0.0$
N	$v = -.075$	$v = 2.1$
CN	$v = -.075$	$v = 0.0$
CNN	$v = -.075$	$v = 0.0$
CO	$f = 1.0 \times 10^{-4}$	$v = 5.8 \times 10^{-5}$
O	$v = -.075$	$v = 0.50$
C+	$f = 0.0$	$v = 9.8$
N+	$f = 0.0$	$v = 2.1$

[a] The symbols f, ϕ and v refer to mixing ratio, flux ($cm^{-2}\ s^{-1}$) and velocity ($cm\ s^{-1}$), respectively. The sign convention for ϕ and v is positive for upward flow.

[b] This boundary condition accounts for flow to the ground at a velocity = K/H, where K is the eddy diffusion coefficient at the ground ($1 \times 10^{5}\ cm^{2}\ s^{-1}$) and H is the scale height for a given species.

[c] Jeans escape velocity.

reactions are not known, we will define a "standard" model, the results of which will then be compared with results from variations of the standard case. In the standard model, only solar radiation is incident on Triton, and the mixing ratio of CO at the ground is assumed to be 10^{-4}. The solar flux used in the model is from Woods and Rottman (1990) for $\lambda \leq 1030$Å, and from Mount and Rottman (1983) for $\lambda \geq 1172.5$Å, with interpolated values used for wavelengths in between.

Several chemical rate constants for reactions involving C and C^+ are unknown; in particular, the rate constants for reactions R191 and R205 (see Table 4) are assumed to be 1×10^{-10} $cm^3 sec^{-1}$ in the standard model. Tables 2, 3, and 4 list the chemical reactions for the standard model only; this set of reactions is condensed from a more complete set of reactions (about 350) available from the authors.

3. Photochemical formation of condensible species

Although Voyager did not detect IR emissions from any molecules in Triton's atmosphere, the photochemical formation of higher hydrocarbons, nitriles and CO_2 is nevertheless of interest. Triton's low temperature results in many of these species being supersaturated and susceptible to condensation. Condensible species may accumulate (Strobel et al., 1990a) in quantities sufficient to be detected from ground-based IR measurements, or may be polymerized by solar radiation and contribute to the coloration of Triton's surface (Thompson and Sagan).

Figure 1 presents in the form of a schematic diagram an overview of the principal

TABLE 2

PHOTOABSORPTION, PHOTODISSOCIATION , AND PHOTOIONIZATION REACTIONS

#		Reaction			Reference
R1	N_2+ hν	absorption			Kirby et al.(1979); Wu et al.(1984)
R2	H_2+ hν	"			a
R3	CH_4+ hν	"			a
R4	C_2H_2+ hν	"			a
R5	C_2H_4+ hν	"			a
R6	C_4H_2 + hν	"			a
R7	CO + hν	"			Thompson et al.(1963); Wright et al.(1976); Lee and Guest(1981); Letzelter et al.(1987); Samson and Haddad(1988); Stark et al.(1991)
R8	HCN + hν	"			West(1975); Nuth and Glicker(1982)
R9	HC_3N + hν	"			Connors et al.(1974); Bruston et al.(1989)
R10	CH + hν	→ C	+ H		van Dishoeck(1987)
R11	CH_4 + hν	→ C(^{1}D)	+2H_2		Rebbert and Ausloos(1972)
R12	HCN + hν	→ H	+ CN		West(1975); Nuth and Glicker(1982)
R13	HC_3N + hν	→ H	+ C_3N		Okabe and Dibeler(1973)
R14	HC_3N + hν	→ C_2H	+ CN		"
R15	N_2 + hν	→2N			Kirby et al. (1979)
R16	N_2 + hν	+e_{ph}	= N	+ N(^{2}D)	assume 0.3*R15
R17	H_2 + hν	→2H			a
R18	$^3CH_2$ + hν	→ CH	+ H		a
R19	CH_3 + hν	→ $^1CH_2$	+ H		a
R20	CH_4 + hν	→ $^1CH_2$	+ H_2		a
R21	CH_4 + hν	→$^3CH_2$	+2H		a
R22	CH_4 + hν	→ CH	+ H	+ H_2	a
R23	C_2H_2 + hν	→ C_2H	+ H		a
R24	C_2H_2 + hν	→ C_2	+ H_2		a
R25	C_2H_4 + hν	→ C_2H_2	+ H_2		a
R26	C_2H_4 + hν	→ C_2H_2	+2H		a
R27	C_2H_4 + hν	→ C_2H_3	+ H		a
R28	CH_2CCH_2 +hν→	C_3H_3	+ H		a
R29	CH_2CCH_2 +hν→	C_3H_2	+ H_2		a
R30	C_4H_2 + hν	→ C_4H	+ H		a
R31	C_4H_2 + hν	→ C_2H_2	+ C_2		a
R32	CO + hν	→ C	+ O		Huber and Herzberg(1979)
R33	H_2CO + hν	→ HCO	+ H		Mentall et al.(1971); Okabe(1978)
R34	H_2CO + hν	→ H_2	+ CO		"
R35	H_2CO + hν	→2H	+ CO		"
R36	CO_2 + hν	→ CO	+ O(^{1}D)		Slanger and Black(1978); Okabe(1978)
R37	CO_2 + hν	→ CO	+ O(^{1}S)		"
R38	CNN + hν	→ CN	+ N		*
R39	CCO + hν	→ C	+ CO		*
R40	C_2H_3CN + hν→	C_2H_3	+ CN		*
R41	N_2 + hν	→ N_2^+	+ e		Kirby et al.(1979); Morioka et al.(1984)
R42	N_2 + hν	→ N^+	+ N	+ e	"
R43	N_2 + hν	+ e_{ph}	→ N_2	+ e	assume 0.2*R41

TABLE 2

PHOTOABSORPTION, PHOTODISSOCIATION , AND PHOTOIONIZATION REACTIONS

#	Reaction					Reference
R44	$N_2 + h\nu$	$+ e_{ph}$	$\rightarrow N^+$	$+ N$	$+ e$	assume 0.2*R42
R45	$N + h\nu$	$\rightarrow N^+$	$+ e$			Le Dourneuf et al.(1979)
R46	$C + h\nu$	$\rightarrow C^+$	$+ e$			Cantu et al.(1981)
R47	$CH_3 + h\nu$	$\rightarrow CH_3^+$	$+ e$			Prasad and Tan(1974)
R48	$C_2H_2 + h\nu$	$\rightarrow C_2H_2^+$	$+ e$			Hayaishi et al. (1982)
R49	$CO + h\nu$	$\rightarrow CO^+$	$+ e$			Wright et al.(1976);Musuoka and Samson(1981)
R50	$NO + h\nu$	$\rightarrow NO^+$	$+ e$			*

* Gladstone,G. R.,M. Allen,Y. L. Yung, Hydrocarbon photochemistry in the upper atmosphere of Jupiter, in press, Icarus.

* assumed value.

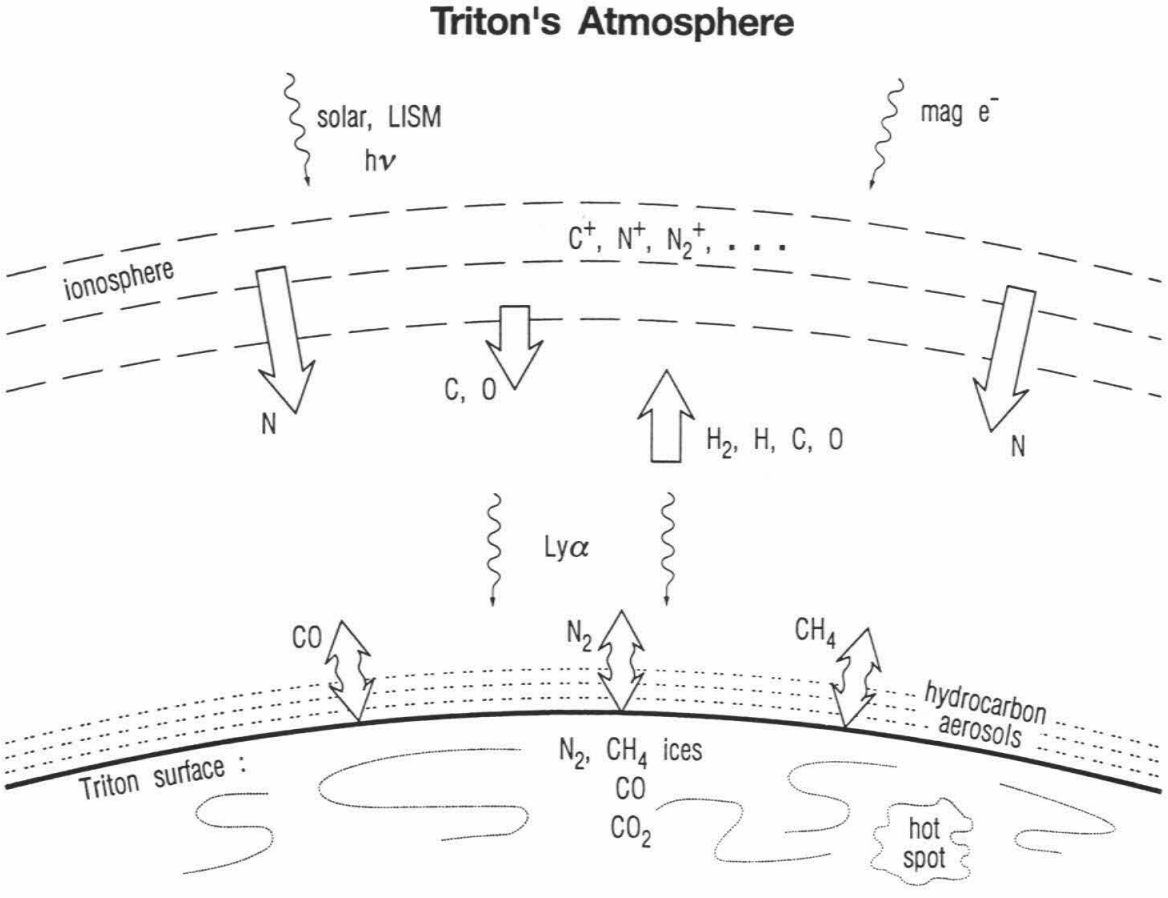

Fig. 1. A schematic diagram showing the important physical and chemical processes in Triton's atmosphere.

photochemical processes occurring in Triton's atmosphere. Ices of N_2, CH_4 and CO are shown condensing and sublimating from the surface; CO_2 has a negligible vapor pressure at such low temperatures. Hot spots may exist on the surface, as evidenced by the lower albedo regions described by Stansberry et al. (1992). Such hot spots may represent regions devoid of N_2 frosts, perhaps exposing patches of pure CH_4, CO or CO_2. If the regions are raised in temperature by a few kelvin as suggested by Stansberry et al. (1992), and CH_4 and/or CO are present, then these volatile species could be saturated in the atmosphere even if they are present only in trace quantities in the N_2 ice. Methane undergoes photodissociation by solar and local interstellar medium (LISM) H Lyman α, which reduces the CH_4 scale height and leads to the production of an aerosol haze (Strobel et al., 1990a). H and H_2, derived from CH_4 dissociation, diffuse to the upper atmosphere where they either escape or participate in ion-molecule chemistry. The ion chemistry is driven by the production of N^+ and N_2^+ by solar EUV and possibly electron impact. Charge exchange from N^+ and N_2^+ to CO produces CO^+, the dissociative recombination of which results in an ionosphere dominated by C^+. A downward flux of N atoms from the ionosphere contributes to the formation of nitriles in the lower atmosphere. Figure 2 shows the temperature and N_2 number density profiles used in the model calculations.

TABLE 3

REACTIONS BETWEEN NEUTRAL SPECIES

#	Reaction	Rate Constant†	Reference‡
R51	$2H + M \rightarrow H_2 + M$	$1.5 \times 10^{-29} T^{-1.3}$	a
R52	$H + {}^3CH_2 \rightarrow CH + H$	$4.7 \times 10^{-10} e^{-370/T}$	a
R53	$H + {}^3CH_2 + M \rightarrow CH_3 + M$	same as R68	a
R54	$H + CH_3 + M \rightarrow CH_4 + M$	$3.8 \times 10^{-28} e^{-19.5/T}$	a
R55	$H + C_2H_3 \rightarrow C_2H_2 + H_2$	6.0×10^{-12}	a
R56	$H + C_3H_2 + M \rightarrow C_3H_3 + M$	10*R54	a
R57	$H + C_3H_3 + M \rightarrow CH_3C_2H + M$	10*R54	a
R58	$C + C \rightarrow C_2 + h\nu$	1.0×10^{-18}	*
R59	$C + N \rightarrow CN + h\nu$	1.0×10^{-18}	*
R60	$C + N + M \rightarrow CN + M$	$2.8 \times 10^{-30} T^{-1.0}$	Fisher et al. (1985)
R61	$C + O \rightarrow CO + h\nu$	1.0×10^{-18}	*
R62	$C + H_2 + M \rightarrow {}^3CH_2 + M$	$2.1 \times 10^{-29} T^{-1.0}$	Husain and Kirsch (1971)
R63	$C + N_2 + M \rightarrow CNN + M$	$2.8 \times 10^{-28} T^{-2.0}$	"
R64	$C + CO + M \rightarrow CCO + M$	$1.9 \times 10^{-29} T^{-1.0}$	"
R65	$C(^1D) + H_2 \rightarrow CH + H$	3.7×10^{-10}	Rebbert and Ausloos (1972)
R66	$C(^1D) + CH_4 \rightarrow C_2H_2 + H_2$	3.2×10^{-11}	"
R67	$C(^1D) + N_2 \rightarrow C + N_2$	2.5×10^{-12}	Braun et al. (1969)
R68	$CH + H_2 + M \rightarrow CH_3 + M$	10*R54	a
R69	$CH + CH_4 \rightarrow C_2H_4 + H$	$3.0 \times 10^{-11} e^{200/T}$	a
R70	$CH + C_2H_2 \rightarrow C_3H_2 + H$	$3.5 \times 10^{-10} e^{61/T}$	a
R71	$CH + C_2H_4 \rightarrow CH_2CCH_2 + H$	$2.2 \times 10^{-10} e^{173/T}$	a
R72	$CH + H \rightarrow H_2 + C$	1.4×10^{-11}	Becker et al. (1989)
R73	$CH + N \rightarrow CN + H$	2.1×10^{-11}	Messing et al. (1981)
R74	$^1CH_2 + M \rightarrow {}^3CH_2 + M$	7.9×10^{-12}	Yung et al. (1984)
R75	$^1CH_2 + H_2 \rightarrow {}^3CH_2 + H_2$	1.3×10^{-11}	a
R76	$^1CH_2 + H_2 \rightarrow CH_3 + H$	9.2×10^{-11}	a
R77	$^1CH_2 + CH_4 \rightarrow {}^3CH_2 + CH_4$	1.2×10^{-11}	a
R78	$^1CH_2 + CH_4 \rightarrow 2CH_3$	5.9×10^{-11}	a
R79	$^3CH_2 + {}^3CH_2 \rightarrow C_2H_2 + 2H$	$2.1 \times 10^{-10} e^{-408/T}$	a
R80	$^3CH_2 + CH_3 \rightarrow C_3H_4 + H$	7.0×10^{-11}	a
R81	$^2CH_3 + M \rightarrow C_2H_6 + M$	1.0×10^{-23}	Laufer et al (1983)
R82	$C_2 + CH_4 \rightarrow C_2H + CH_3$	$5.1 \times 10^{-11} e^{-297/T}$	a
R83	$C_2 + N \rightarrow CN + C$	5.0×10^{-11}	*
R84	$C_2 + O \rightarrow CO + C$	$1.0 \times 10^{-10} e^{-250/T}$	a
R86	$C_2H + C_2H_2 \rightarrow C_4H_2 + H$	1.5×10^{-10}	a
R87	$C_2H + C_2H_4 \rightarrow C_4H_4 + H$	2.0×10^{-11}	a
R88	$C_2H + C_4H_2 \rightarrow C_6H_2 + H$	same as R86	a
R89	$C_2H + N \rightarrow CN + CH$	1.0×10^{-10}	*
R90	$C_2H + O \rightarrow CO + CH$	3.0×10^{-11}	Tsang and Hampson (1986)
R91	$C_2H_3 + O \rightarrow CH_2CO + H$	4.5×10^{-11}	Heinemann et al. (1988)
R92	$C_2H_3 + N \rightarrow H_2C_2N + H$	1.0×10^{-10}	*
R93	$C_3H_2 + C_2H_2 \rightarrow C_4H_2 + {}^3CH_2$	5.0×10^{-13}	a
R94	$CN + N \rightarrow C + N_2$	1.0×10^{-10}	Whyte and Phillips (1983)
R95	$CN + C_2H_2 \rightarrow HC_3N + H$	1.0×10^{-10}	Lichtin and Lin (1986)
R96	$CN + C_2H_4 \rightarrow C_2H_3CN + H$	1.0×10^{-10}	"

TABLE 3

REACTIONS BETWEEN NEUTRAL SPECIES

#	Reaction	Rate Constant†	Reference‡
R97	CNN + N → CN + N_2	1.0×10^{-10}	*
R98	CNN + H → CH + N_2	5.0×10^{-11}	*
R99	CNN + C → CN + CN	1.0×10^{-10}	*
R100	CNN + H → CN + NH	5.0×10^{-11}	*
R101	CNN + O → CN + CO	5.0×10^{-11}	*
R102	CNN + C_2H_2 → HC_3N + NH	1.0×10^{-10}	*
R103	CNN + C_2H_4 → C_2H_3CN + NH	1.0×10^{-10}	*
R104	C_3N + C_2H_2 → PROD	1.0×10^{-10}	*
R105	C_3N + C_2H_4 → PROD	1.0×10^{-10}	*
R106	2N + M → M	6.5×10^{-28} $T^{-2.0}$	Yamashita (1979)
R107	N + H → NH	1.0×10^{-18}	*
R108	N + H + M → NH + M	4.5×10^{-27} $T^{-2.0}$	Brown (1973)
R109	N + NH → H	1.1×10^{-11} $T^{0.50}$	Yung et al. (1984)
R110	N + $^3CH_2$ → HCN + H	4.3×10^{-10} $e^{-420/T}$	*
R111	N + CH_3 → H_2CN + H	4.3×10^{-10} $e^{-420/T}$	Marston et al.(1989)
R112	N + NO → O	3.4×10^{-11}	DeMore et al. (1992)
R113	N + OH → NO + H	5.1×10^{-11}	Atkinson et al (1989)
R114	N + O → NO	1.0×10^{-18}	*
R115	$N(^2D)$ + U → N + U	2.3×10^{-05}	Yung et al. (1984)
R116	$N(^2D)$ + H_2 → NH + H	5.0×10^{-12}	Black et al. (1969)
R117	$N(^2D)$ + N_2 → N + N_2	6.0×10^{-15}	"
R118	$N(^2D)$ + CO → N + CO	6.0×10^{-12}	"
R119	NH + O → NO + H	1.2×10^{-10}	Cohen and Westberg (1991)
R120	NH + O → OH + N	1.2×10^{-11}	"
R121	NH + NO → N_2 + OH	4.5×10^{-11}	Yamasaki et al. (1991)
R122	NH + $^3CH_2$ → PROD	2.0×10^{-11}	*
R123	NH + CH_3 → PROD	2.0×10^{-11}	*
R124	NH + C → CN + H	5.0×10^{-11}	*
R125	NO + CH → CO + NH	2.5×10^{-10}	Lichtin et al. (1984)
R126	NO + HCO → HNO + CO	1.2×10^{-10} $T^{-0.40}$	Veyret and Lesclaus (1981)
R127	NO + $^3CH_2$ → PROD	3.7×10^{-11}	Seidler et al. (1989)
R128	NO + C → CN + O	1.6×10^{-11}	Becker et al. (1988)
R129	O + $^3CH_2$ → HCO + H	2.0×10^{-11}	Tsang and Hampson (1986)
R130	O + CH_3 → H_2CO + H	1.1×10^{-10}	DeMore et al. (1992)
R131	O + N + M → NO + M	5.5×10^{-33} $e^{155/T}$	Campbell and Gray (1973)
R132	O + H + M → OH + M	1.3×10^{-29} $T^{1.00}$	Tsang and Hampson(1986)
R133	O + CN → CO + N	1.7×10^{-11}	Baulch et al. (1981)
R134	O + CH → CO + H	6.6×10^{-11}	Warnatz (1984)
R135	OH + C → CO + H	1.0×10^{-11}	*
R136	CO + OH → CO_2 + H	1.4×10^{-13} $e^{-31/T}$	DeMore et al. (1992)
R137	HCO + O → CO_2 + H	5.0×10^{-11}	Tsang and Hampson (1986)
R138	HCO + H → CO + H_2	2.0×10^{-10}	"
R139	HCO + O → CO + OH	5.0×10^{-11}	"
R140	CCO + H → CH + CO	2.2×10^{-11}	Bauer et al. (1985)
R141	CCO + O → CO + CO	8.6×10^{-11}	"
R142	CCO + N → CN + CO	5.0×10^{-11}	*
R143	CCO + C → C_2 + CO	5.0×10^{-11}	*
R144	C_2H_2 condensation onto aerosols	see text	
R145	C_2H_4 "	"	
R146	C_2H_6 "	"	
R147	C_4H_2 "	"	
R148	HCN "	"	
R149	HC_3N "	"	
R150	C_2H_3CN "	"	

TABLE 3

REACTIONS BETWEEN NEUTRAL SPECIES

#		Reaction	Rate Constant†	Reference‡
R151	H_2CO	"	"	
R152	CO_2	"	"	
R153	C	scavenging by aerosols	"	
R154	N	"	"	
R155	H	"	"	
R156	O	"	"	

† Units are cm^3 sec^{-1} for bimolecular reactions; cm^6 sec^{-1} for termolecular reactions.

* Gladstone,G. R.,M. Allen,Y. L. Yung, Hydrocarbon photochemistry in the upper atmosphere of Jupiter, in press, Icarus.

• assumed value

‡ For additional references see F. Westley et. al., NIST Chemical Kinetics Database, version 4.0, 1992.

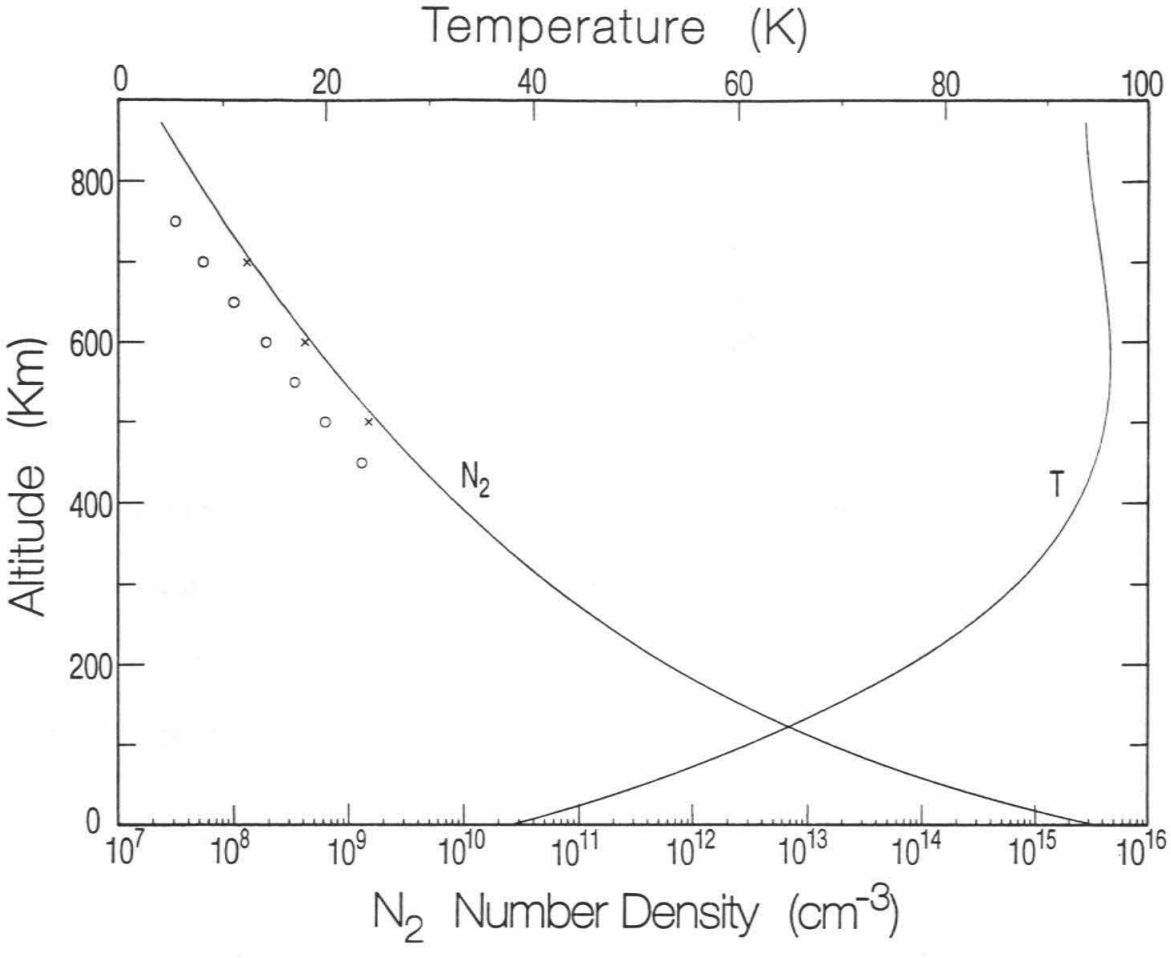

Fig. 2. The temperature and N_2 density profiles used in the model. For comparison, several values of the N_2 density profiles of Krasnolpolsky et al. (1993) (open circles) and Summers and Strobel (1992) (crosses) are shown.

The dissociation production rates for the three parent gases in the photochemical model are shown in Figure 3. Methane photolysis proceeds by the reactions (Strobel et al., 1991; Yung et al., 1984)

$$CH_4 + h\nu \rightarrow {}^1CH_2 + H_2 \quad \text{(R20)}$$
$$\rightarrow {}^3CH_2 + 2H \quad \text{(R21)}$$
$$\rightarrow CH + H_2 + H \quad \text{(R22)}$$

with peak production rates occurring at about 20 km. (Recent measurements of CH_4 photodissociation products (Mordaunt et al., 1993) suggest that R20-R22 may not be correct; however we have not yet incorporated these results into the model presented here.) CO photolysis,

$$CO + h\nu \rightarrow C + O \quad \text{(R32)}$$

also peaks in the lower atmosphere but with a much smaller rate; for larger CO mixing ratios the altitude of peak dissociation will increase but the rate increases only slightly. The production of nitrogen atoms occurs both by the direct dissociation of N_2 by photons and electrons and by ion reactions, in particular the recombination of N_2^+. Figure 3 shows the total production rate of nitrogen atoms due to both solar and photoelectron impact

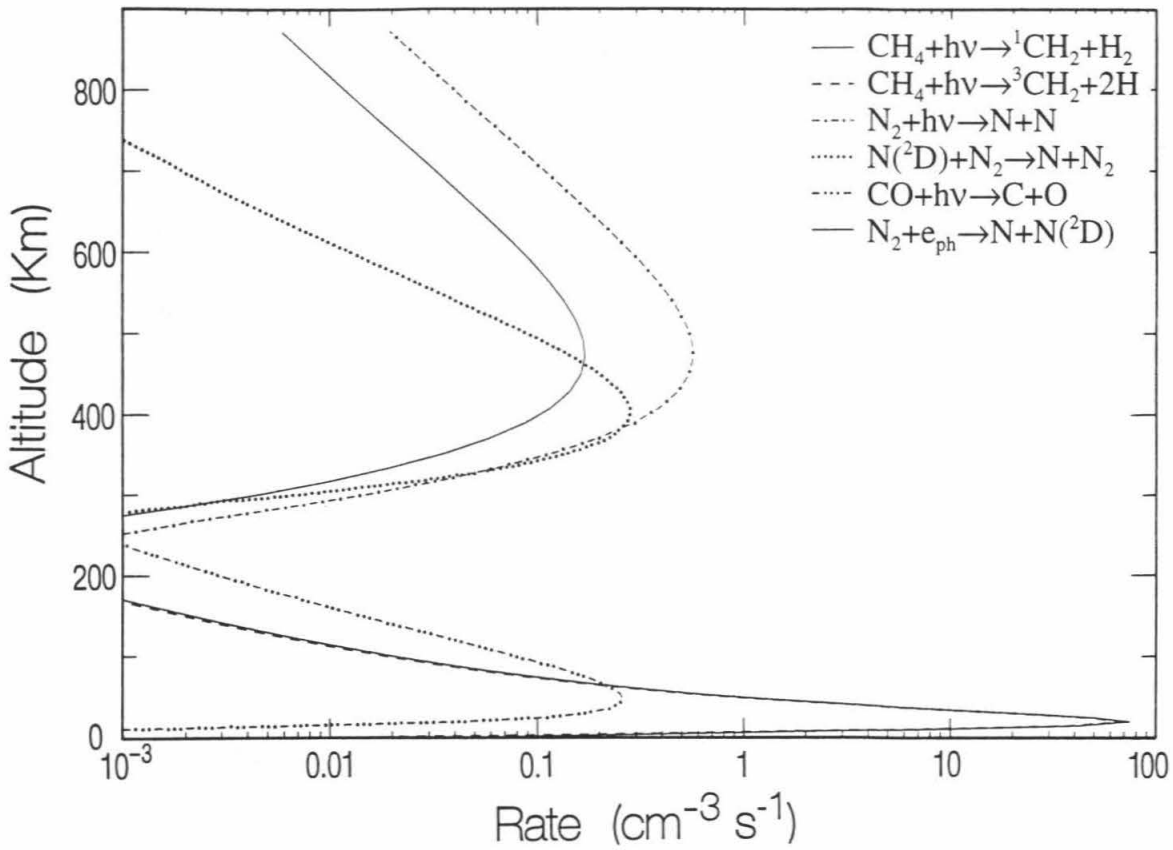

Fig. 3. Column dissociation rates for N_2, CH_4, CO.

processes. A discussion of the specific chemistry leading to N production will be given in the next section. The downward flux of N (normalized to the ground to account for the sphericity of the atmosphere) for the standard model is about 1×10^8 cm^{-2} sec^{-1} at the bottom of the ionosphere.

An estimate of the eddy diffusion coefficient can be made by comparing the photolysis rate of CH_4 to the observed CH_4 scale height. Preliminary estimates (Strobel et al., 1990a) yielded eddy coefficients ~ 6000 cm^2 sec^{-1}. A more recent analysis (Summers and Strobel, 1992) incorporating the revised CH_4 profile of Herbert and Sandel (1991) yields eddy coefficients ~ 300 cm^2 sec^{-1}, the value predicted by Yelle et al. (1991). Figure 4 shows the methane profile obtained for an eddy coefficient K = 300 cm^2 sec^{-1} above 9 km, and K = $10^5 cm^2$ sec^{-1} below 9 km. The methane densities obtained by Herbert and Sandel (1991) are also shown. As can be seen from the figure, the model profile is intermediate between the measured summer and winter profiles. Ion chemistry rapidly consumes CH_4 above 200 km.

The density profiles of parent species and some of their dissociation products are shown in Figure 5. The small falloff with height of CO results from weak photodissociation, so CO has nearly the same scale height as N_2. H_2 is escaping at the diffusive limit and therefore also has a scale height comparable to N_2. Atomic nitrogen peaks at about 135 km, below which recombination and scavenging by aerosols rapidly consume it. The profiles of O and C are qualitatively similar to N except that their densities are much lower. Atomic hydrogen, which is involved in many reactions and is rapidly scavenged by aerosol particels (Table 4), peaks closer to the ground due to the

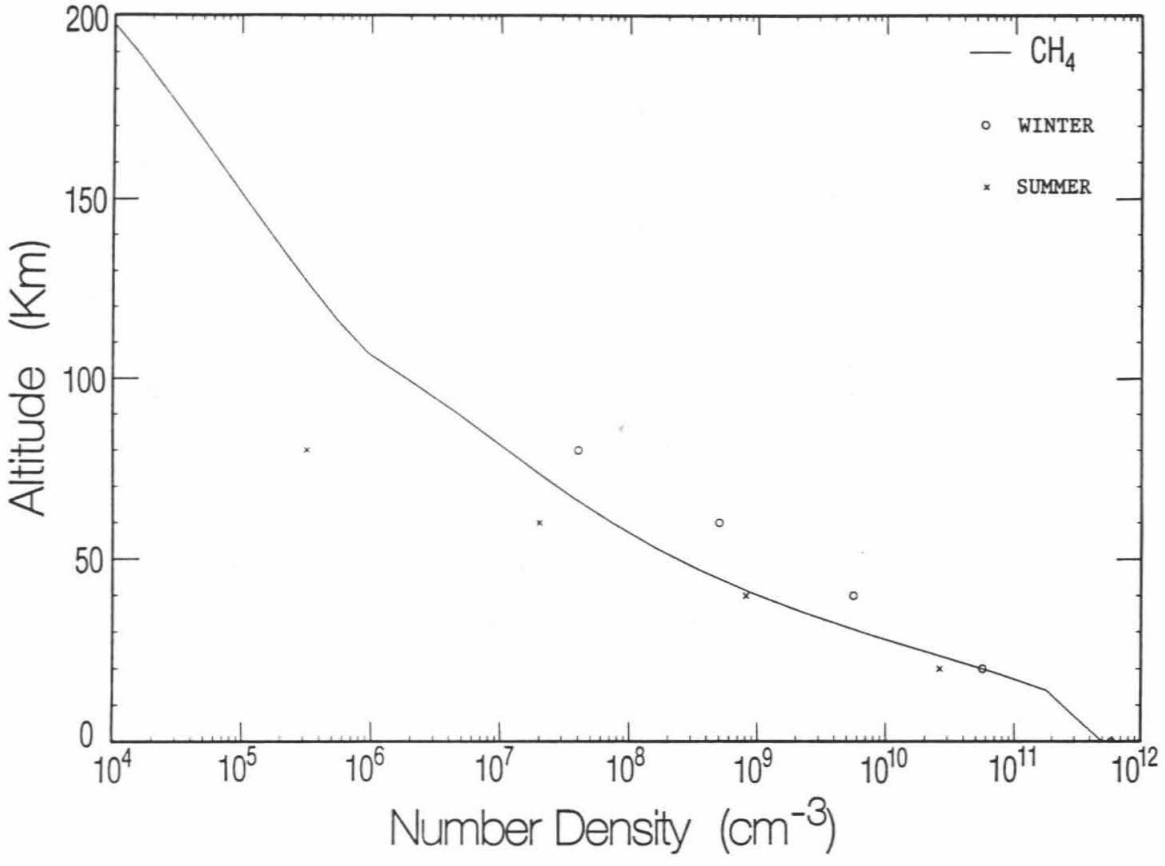

Fig. 4. Methane profile with summer and winter data points as determined by Herbert and Sandel (1991).

TABLE 4.

ION-MOLECULE AND ION RECOMBINATION REACTIONS

#	Reaction	Rate Constant‡	Reference
R157	$H^+ + O = O^+ + H$	3.8×10^{-10}	a
R158	$C^+ + CH_4 = C_2H_2^+ + H_2$	4.5×10^{-10}	a
R159	$C^+ + CH_4 = C_2H_3^+ + H$	9.5×10^{-10}	a
R160	$C^+ + C_2H_2 = C_3H^+ + H$	2.6×10^{-9}	a
R161	$C^+ + HCN = C_2N^+ + H$	2.9×10^{-9}	a
R162	$C^+ + C_2H_4 = C_3H_m^+ + H$	1.5×10^{-9}	a
R163	$C^+ + NO = NO^+ + C$	7.5×10^{-10}	a
R164	$C^+ + N_2 + M = CNN^+ + M$	6.0×10^{-30}	*
R165	$C^+ + H_2 = CH^+ + H$	1.2×10^{-16}	a
R166	$C^+ + e = C + h\upsilon$	5.0×10^{-12}	*
R167	$CNN^+ + e = CN + N$	3.0×10^{-7}	*
R168	$C_2H_2^+ + H_2 = C_2H_3^+ + H$	1.0×10^{-11}	a
R169	$C_2H_2^+ + N = H^+ + HCN + C$	2.5×10^{-11}	a
R170	$C_2H_2^+ + N = C_2N^+ + H_2$	7.5×10^{-11}	a
R171	$C_2H_2^+ + N = CHCN^+ + H$	1.5×10^{-10}	a
R172	$C_2H_3^+ + CH_4 = C_3H_m^+ + H_2$	1.9×10^{-10}	a
R173	$C_2H_3^+ + N = CHCN^+ + H_2$	2.2×10^{-10}	a
R174	$C_2H_3^+ + e = C_2H_2 + H$	7.8×10^{-7}	c
R175	$C_2N^+ + e = CN + C$	5.0×10^{-7}	*
R176	$C_2N^+ + CH_4 = C_2H_3^+ + HCN$	7.0×10^{-10}	a
R177	$CHCN^+ + e = CH + CN$	2.0×10^{-7}	*
R178	$CHCN^+ + e = C + HCN$	2.0×10^{-7}	*
R179	$N^+ + H_2 = NH^+ + H$	2.4×10^{-10}	b
R180	$N^+ + C = C^+ + N$	1.0×10^{-12}	*
R181	$N^+ + CO = CO^+ + N$	9.4×10^{-10}	b
R182	$N^+ + CO = NO^+ + C$	1.6×10^{-10}	a
R183	$N^+ + O = O^+ + N$	1.0×10^{-12}	*
R184	$N^+ + e = N + h\upsilon$	5.0×10^{-12}	*
R185	$NH^+ + N_2 = N_2H^+ + N$	6.5×10^{-10}	a
R186	$NH^+ + e = N + H$	7.5×10^{-8}	c
R187	$NO^+ + e = N + O$	6.5×10^{-7}	c
R188	$N_2^+ + H_2 = N_2H^+ + H$	2.0×10^{-9}	a
R189	$N_2^+ + H = H^+ + N_2$	1.0×10^{-11}	a
R190	$N_2^+ + N = N^+ + N_2$	1.0×10^{-11}	a
R191	$N_2^+ + C = C^+ + N_2$	1.0×10^{-10}	*
R192	$N_2^+ + O = NO^+ + N$	1.3×10^{-10}	a
R193	$N_2^+ + O = O^+ + N_2$	0.1×10^{-10}	a
R194	$N_2^+ + e = N(^2D) + N$	5.7×10^{-8}	c
R195	$N_2^+ + CO = CO^+ + N_2$	7.4×10^{-11}	a
R196	$N_2H^+ + CO = HCO^+ + N_2$	8.8×10^{-10}	a

TABLE 4.

ION-MOLECULE AND ION RECOMBINATION REACTIONS

#	Reaction					Rate Constant‡	Reference
R197	N_2H^+	+ O	=	N_2H^+	+ O	1.4×10^{-10}	a
R198	N_2H^+	+ e	=	H	+ N_2	6.5×10^{-7}	c
R199	H_2CN^+	+ HC_3N	=	$H_2C_3N^+$	+ HCN	3.4×10^{-9}	a
R200	H_2CN^+	+ e	=	HCN	+ H	6.1×10^{-7}	c
R201	O^+	+ N_2	=	NO^+	+ N	1.2×10^{-12}	a
R202	O^+	+ H_2	=	N_2H^+	+ O	1.7×10^{-9}	a
R203	CO^+	+ H_2	=	N_2H^+	+ CO	7.0×10^{-10}	a
R204	CO^+	+ O	=	O^+	+ CO	1.4×10^{-10}	a
R205	CO^+	+ C	=	C^+	+ CO	1.0×10^{-10}	*
R206	CO^+	+ H_2	=	HCO^+	+ H	7.0×10^{-10}	a
R207	CO^+	+ H	=	H^+	+ CO	7.5×10^{-10}	a
R208	CO^+	+ e	=	C	+ O	1.7×10^{-7}	c
R209	HCO^+	+ C_2H_2	=	$C_2H_3^+$	+ CO	1.4×10^{-9}	a
R210	HCO^+	+ HCN	=	H_2CN^+	+ CO	3.5×10^{-9}	a
R211	HCO^+	+ e	=	CO	+ H	5.1×10^{-7}	c

‡ Units are $cm^3\ s^{-1}$ for bimolecular reactions; $cm^6\ s^{-1}$ for termolecular reactions.

[a] V. G. Anicich, Evaluated bimolecular ion-molecule gas phase kinetics of positive ions, submitted *J. Phys. Chem. Ref. Data*, 1992.

[b] V. G. Anicich, A survey of bimolecular ion-molecule reactions for use in modeling the chemistry of planetary atmospheres, cometary comae, and interstellar clouds: 1992 supplement, submitted *Ap. J. Suppl. Series*, 1992.

[c] J. B. A. Mitchell, The dissociative recombination of molecular ions, *Physics Reports* **186, No. 5**, 215-248, 1990.

* assumed value

relatively large methane dissociation rate.

Many condensible chemical species are produced in Triton's atmosphere via pathways very similar to those proposed for Titan (Yung et al., 1984). Strobel et al. (1990a) first described the production of C_2 and C_4 hydrocarbons for Triton. Lyons et al. (1992) and Summers and Strobel (1992) described some of the nitriles produced. Here, we will simply outline the principal chemical pathways forming various species. The most produced condensible compound is C_2H_4 via the reactions

R69

$$CH + CH_4 \rightarrow C_2H_4 + H$$

R80

$$CH_3 + {}^3CH_2 \rightarrow C_2H_4 + H$$

Acetylene, with the next highest production rate, is produced by

$$^3CH_2 + {}^3CH_2 \rightarrow C_2H_2 + H \qquad \text{R79}$$

and by photolysis of C_2H_4. The compound CH_2CCH_2 results from

$$CH + C_2H_4 \rightarrow CH_2CCH_2 + H \qquad \text{R71}$$

which has a reaction rate more than two orders of magnitude below that of R69. Other hydrocarbon species produced include C_2H_6, C_4H_2, C_3H_2 and C_4H_4. Several nitriles are expected due to reaction of N with CH_4 photodissociation products. Hydrogen cyanide is produced by the reaction

TABLE 5.

CONDENSATION AND SCAVENGING COLUMN REACTION RATES

#	Species	Column Rate (cm^{-2} sec^{-1})	#	Species	Column Rate (cm^{-2} sec^{-1})
R144	C_2H_2	1.5×10^{7}	R151	H_2CO	6.7×10^{3}
R145	C_2H_4	1.7×10^{8}	R152	CO_2	1.3×10^{5}
R146	C_2H_6	1.3×10^{4}	R153	C	2.6×10^{3}
R147	C_4H_2	4.0×10^{4}	R154	N	1.4×10^{5}
R148	HCN	1.2×10^{4}	R155	H	2.7×10^{8}
R149	HC_3N	1.3×10^{5}	R156	O	7.2×10^{4}
R150	C_2H_3CN	4.8×10^{5}			

TABLE 6.

ESCAPE FLUXES FROM TOP OF ATMOSPHERE

Species	Flux (cm^{-2} sec^{-1})	Species	Flux (cm^{-2} sec^{-1})
H	1.7×10^7	O	5.8×10^4
H_2	2.6×10^8	CO	1.3×10^4
C	2.5×10^6	C^+	1.7×10^5 (thermal)
N	1.1×10^7		4.8×10^5 (nonthermal)
$N(^2D)$	2.3×10^5	N^+	1.4×10^4

$$N + {}^3CH_2 \rightarrow HCN + H \qquad \text{R110}$$

and also by dissociative recombination of H_2CN^+ in the ionosphere. The cyanide radical is involved in the formation of HC_3N and C_2H_3CN via the reactions

$$CN + C_2H_4 \rightarrow C_2H_3CN + H \qquad \text{R96}$$

$$CN + C_2H_2 \rightarrow HC_3N + H \qquad \text{R95}$$

Other condensible species are formed by the reaction of oxygen atoms, produced during photolysis of CO, with CH_4 dissociation products. Formaldehyde is generated by

$$O + CH_3 \rightarrow H_2CO + H \qquad \text{R130}$$

and CO_2 is generated by

$$CO + OH \rightarrow CO_2 + H \qquad \text{R136}$$

In the standard model the rates of these reactions are about four orders of magnitude below that of R69 producing C_2H_4, so the formation of H_2CO and CO_2 is negligible compared to some of the species already discussed. Note that, in contrast to Titan (Yung et al., 1984), the production of C_2H_6 is negligible compared to acetylene and ethylene, although the rate constants estimated for the recombination of methyl radicals (Laufer et al., 1983; Macpherson et al., 1985; Slagle et al., 1988) vary by nearly ten orders of magnitude at 50 K.

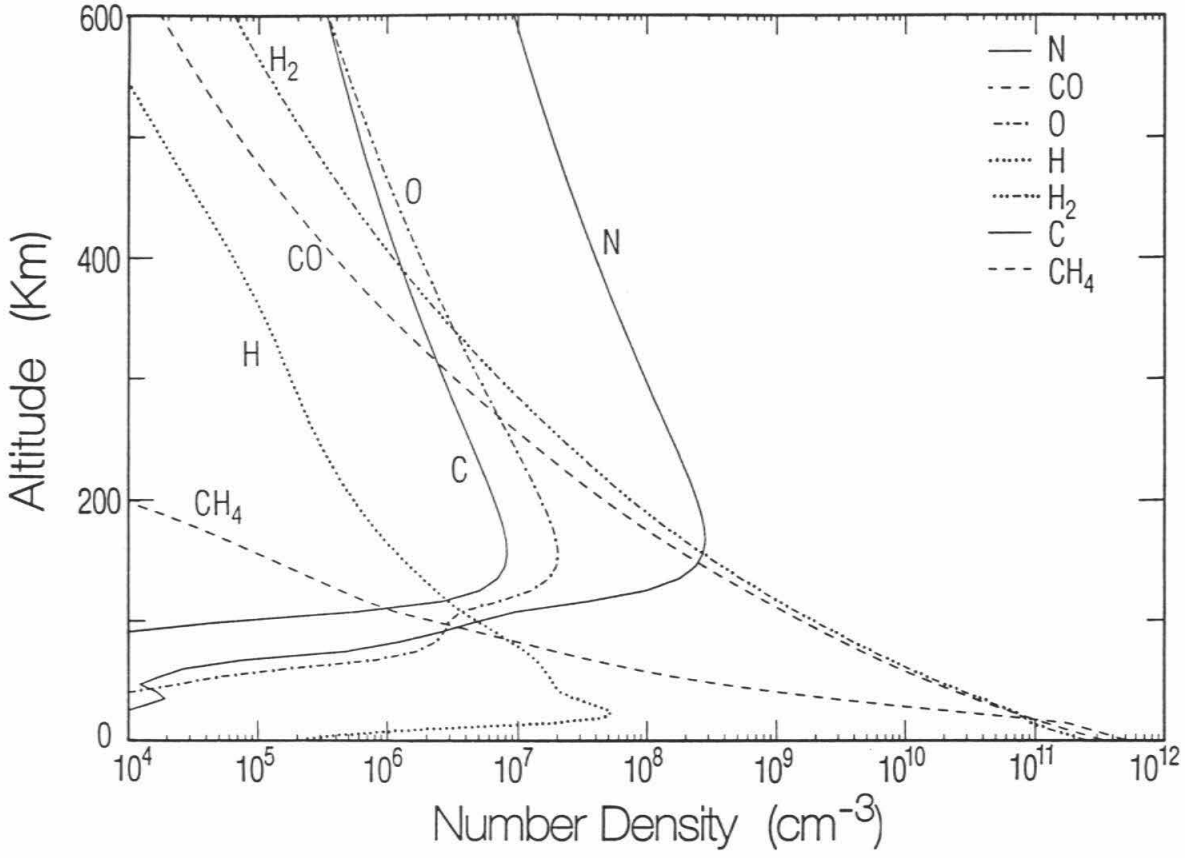

Fig. 5. Model density profiles for parent species, atomics, and H_2.

The principal loss process for all these species is condensation. A unimolecular condensation rate coefficient is defined as (Yung et al., 1984; Summers and Strobel, 1992)

$$k_i = \frac{n_i - n_{i,sat}}{\tau_c}$$

where n_i is the number density of the ith supersaturated species and $n_{i,sat}$ is the saturation number density for the ith species. τ_c is the condensation time constant which describes the time between collisions of the supersaturated species with aerosol particles, and which varies with height according to

$$\tau_c = \tau_0 e^{+\frac{z - z_0}{H_{haze}}}$$

where H_{haze} = 10 km is the scale height of the photochemical haze, (Krasnopolsky et al.,1992), and z_0 is the tropopause height. τ_0 is determined from the observed haze opacity and is about 10^5 seconds for Triton's atmosphere (Summers and Strobel, 1992). Table 5 contains a list of the column condensation rates for the supersaturated species photochemically produced in the model, and includes the column scavenging rates of atomic species by aerosols. Figure 6 plots the number density profiles for several of the species in Table 5. Scavenging of key radical species, in particular CH_2, has not been included in the model but could significantly modify the gas-phase production of higher hydrocarbons.

The recent detection of CO_2 ice in IR reflectance measurements (Cruikshank et al., 1991), poses an interesting challenge to photochemical modelers. Surprisingly, CO_2

TABLE 7.

RECOMMENDED LIST OF FUTURE CHEMICAL KINETICS EXPERIMENTS RELEVANT TO TRITON

#	Reaction	Comment
R191	$N_2^+ + C = C^+ + N_2$	Key ion reaction
R205	$CO^+ + C = C^+ + CO$	"
R214	$N_2H^+ + C = CH^+ + N_2$	May be important
R215	$HCO^+ + C = CH^+ + CO$	"
R218	$CN^+ + N = C^+ + N_2$	"
R66	$C + N_2 + M = CNN + M$	At low temp
R97	$CNN + N = CN + N_2$	At any temp
R94	$CN + N = C + N_2$	At low temp

ice covers as much as 10 % of the surface (Cruikshank et al., 1993). The model condensation rate of CO_2 (Table 5), assumed to be constant over the age of the solar system, corresponds to about one centimeter of ice. Because of the relatively large absorption coefficient of CO_2 ice, the IR measurements are sensitive to only the top one millimeter of ice (R. H. Brown, private communication). Hence, R136 may be able to account for the observed CO_2. Heterogeneous recombination of O and CO on the surface of aerosol particles could provide an additional CO_2 formation pathway. The column photolysis rate of CO in the standard model is about 1×10^6 $cm^{-2}sec^{-1}$. However, the rate of O scavenging (Table 5) is only about one half of the gas-phase CO_2 condensation rate (also in Table 5), suggesting that heterogeneous reactions may be an important but not dominant means of forming CO_2. It is also possible that the CO_2 was formed during Triton's capture as a result of tidal heating, although we do not consider this here. Irradiation of CO ice can convert CO ice to CO_2 ice (Anicich et al., 1988), especially during periods of very low atmospheric opacity. The nondetection of CO_2 ice on Pluto (Owen et al.,1992) may support the tidal heating hypothesis for Triton, or may simply be the result of a lower CO mixing ratio or a higher atmospheric opacity on Pluto.

Contrasting the condensation rates of CO_2 and C_2H_4 raises an apparent inconsistency (Cruikshank et al., 1993) between the predictions of the photochemical models and the results of the IR measurements. The condensation rate of C_2H_4 corresponds to roughly a 1 micron layer being deposited each Triton season. In about 10^6 years enough C_2H_4 ice will have accumulated to be detectable, and over the age of the

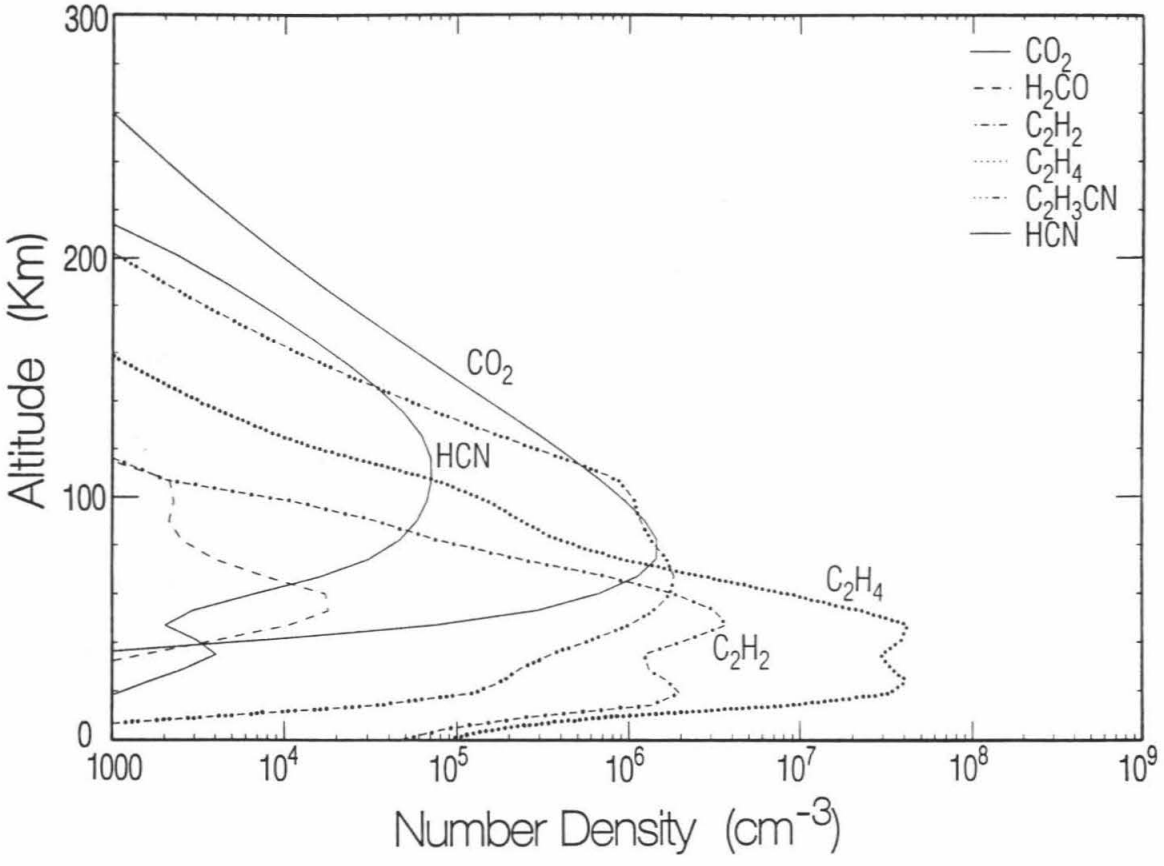

Fig. 6. Model number density profiles for several condensible species.

solar system meters of ice should accumulate (Strobel and Summers, 1990). Yet C_2H_4 is not detected in IR measurements. There are several possible reasons C_2H_4 is not seen. The C_2H_4 ice may be rapidly polymerized by UV radiation, especially if the surface HLyα opacity drops below unity due to orbital variations (Trafton, 1984). (The vertical HLyα opacity in the model is 7.5 with an uncertainty of about 50%.) It is also possible that C_2H_4 is modified by heterogeneous chemistry on aerosol particles. In particular, because the scavenging rate of H (Table 5) is comparable to the condensation rate of C_2H_4, hydrogenation of ethylene, yielding perhaps C_2H_5, C_2H_6 or other more complex hydrocarbons, could occur. On the other hand, it may simply be argued that the photochemical models are incorrect in predicting substantial C_2 hydrocarbon production and condensation. The fair agreement obtained between measurements and photochemical model predictions for Titan's atmosphere (Yung et al., 1984) may not be a good indicator for Triton given the significantly lower temperature of Triton's atmosphere.

4. The abundance of atomic nitrogen

The determination of the atomic nitrogen profile in Triton's upper atmosphere by Krasnopolsky et al. (1993) provides a key test of model predictions. Atomic nitrogen is produced by N_2 photodissociation in the reaction

$$N_2 + h\nu(\lambda<800\text{Å}) \rightarrow N + N \qquad \text{R15}$$

and also by photoelectron impact according to

$$N_2 + e_{ph} \rightarrow N + N(^2D) \qquad \text{R16}$$

R16 is assumed to proceed at 30% of the rate of R15. Precipitating electrons from the magnetosphere will contribute to N_2 dissociation but are not included in the standard model. The production of $N(^2D)$ occurs by R16 and also by the recombination of N_2^+, R194. $N(^2D)$ returns to the ground state by collisions with N_2,

$$N(^2D) + N_2 \rightarrow N + N_2 \qquad \text{R111}$$

and by spontaneous emission,

$$N(^2D) \rightarrow N + h\nu \qquad \text{R109}$$

N is also produced by ion-molecule reactions, most notably R185 and R194. The total column production rate of ground state N in the standard model is 1.1×10^8 $cm^{-2}sec^{-1}$, with peak production from 200 to 500 km as shown in Figure 3.

N produced in the ionosphere diffuses to lower altitudes where 3-body recombination occurs, resulting in a N peak at about 135 km. In the standard model the principal recombination pathway involves atomic C, CN and CNN. As discussed in a footnote in Lyons et al. (1992) and by Summers and Strobel (1992), C can form the compound CNN through the reaction

$$C + N_2 + M \rightarrow CNN + M \qquad \text{R63}$$

The rate coefficient of this reaction has been measured (Husain, 1971) at 300 K; we assume a T^{-2} temperature dependence in the standard model. CNN has been studied very little in the laboratory, but it is believed to have a triplet ground state (Milligan and

Jacox, 1966). There have been no laboratory studies of CNN in reaction with other species, so we must assume both the reactions that occur and their rates. By analogy with CN we assume that the reaction of CNN with CH_4 and H_2 occurs very slowly due to large activation energies, but that reaction with C_2H_2 and C_2H_4 proceeds rapidly to produce nitriles.(The reaction of CNN with these hydrocarbon species is assumed to proceed at the gas-kinetic rate of 1×10^{-10} $cm^{-3}sec^{-1}$, by analogy with CN.) CNN is also assumed to react with atomic species, of which reaction with N occurs as

$$CNN + N \rightarrow CN + N_2 \qquad \text{R97}$$

Again by analogy with CN, we assume that this reaction proceeds at the gas-kinetic rate. The corresponding reaction for CN is

$$CN + N \rightarrow C + N_2 \qquad \text{R94}$$

The three reactions, R63, R94 and R97, constitute a recombination cycle for nitrogen atoms in which C acts as a catalyst. In the standard model, this reaction sequence accounts for 96% of the recombination of N to N_2, while the reaction

$$NH + N \rightarrow N_2 + H \qquad \text{R212}$$

accounts for only a few percent. In Titan's upper atmosphere (Yung et al., 1984) NH is produced by $N(^2D)$ attacking CH_4 and H_2, and R212 is the principal mechanism for recombining N; it seems likely that this will be true for Pluto as well if the CH_4 abundance is substantial (Yelle and Lunine, 1989). In the Earth's atmosphere, $N(^2D)$ attacks O_2 to produce NO, and the latter reacts with N to yield N_2 and O.

Figure 7a shows number density profiles for the key species involved in the C-N cycle leading to recombination of nitrogen atoms in the standard model. The values determined by Krasnopolsky et al. (1993) are shown for altitudes from 200 to 500 km. The model values are low by about a factor of two. The model profile could be brought into agreement by adding magnetospheric electron impact; however, the uncertainties in the model result are likely to be larger than the discrepancy. The model N profile is affected by many parameters, including the rates of R94 and R97 and the temperature dependence of R63, the carbon atom profile, and, as just mentioned, a flux of precipitating electrons. Because of the uncertainty in these parameters, it is unlikely that the observed N densities will add sufficient information to allow the ratios of solar to magnetospheric energy input to be unambiguously determined. Figure 7b shows the same profiles as Figure 7a, except that the CNN formation reaction, R63, is turned off. In this case the model N profile is nearly in agreement with the measured values. However, as is apparent from Figure 5, the model N_2 density is higher by about a factor of two than the N_2 densities determined by Krasnopolsky et al. (1993), which would yield an even lower N abundance. Thus, the measured N profiles seem to require either smaller N loss rates than in the standard model, or higher production rates. The latter could be evidence for electron precipitation with an orbitally-averaged energy flux comparable to the solar EUV energy flux. Note that when CNN is not included in the model the principal N recombination pathway is direct recombination,

$$N + N + M \rightarrow N_2 + M \qquad \text{R106}$$

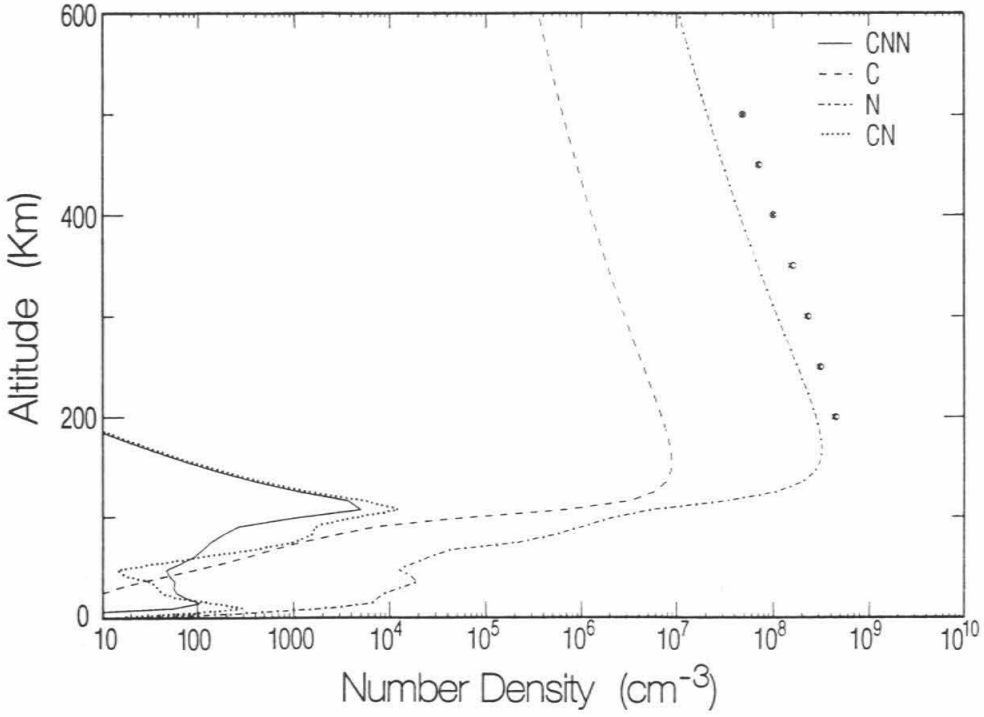

Fig. 7a. Model C, CN, CNN and N number densities, with Krasnolpolsky et al. (1993) N densities at several altitudes.

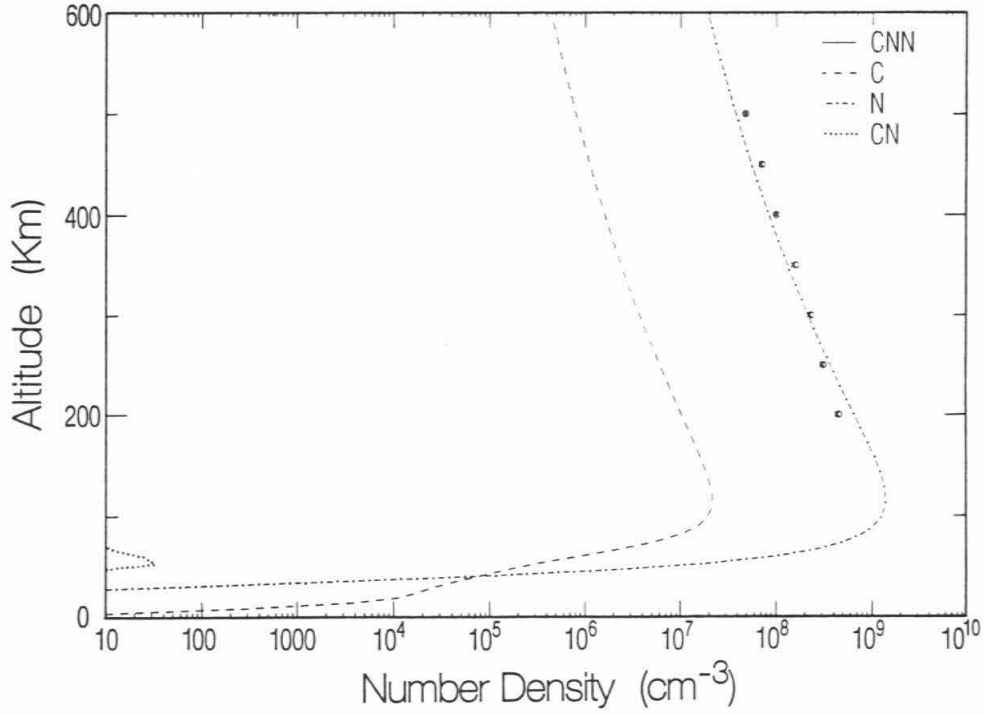

Fig. 7b. Same a Fig. 7a., but with no CNN formation turned off.

In the standard model production and loss of C is dominated by R94 and R63, respectively, with peak rates at about 100 km. The original sources of C are the parent species CO and CH_4 and their products. In the bottom of the atmosphere, direct photolysis of these species produces C by reactions R32 and

$$CH_4 + h\nu \rightarrow C(^1D) + 2H_2 \qquad \text{R11}$$

where $C(^1D)$ is rapidly quenched to the ground state by collisions with N_2. Photolysis of HCN, yielding CN, also produces C by R94. However, the largest sources of carbon atoms are the dissociative recombination of CO^+ in the ionosphere and the photolysis of CO in the lower atmosphere. CO^+ is formed by charge exchange between N^+ and CO (Delitsky et al.,1992; Summers and Strobel, 1992). Below about 150 km, the main loss of C is R63, but in the ionosphere the principal loss of C is by charge exchange with N_2^+, reaction R191. In the model of Lyons et al. (1992), C was produced primarily by R94 in the lower atmosphere and then diffused up to the ionosphere.

5. Ion chemistry

The inclusion of CO in Triton's atmosphere results in ionospheric chemistry that is both complex and interesting. The ion chemistry is driven by the formation of N_2^+ and N^+ by solar photons (R41 and R42) and by photoelectron impact (R43 and R44). The production rates for these two species in the standard model are shown in Figure 8a. As has been discussed by many authors (see section I), N_2^+ and N^+ have relatively short

chemical lifetimes in Triton's atmosphere. N_2^+ is lost by reaction with H_2 (R188), by charge exchange with N (R190) and by dissociative recombination (R194). N^+ is lost mainly by the reactions

$$N^+ + H_2 \rightarrow NH^+ + H \qquad \text{R179}$$

$$N^+ + CO \rightarrow CO^+ + N \qquad \text{R181}$$

The relatively large electron densities observed in Triton's ionosphere suggest an atomic ion as the principal species present. An N^+ ionosphere would require a magnetospheric electron flux ≈30 times the solar EUV flux to be ionizing Triton's atmosphere within about one hour of the time Voyager's measurements of Triton's ionosphere were made (Strobel et al., 1990b). Protons, formed by

$$CO^+ + H \rightarrow H^+ + CO \qquad \text{R207}$$

are lost via rapid charge exchange between H^+ and O,

$$H^+ + O \rightarrow O^+ + H \qquad \text{R157}$$

Because O^+ reacts with both N_2 and H_2 to form molecular ions, this pathway precludes the possibility of a significant quantity of either O^+ or H^+ in the ionosphere. Lyons et al. (1992) proposed that C^+, formed in the reaction

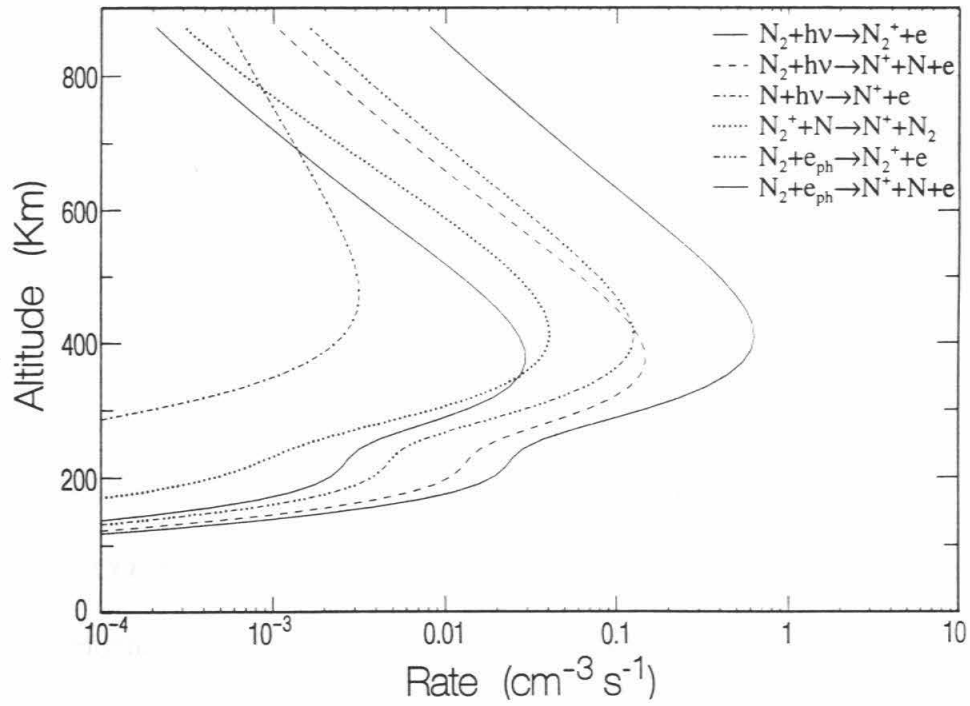

Fig. 8a. Model column production rates for N_2^+ and N^+.

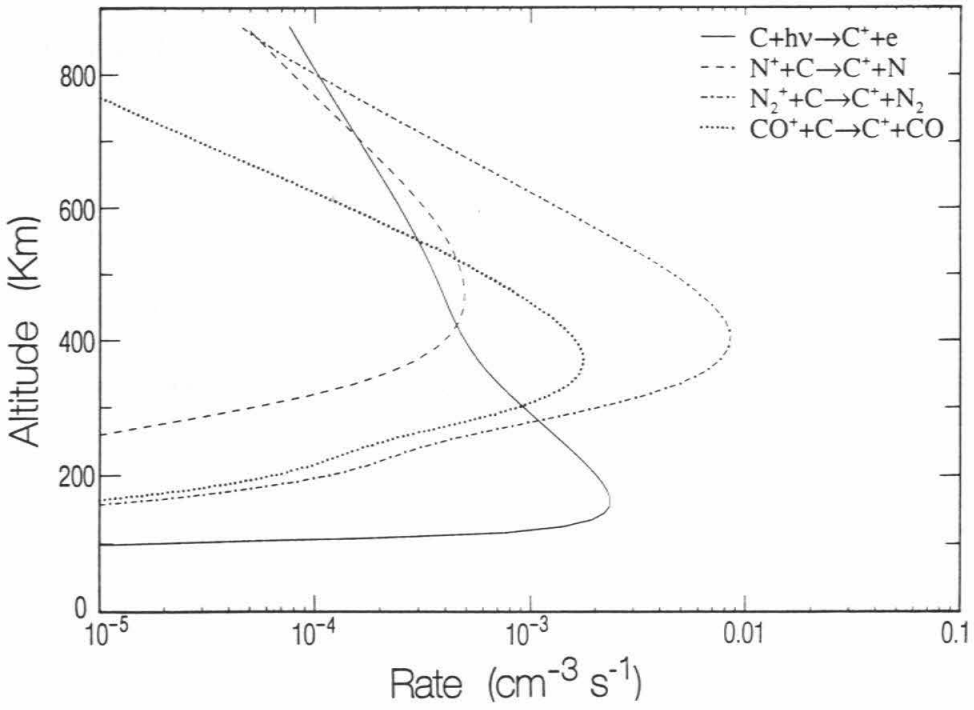

Fig. 8b. Model column production rates for C^+.

$$N_2^+ + C \rightarrow C^+ + N_2 \qquad \text{R191}$$

was a likely candidate for the dominant ion, since C^+ does not react with either H_2 or N_2. Neither reaction R191 nor any other ion reaction involving neutral carbon has been studied in the laboratory, so Lyons et al. had to assume a rate coefficient. For a rate coefficient of 1×10^{-9} cm^3sec^{-1}, which is rapid for a charge exchange reaction, the result was a solar-maintained ionosphere with C^+ as the dominant ion. However, their model did not include CO photochemistry. The inclusion of CO even at a mixing ratio as low as 10^{-4} greatly strengthens the case for a solar-maintained C^+ ionosphere. In the standard model presented here, we assume a rate for R191 of 1×10^{-10} $cm^{-3}sec^{-1}$, an order of magnitude lower than assumed in Lyons et al. (1992). In addition to R191, C^+ is formed by solar ionization of C, R46, and by the reaction

$$CO^+ + C \rightarrow C^+ + CO \qquad \text{R205}$$

Figure 8b shows the production rates for C^+ in the standard model. As mentioned above, the principal source of C in the ionosphere is dissociative recombination of CO^+, where the latter is produced by R181 (Delitsky et al., 1992; Summers and Strobel, 1992).

The density profiles of the ion species computed in the standard model are shown in Figure 9a. The agreement between the modelled and observed electron densities is fairly good, although the peak model density is about 20 km too low. The model electron density above 600 km suggests that nonthermal escape may be an important loss process for C^+. Carbon ions are lost primarily by reaction with HCN and CH_4 in reactions R161,

R158 and R159 in the lower ionosphere and by radiative recombination, R166, at and above the peak. We also assume that the species CNN^+ is formed by three-body reaction of C^+ with N_2. The ion product of R161 is C_2N^+, which we assume dissociatively recombines to produce C and CN. (Actually, it is not clear from the laboratory data whether CCN^+ or CNC^+ is formed in R161; the subsequent ion-molecule chemistry is different for these two species (Anicich,1992)). Reactions R158 and R159 yield $C_2H_2^+$ and $C_2H_3^+$. These ions react rapidly with N to produce mainly the species $CHCN^+$, which then dissociatively recombines to produce C and HCN. Thus, the principal loss pathways for C^+ actually recycle C back to the ionosphere. However, it must be emphasized that the species C_2N^+ and $CHCN^+$ have not been studied extensively, so there could be ionospheric pathways that are true sinks of C.

Figure 9b shows the ion profiles for the standard model except that the rates of R191 and R205 are 1×10^{-11} cm^{-3} sec^{-1}, an order of magnitude slower than the standard model. If the charge exchange reactions are this slow, then magnetospheric electron impact is necessary to provide the additional ionization. The required electron flux would be about twice the solar EUV flux. Figure 9c shows the ion profiles for the standard model with the CNN formation reaction, R63, turned off. This case would require a relatively small flux of precipitating electrons to form the bottom side ionosphere. Figure 9d shows the effect of nonthermal (i.e., faster than Jeans) escape of C^+ on the electron profile of the standard model. Electron impact would be needed to fill in the observed electron bulge at 500 km. It should be noted that several authors (Stevens et al., 1992; Krasnopolsky et al., 1993) have proposed that heating by electron impact is necessary to

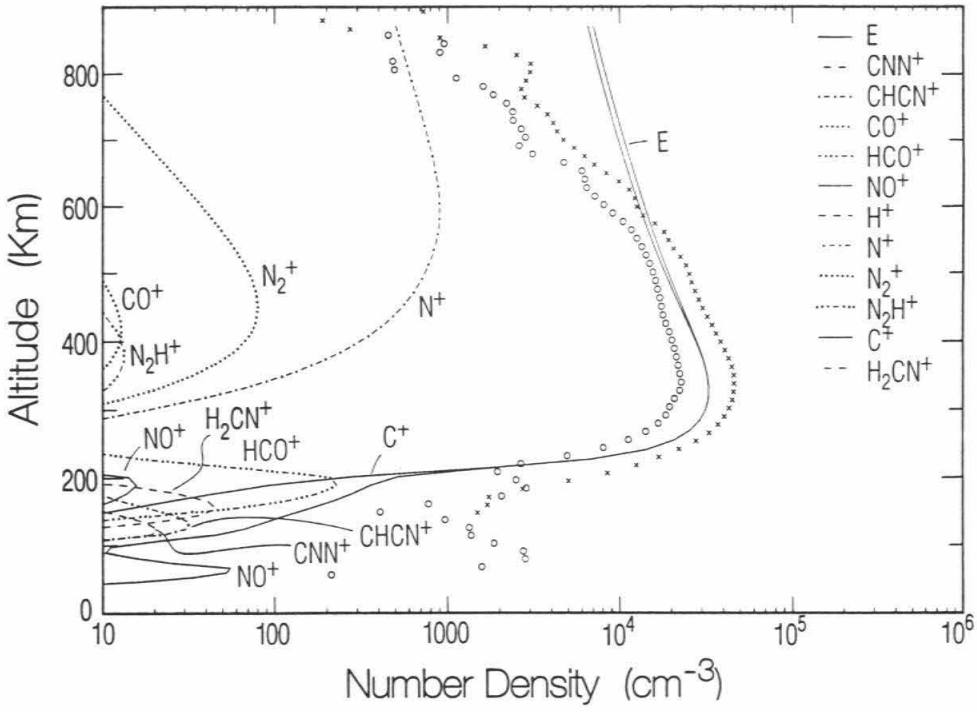

Fig. 9a. Model ion densities computed for the standard model, and observed electron densities.

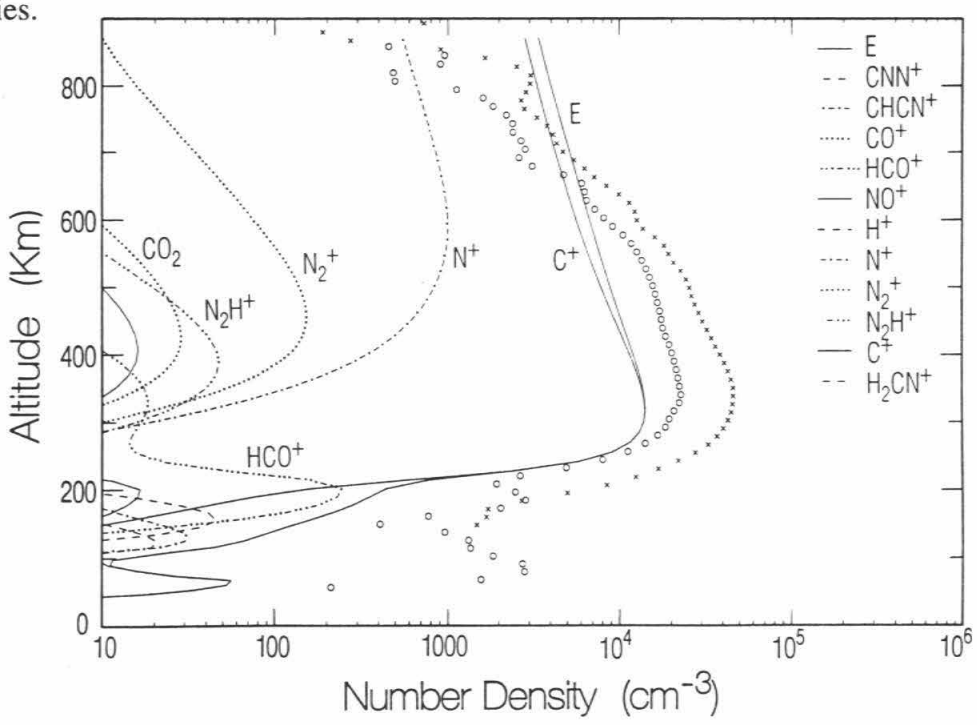

Fig. 9b. Same as Fig. 9a, but rate coefficients of R191 and R205 set to 1×10^{-11} cm^3 sec^{-1}.

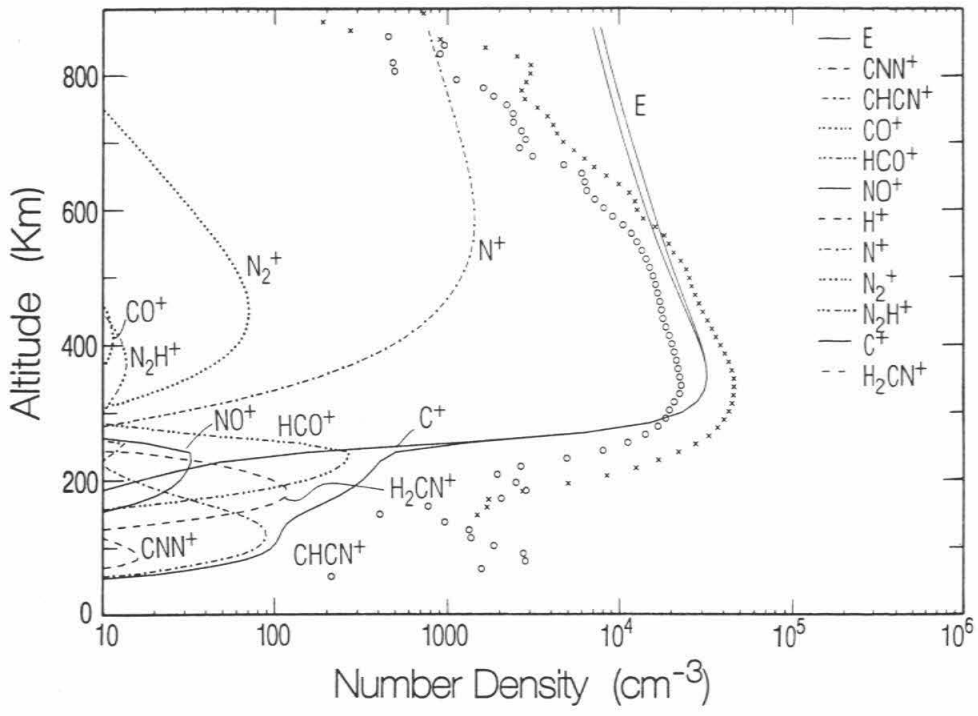

Fig. 9c. Same as Fig. 9a, but CNN formation (R63) turned off.

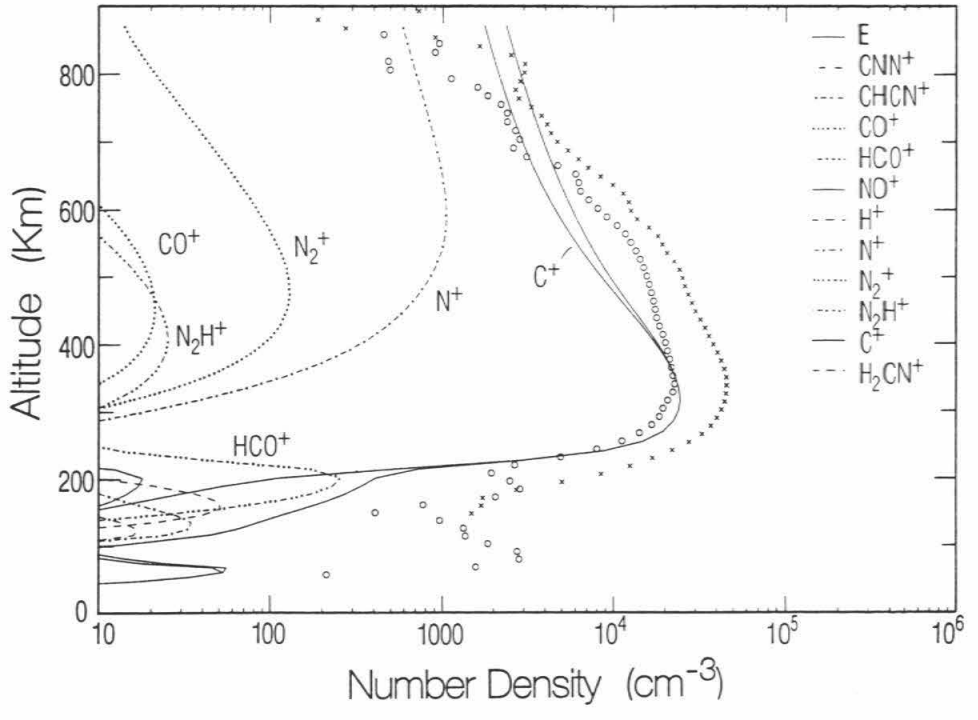

Fig. 9d. Same as Fig. 9a, but with nonthermal escape of C^+ at a velocity of 100 cm sec^{-1}.

explain Triton's thermospheric temperature. We do not address this issue here, except to say that heating by electron impact would be consistent with low rates for R191 and R205. Table 6 gives the thermal escape fluxes of various species for the standard model, including the (imposed) nonthermal escape flux of C^+ corresponding to Figure 9d.

Comparing our results with those of Summers and Strobel (1992) points out the key difference between the various photochemical models. Summers and Strobel obtain a C^+ ionosphere for a CO mixing ratio of 3×10^{-4}, but only when an instantaneous (i.e., not orbitally averaged) electron impact energy flux of about five times the solar EUV flux is included. They also obtain a large H^+ abundance, primarily because they have neglected R157, but also because their rate constant for charge exchange between N_2^+ is too high. It is not entirely clear why the results of the two models differ so greatly with regard to C^+ densities, but it would appear to be in part due to the column abundance of neutral carbon. In the present model C densities are higher, with the result that photoionization of C produces C^+ at a rate capable of consuming CH_4 in the bottomside ionosphere.

Other shorter-lived molecular ions that appear in the lower ionosphere in the standard model include HCO^+, H_2CN^+, and NO^+. HCO^+ is formed in the reactions

$$N_2H^+ + CO \rightarrow HCO^+ + N_2 \qquad \text{R196}$$

and (Krasnopolsky et al., 1993; Summers and Strobel, 1992)

$$CO^+ + H_2 \rightarrow HCO^+ + H \qquad \text{R206}$$

and is lost by dissociative recombination. (In R206 the isomer HOC^+ is also produced, but reacts rapidly with N_2 to produce N_2H^+.) Because the proton affinity of HCN is larger than that of N_2 and CO (Huntress, 1977), $H_2CN^+$is formed via the reactions

$$HCO^+ + HCN \rightarrow H_2CN^+ + CO \qquad \text{R210}$$

$$N_2H^+ + HCN \rightarrow H_2CN^+ + N_2 \qquad \text{R213}$$

although the latter is slow in the standard model. The ultimate fate of H_2CN^+ is dissociative recombination yielding HCN and H. NO^+ is formed by reactions R182, R192, and R201, and is also lost by dissociative recombination.

Comparing the proton affinities (Huntress,1977) of C with CO and N_2 suggests two other ion-molecule reactions of potential importance in Triton's ionosphere:

$$N_2H^+ + C \rightarrow CH^+ + N_2 \qquad \text{R214}$$

and

$$HCO^+ + C \rightarrow CH^+ + CO \qquad \text{R215}$$

These reactions have not been measured for the same reason that R191 and R205 have not been measured: the difficulty of generating C efficiently in rate coefficient measurement systems (V. Anicich, private communication). In fact, to the best of our knowledge, the rate coefficient of an ion-molecule reaction in which atomic carbon is the neutral reactant has never been measured for any ion! Given the potential importance of

C in Triton's atmosphere, this represents a significant limitation to our abiltity to determine the governing chemical processes. CH^+, however, has been well studied (Anicich and Huntress, 1986; Anicich, 1992), so we can determine its fate in Triton's ionosphere. CH^+ reacts rapidly with N and H_2 according to

$$CH^+ + N \rightarrow CN^+ + H \qquad \text{R216}$$

$$CH^+ + H_2 \rightarrow CH_2^+ + H \qquad \text{R217}$$

Similarly, CH_2^+ reacts with N to yield CN^+ and HCN^+ and with H_2 to yield CH_3^+; CH_3^+ is lost via reaction with N. The fate of CN^+ is less certain because the reaction with N has never been studied. We propose the reaction

$$CN^+ + N \rightarrow C^+ + N_2 \qquad \text{R218}$$

This is the most exothermic branch, but others are possible: charge exchange from $CN^+$to N may occur, since the ionization potentials of CN and N are similar, and the formation of N_2^+ and C is exothermic by about 0.7 eV. CN^+ will also react with H_2 to form HCN^+ and HNC^+. The above sequence of reactions, starting with R214 and R215, has not been included in the model presented here, but shows that if R214 and R215 do occur then C is likely to be recycled back to either C or C^+.

6. Summary and conclusions

We have developed a one-dimensional photochemical model of Triton's atmosphere and ionosphere. The model has 55 neutral and ion species and 211 reactions.

We define a "standard" model as having N_2 and CH_4 at saturation pressure at the ground, and CO subsaturated with a mixing ratio of 10^{-4} at the ground as suggested by Cruikshank et al. (1993). In the standard model only solar EUV radiation is included (i.e., there is no magnetospheric electron impact). The rate coefficients of R191 and R205 are assumed to be $1\times10^{-10}cm^3sec^{-1}$.

The condensation rates of supersaturated hydrocarbons and nitriles have been computed assuming heterogeneous nucleation on aerosol haze particles (Strobel and Summers,1991). The IR observations of Cruikshank et al. (1991) pose two questions regarding condensation. First, the detection of CO_2 ice on Triton's surface raises the question of whether the CO_2 is deposited as a result of photochemical processing of gas-phase CO. We find that for present Triton conditions, gas-phase chemical reactions (R136) are able to produce detectable amounts of CO_2, assuming a constant rate over the age of the solar system (which is likely to be an incorrect assumption). Heterogeneous recombination of O and CO on aerosol particle surfaces may also produce detectable quantities of CO_2. We note also that conversion of CO ice to CO_2 ice may occur when the former is exposed to Lyman alpha radiation (Anicich et al., 1989). We have not considered the photochemical implications of variations in surface pressure, as predicted to occur as Triton's obliquity changes (Trafton, 1984). Recent IR measurements of Pluto (Owen et al,1992) do not indicate the presence of CO_2 ice. Why the same photochemical processes would not also produce detectable quantities of CO_2 ice on Pluto is not obvious but may simply be the result of a lower CO mixing ratio or a lower CO photolysis rate higher (due to a higher optical depth) than on Triton. We have not considered the

possibility that Triton's CO_2 is a result of chemical processing that occurred during capture by Neptune. The second question posed by the IR data concerns the lack of detection of C_2H_4 ice on Triton, even though photochemical models predict that detectable quantities of ethylene should accumulate in about 10^6 years. We propose that C_2H_4 ice is either easily polymerized to more complex hydrocarbons by UV radiation, is difficult to distinguish from CH_4 ice, or is modified by heterogeneous reactions on aerosol particles. Dissly (1995) demonstrated that C_2H_4 ice is readily dissociated to C_2H_2 ice at wavelengths < 1849 Å at a rate sufficiently fast to prevent the accumulation of a detectable layer of C_2H_4 ice on Triton. The color of Triton's surface (Thompson and Sagan, 1991) may be a result of the polymerization of ethylene or acetylene. Alternatively, the photochemical models may simply be incorrect in their predictions for some species, especially at such low temperatures.

The determination of N densities in the upper atmosphere of Triton (Krasnopolsky et al., 1993) places an important constraint on the models. We find that N produced in the ionosphere by dissociation and ion recombination was lost primarily by 3-body recombination catalyzed by carbon atoms. The species CNN is formed by reaction R63, and we propose that CN is produced by reaction of CNN with N (R97). The nitrogen atom recombination step is then $CN + N \rightarrow C + N_2$. The reaction $NH + N \rightarrow H + N_2$ accounts for only a few percent of the recombination of nitrogen atoms. This results in model N densities about a factor of two lower than the measured values, suggesting that additional production of N may be occurring, possibly as a result of electron impact. Turning off the reaction forming CNN (R63) raises the nitrogen atom densities by about

a factor of two, in better agreement with the measured N profile. The C-N cycle mentioned above is also important in determining the C density profile.

In the ionosphere, CO charge exchanges with N^+ to form CO^+ (Delitsky et al., 1992; Summers and Strobel, 1992), and the latter dissociatively recombines becoming a source of O and C. In the standard model C^+, produced by charge exchange with N_2^+ and CO^+, is the dominant ion. Thus the addition of CO reinforces the suggestion (Lyons et al., 1992) of a solar-controlled atmosphere with C^+ as the dominant ion. We have not explored the sensitivity of the model to the mixing ratio of CO, but a larger abundance of CO will result in faster rates of C production in the ionosphere. A mixing ratio of 10^{-4} is probably a reasonable lower limit to the CO abundance given an ice mass fraction of about 0.1% (Cruikshank et al., 1993). Depending on the rates of R191 and R205 and the ultimate fate of CNN, some magnetospheric electron precipitation may be necessary, but the precipitating electron energy flux is far less than earlier models were predicting. The importance of H^+ in our model is minimal due to rapid charge exchange between H^+ and O. Ions formed in the lower ionosphere include HCO^+, H_2CN^+, $CHCN^+$ and NO^+; the ultimate fate of these ions is apparently dissociative recombination. Comparing the model and observed topside electron densities suggests that nonthermal escape of C^+ may occur. Hence, C^+ may have been detected in Neptunes's magnetosphere (Richardson et al, 1990).

We have identified several species and reactions, listed in Table 7, of importance in Triton's atmosphere for which there is either no or very little laboratory data available. Most notably, ion-neutral reactions in which carbon atoms are the neutral reactant have apparantly never been studied in the laboratory for the purpose of determining a rate

coefficient. This significantly limits our ability to accurately model chemical processes in Triton's ionosphere. In particular, the ion reactions R191 and R205 are important on Triton. Depending on the rates of R191 and R205, reactions R214, R215 and R218 may also be important. With regard to neutral chemistry, the species CNN is most in need of laboratory study. The reaction R97 and the temperature dependence of R63 are especially relevant. Until some of these reactions have been studied in the laboratory, it will not be possible to definitively state whether Triton's upper atmosphere is solar or magnetosphere controlled.

Acknowledgements

The authors thank V. Krasnopolsky and M. Summers for preprints of related papers. Discussions with V. Anicich and R. H. Brown are also gratefully acknowledged. This work was supported by the Neptune Data Analysis Program, grant number NAGW-2362.

References

Anicich, V. G. in press. A survey of bimolecular ion-molecule reactions for use in modeling the chemistry of planetary atmospheres, cometary comae, and interstellar clouds: 1992 supplement, *Ap. J. Supplement Series.*

Anicich, V. G. and W. T. Huntress 1986. A survey of bimolecular ion-molecule reactions for use in modeling the chemistry of planetary atmospheres, cometary comae, and interstellar clouds, *Ap. J. Supplement Series* **62**, 553-672.

Anicich, V. G., T. Arakelian and M. S. Hanner 1990. Photolysis of cometary materials: CO and CO_2 ices, *B. A. A. S.* **22**, 1099.

Atkinson, R., D. L. Baulch, R. A. Cox, R. F. Hampson,Jr., J. A. Kerr, J. Troe 1989. Evaluated kinetic and photochemical data for atmospheric chemistry: Supplement III, *J. Phys. Chem. Ref. Data* **18**, 881-1097.

Bauer, W., K. H. Becker, R. Menser 1985. Laser-induced flourescence studies on C_2O and CH radicals, *Ber. Bunsenges. Phys. Chem.* **89**, 340-341.

Baulch, D. L., J. Duxbury, S. J. Grant, D. C. Montague 1981. Evaluated kinetic data for high temperature reactions. Volume 4. Homogeneous gas phase reactions of halogen- and cyanide-containing species, *J. Phys. Chem. Ref. Data* **10**, Suppl. 1, 1-1.

Becker, K. H., B. Engelhardt, P. Wiesen 1989. Rate constants for CH(X2Π) reactions at low total pressures, *Chem. Phys. Lett.* **154**, 342-348.

Becker, K. H., K. J. Brockmann, P. Wiesen 1988. Spectroscopic identification of $C(^3P)$ atoms in halogenomethane + H flame systems and measurements of $C(^3P)$ reaction rate constants by two-photon laser-induced flourescence, *J. Chem. Soc. Faraday Trans. 2,* **84,** 455.

Black, G., T. G. Slanger, G. A. St. John, R. A. Young 1969. Vacuum-ultraviolet photolysis of N_2O. IV. Deactivation of $N(^2D)$, *J. Chem. Phys.* **51**, 116-121.

Braun, W., A. M. Bass, D. D. Davis, J. D. Simmons 1969. Flash photolysis of carbon suboxide: absolute rate constants for reactions of $C(^3P)$ and $C(^1D)$ with H, N, CO, NO, O_2 and CH_4, *Proc. Roy. Soc.* **A312**, 417-434.

Broadfoot, A. L., S. K. Atreya, J. L. Bertaux, J. E. Blamont, A. J. Dessler, T. M. Donahue, W. T. Forrester, D. T. Hall, F. Herbert, J. B. Holberg, D. M. Hunten, V. A. Krasnopolsky, S. Linick, J. I. Lunine, J. C. McConnell, H. W. Moos, B. R. Sandel, N. M. Schneider, D. E. Shemansky, G. R. Smith, D. F. Strobel, R. V. Yelle 1989. Ultraviolet spectrometer observations of Neptune and Triton, *Science* **246**, 1459-1466.

Brown, R. L. 1973. A measurement of the rate of the reaction N+H+M→NH+M, *Int. J. Chem. Kinet.* **5**, 663-668.

Bruston, P., H. Poncet, F. Raulin, C. Cossart-Magos, R. Courtin 1989. UV spectroscopy of Titan's atmosphere, planetary organic chemistry, and prebiological synthesis. 1. Absorption spectra of gaseous propynenitrile and 2-butynenitrile in the 185 to 250 nm region, *Icarus* **78,** 38-53.

Campbell, I. M. and C. N. Gray 1973. Rate constants for $O(^3P)$ recombination and association with $N(^4S)$, *Chem. Phys. Lett.* **18**, 607-609.

Cantu, A. M., M. Mazzoni, M. Pettini, G. P. Tozzi 1981. Photoionization spectrum of the ^3P ground state of neutral carbon, *Phys. Rev. A* **23**, 1223-1228.

Cohen, N. and K. R. Westberg 1991. Chemical kinetic data sheets for high-temperature reactions. Part II, *J. Phys. Chem. Ref. Data* **20**, 1211-1311.

Connors, R. E., J. L. Roebber, K. Weiss 1974. Vacuum ultraviolet spectroscopy of cyanogen and cyanoacetylenes, *J. Chem. Phys.* **60**, 5011-5024.

Conrath, B., F. M. Flaser, R. Hanel, V. Kunde, W. Maguire, J. Pearl, J. Pirraglia, R. Samuelson, P. Gierasch, A. Weir, B. Bezard, D. Gautier, D. Cruikshank, L. Horn, R. Springer, W. Shaffer 1989. Infrared observations of the Neptunian system, *Science* **246**, 1454-1459.

Cruikshank, D. P., T. C. Owen, T. R. Geballe, B. Schmitt, C. de Bergh, J-P. Maillard, B. L. Lutz, R. H. Brown 1991. Tentative detection of CO and CO_2 ices on Triton, *B. A. A. S.* **23,** 1208.

Cruikshank, D. P., T. L. Roush, T. C. Owen, T. R. Geballe, C. de Bergh, B. Schmitt, R. H. Brown, M. J. Bartholomew 1993. Ices on the surface of Triton, submitted to *Science.*

Delitsky, M. L., R. P. Turco, and M. Z. Jacobson 1990. Nitrogen ion clusters in Triton's atmosphere, *Geophys. Res. Lett.* **17**, 1725-1728.

Delitsky, M. L., M. Z. Jacobson, and R. P. Turco 1992. The effect of oxidized species on Triton's ion chemistry, *Neptune/Triton Conference abstract volume*, p. 20.

DeMore, W. B., S. P. Sander, D. M. Golden, R. F. Hampson, M. J. Kurylo, C. J. Howard,A. R. Ravishankara, C. E. Kolb, M. J. Molina 1992. Chemical kinetics and photochemical data for use in stratospheric modeling 1992, Evaluation Number 10, *JPL publication* **92-20.**

Dissly, R. W. 1995. Laboratory Studies of Astrophysical Ices, Thesis, California Institute of Technology.

Fisher, W. H., T. Carrington, C. M. Sadowski 1985. The reactions of $C(2^1D_2)$ with H_2, D_2 and HD: product rotational energies, isotope effects and the CD/CH branching ratio, *Chem. Phys.* **97**, 433-448.

Hayaishi, T., S. Iwata, M. Sasanuma, E. Ishiguro, Y. Morioka, Y. Iida, M. Nakamura 1982. Photoionization mass spectrometric study of acetylene in the VUV region, *J. Phys. B. At. Mol. Phys.* **15,** 79-92.

Heinemann, P., R. Hofmann-Sievert, K. Hoyermann 1988. Direct study of the reactions of vinyl radicals with hydrogen and oxygen atoms, *Proc. Symp. (Int.) Combust.* **21**, 865.

Herbert, F. and B. R. Sandel 1991. CH_4 and haze in Triton's lower atmosphere, *J. Geophys. Res.* **96**, 19241-19252.

Huber, K. P. and G. Herzberg 1979. *Molecular Spectra and Molecular Structure IV. Constants of Diatomic Molecules,* Van Nostrand (New York).

Huntress, W. T. 1977. Laboratory studies of bimolecular reactions of positive ions in interstellar clouds , in comets, and in planetary atmospheres of reducing composition, *Ap. J. Suppl. Series* **33**, 495-514.

Husain, D. and L. J. Kirsch 1971. Reactions of atomic carbon $C(2^3P_j)$ by kinetic absorption spectroscopy in the vacuum ultraviolet, *Trans. Faraday Soc.* **67**, 2025-2035.

Ip, W. -H. 1990. On the ionosphere of Triton: An evaluation of the magnetospheric electron precipitation and photoionization effects, *Geophys. Res. Lett.* **17**, 1713-1716.

Kirby, K., E. R. Constantinides, S. Babeu, M. Oppenheimer, G. A. Victor 1979. Photoionization and photoabsorption cross sections of He, O, N_2 and O_2 for aeronomic calculations, *Atomic Data and Nuclear Data Table* **23**, 63-81.

Krasnopolsky, V. A., B. R. Sandel, F. Herbert, and R. J. Vervack, Jr. 1993. Temperature, N_2, and N density profiles of Triton's atmosphere: Observations and model, *J. Geophys. Res.* **98,** 3065-3078.

Krasnopolsky, V. A., B. R. Sandel, and F. Herbert 1992. Properties of haze in the atmosphere of Triton, *Neptune/ Triton conference abstract volume*, p. 39.

Laufer, A. H., E. P. Gardner, T. L. Kwok, Y. L. Yung 1983. Computations and estimates of rate coefficients for hydrocarbon reactions of interest to the atmospheres of the outer solar system, *Icarus* **56**, 560-567.

Le Dourneuf, M., V. Ky Lan, C. J. Zeippen 1979. The photoionisation of the $^4S^0$ ground state of atomic nitrogen, *J. Phys. B. At. Mol. Phys.* **12**, 2449-2463.

Lee, L. C. and J. A. Guest 1981. Quantitative absorption and flourescence studies of CO from 1060 to 1550 Å, *J. Phys. B.* **14**, 3415-3421.

Letzelter, C., M. Eidelsberg, F. Rostas, J. Breton, B. Thieblemont 1987. Photoabsorption and photodissociation cross sections of CO between 88.5 and 115 nm, *Chem. Phys.* **114**, 273-288.

Lichtin, D. A. and M. C. Lin 1986. Temperature dependence of the CN radical reactions with C_2H_2 and C_2H_4, *Chem. Phys.* **104**, 325-330.

Lichtin, D. A., M. R. Berman, M. C. Lin 1984. NH($A^3\Pi \rightarrow X^3\Sigma^-$) chemiluminescence from the CH($X^2\Pi$)+NO reaction, *Chem. Phys. Lett.* **108**, 18-24.

Lyons, J. R., Y. L. Yung, and M. Allen 1992. Solar control of the upper atmosphere of Triton, *Science* **256**, 204-206.

Macpherson, M. T., M. J. Pilling, M. J. C. Smith 1985. Determination of the absorption cross section for CH_3 at 216.36 nm and the absolute rate constant for methyl radical recombination over the temperature range 296-577 K, *J. Chem. Phys.* **89**, 2268-2274.

Majeed, T., J. C. McConnell, D. F. Strobel, and M. E. Summers 1990. The ionosphere of Triton, *Geophys. Res. Lett.* **17**, 1721-1724.

Marston, G., F. L. Nesbitt, D. F. Nava, W. A. Payne, L. J. Stief 1989. Temperature dependence of the reaction of nitrogen atoms with methyl radicals, *J. Phys. Chem.* **93**, 5769-5774.

Marston, G., F. L. Nesbitt, L. J. Stief 1989. Branching ratios in the N+CH_3 reaction: formation of the methylene amidogen (H_2CN) radical, *J. Chem. Phys.* **91**, 3483-3491.

Mentall, J. E., E. P. Gentieu, M. Krauss, D. Neumann 1971. Photoionization and absorption spectrum of formaldehyde in the vacuum ultraviolet, *J. Chem. Phys.* **55**, 5471-5479.

Messing, I., S. V. Filseth, C. M. Sadowski, T. Carrington 1981. Absolute rate constants for the reactions of CH with O and N atoms, *J. Chem. Phys.* **74**, 3874-3881.

Milligan, D. E. and M. E. Jacox 1966. Matrix-isolation study of the infrared and ultraviolet spectra of the free radical CNN, *J. Chem. Phys.* **44**, 2850-2856.

Mordaunt, D. H., I. R. Lambert, G. P. Morley, M. N. R. Ashfold, R. N. Dixon, C. M. Western, L. Schnieder, K. H. Welge 1993. Primary product channels in the photodissociation of methane at 121.6 nm, *J. Chem. Phys.* **98**, 2054-2065.

Morioka, Y., S. Aoyama, Y. Kageyama, T. Hayaishi, I. H. Suzuki, G. Isoyama, S. Asaoka, E. Ishiguro, M. Nakamura 1984. Dissociative photoionization of N_2 from threshold to 29 eV, *J. Phys. B. At. Mol. Phys.* **18**, 2795-2802.

Mount, G. H. and G. J. Rottman 1983. The solar absolute spectral irradiance 1150 - 3173 Å: 17 May 1982, *J. Geophys. Res.* **88**, 5403-5410.

Musuoka, T. and J. A. R. Samson 1981. Dissociative and double photoionization of CO from threshold to 90 Å, *J. Chem. Phys.* **74**, 1093-1097.

Nuth, J. A. and S. Glicker 1982. The vacuum ultraviolet spectra of HCN, C_2N_2 and CH_3CN, *J. Quant. Spect. Rad. Trans.* **28**, 223-231.

Okabe, H. and V. H. Dibeler 1973. Photon impact studies of C_2HCN and CH_3CN in the vacuum ultraviolet; heats of formation of C_2H and CH_3CN, *J. Chem. Phys.* **59**, 2430-2434.

Okabe, H. 1978. *Photochemistry of Small Molecules*, Wiley-Interscience (New York).

Owen, T., T. Geballe, C. de Bergh, L. Young, J. Elliot, D. Cruikshank, T. Roush, B. Schmitt, R. H. Brown, J. Green 1992. Detection of nitrogen and carbon monoxide on the surface of Pluto, *B. A. A. S.* **24**, 961.

Prasad, S. S. and A. Tan 1974. The Jovian ionosphere, *Geophys. Res. Lett.* **1**, 337-340.

Rebbert, R. E. and P. Ausloos 1972. Photolysis of methane: quantum yield of $C(^1D)$ and CH, *J. Photochem.* **1**, 171-176.

Richardson, J. D. , A. Eviatar and M. L. Delitsky 1990. The Triton torus revisited, *Geophys. Res. Lett.* **17**, 1673-1676 .

Samson, J. A. R. and G. Haddad 1988. in Absolute Cross-sections for molecular photoabsorption, partial photoionization, and ionic photofragmentation processes, edited by J. W. Gallagher, C. E. Brion, J. A. R. Samson, P. W. Langhoff, *J. Phys. Chem. Ref. Data* **17**, 48.

Seidler, V., F. Temps, H. G. Wagner, M. Wolf 1989. Kinetics of the reactions of $CH_2(X^3B_1)$ radicals with NO and NO_2, *J. Phys. Chem.* **93**, 1070-1073.

Slagle, I. R., D. Gutman, J. W. Davies, M. J. Pilling 1988. Study of the recombination reaction $CH_3+CH_3 \rightarrow C_2H_6$. 1. Experiment, *J. Phys. Chem* **92**, 2455-2462.

Slanger, T. G. and G. Black 1978. CO_2 photolysis revisited, *J. Chem. Phys.* **68**, 1844-1849.

Stansberry, J. A., R. V. Yelle, J. I. Lunine, and A. S. McEwan 1992. Triton's surface-atmosphere energy balance, *Icarus* **99**, 242-260.

Stark, G., K. Yoshino, P. L. Smith, K. Ito, W. H. Parkinson 1991. High resolution absorption cross sections of carbon monoxide bands at 295 K between 91.7 and 100.4 nanometers, *Astrophys. J.* **369**, 574-580.

Stevens, M. H., D. F. Strobel, M. E. Summers, and R. V. Yelle 1992. On the thermal structure of Triton's thermosphere, *Geophys. Res. Lett.* **19**, 669-672.

Strobel, D. F., M. E. Summers, F. Herbert, and B. R. Sandel 1990a., The photochemistry of methane in the atmosphere of Triton, *Geophys. Res. Lett.* **17**, 1729-1732.

Strobel, D. F., A. F. Cheng, M. E. Summers, and D. J. Strickland 1990b. Magnetospheric interaction with Triton's ionosphere, *ibid.*, 1661-1664.

Summers, M. E. and D. F. Strobel 1992. Triton's ionosphere: A case for CO, submitted to *Icarus.*

Thompson, B. A., P. Harteck and R. R. Reeves, Jr. 1963. Ultraviolet absorption coefficients of CO_2, CO, O_2, H_2O, N_2O, NH_3, NO, SO_2 and CH_4 between 1850 and 4000 Å, *J. Geophys. Res.* **68**, 6431-6436.

Thompson, W. R. and C. Sagan 1992. Color and Chemistry on Triton, *Science* **250**, 415-418.

Trafton, L. M. 1984. Seasonal variations in Triton's atmospheric mass and composition, *Uranus and Neptune*, NASA conference publication 2330, J. Bergstralh (ed.), 481-493.

Tsang, W. and R. F. Hampson 1986. Chemical kinetic database for combustion chemistry. Part I. Methane and related compounds, *J. Phys. Chem. Ref. Data* **15**, 1087-1279.

Tyler, G. L., D. N. Sweetnam, J. D. Anderson, S. E. Borutzki, J. K. Campbell, V. R. Eshleman, D. L. Gresh, E. M. Gurrola, D. P. Hinson, N. Kawashima, E. R. Kursinskim G. S. Levy, G. F. Lindal, J. R. Lyons, E. A. Marouf, P. A. Rosen, R. A. Simpson, G. E. Wood 1989. Voyager radio science observations of Neptune and Triton, *Science* **246**, 1466-1473.

van Dishoeck, E. F. 1987. Photodissociation processes in the CH molecule, *J. Chem. Phys.* **86,** 196-214.

Veyret, B. and R. Lesclaux 1981. Absolute rate constants for the reactions of HCO with O_2 and NO from 298 to 503 K, *J. Phys. Chem.* **85**, 1918-1922.

Warnatz, J. 1984. Rate coefficients in the C/H/O system, *Combustion Chemistry* (ed. W. C. Gardiner, Jr.), Springer-Verlag, New York, p.197.

West, G. A. 1985. Cyanide radical molecular electronic and vibrational chemical lasers; hydrogen cyanide polyatomic chemical lasers, thesis, University of Wisconsin-Madison.

Whyte, A. R. and L. F. Phillips 1983. Rate of reaction of N with CN(v=0,1), *Chem. Phys. Lett.* **98**, 590-593.

Woods, T. N. and G. J. Rottman 1990. Solar EUV irradiance from a sounding rocket experiment on November 10, 1988, *J. Geophys. Res.* **95**, 6227-6236.

Wright, G. R., M. J. Van der Wiel, C. E. Brion 1976. Dipole excitaton and fragmentation of N_2 and CO in the 10 - 60 eV region, *J. Phys. B.* **9**, 675-689.

Wu, C. Y. R., L. C. Lee, D. L. Judge 1984. Flourescence from photofragments as an aid in identifying new molecular states: the N_2 case, *J. Chem. Phys.* **80**, 4682-4685.

Yamasaki, K., S. Okada, M. Koshi, H. Matsui 1991. Selective product channels in the reactions of $NH(a^1\Delta)$ and $NH(X^3\Sigma\text{-})$ with NO, *J. Chem. Phys.* **95**, 5087-5096.

Yamashita, T. 1979. Rate of recombination of nitrogen atoms, *J. Chem. Phys.* **70**, 4248-4253.

Yelle, R. V. and J. I. Lunine 1989. Evidence for a molecule heavier than methane in the atmosphere of Pluto, *Nature* **339**, 288-290.

Yelle, R. V., J. I. Lunine, and D. M. Hunten 1991. Energy balance and plume dynamics in Triton's lower atmosphere, *Icarus* **89**, 347-358.

Yung, Y. L. and J. R. Lyons 1990. Triton: Topside ionosphere and nitrogen escape, *Geophys. Res. Lett.* **17**, 1717-1720.

Yung, Y. L., M. Allen, and J. P. Pinto 1984. Photochemistry of the atmosphere of Titan: Comparison between model and observations, *Ap. J. Suppl. Series* **55**, 465-506.

PAPER II

Metal ions in the atmosphere of Neptune

James R. Lyons

Division of Geological and Planetary Sciences

California Institute of Technology

Pasadena, California 91125

published in Science

April , 1995

Abstract

Microwave propagation experiments performed with Voyager 2 at Neptune revealed sharp layers of electrons with densities ~ 10^4 cm^{-3} in Neptune's lower ionosphere. These layers are reminiscent of terrestrial sporadic-E layers, and, when taken together with data from the other giant planets, confirm the importance of the magnetic field in layer formation. A photochemical model which incorporates species produced by meteoroid ablation predicts that Mg^+ is the most likely metal comprising the layers, although laboratory data on the kinetics of metallic atoms and ions in a reducing environment are lacking. The metal chemistry discussed here is directly relevant to the abundant metals observed at the impact site of the G fragment of Comet Shoemaker Levy 9 on Jupiter.

1. Introduction

With the completion of the planetary component of the Voyager mission (Stone and Miner 1989), we now have spacecraft data for nine ionospheres in the solar system. These data, taken together with the wealth of information on Earth's ionosphere, provide an excellent opportunity for comparative planetology. Seven of the ionospheres studied reside in the outer solar system (Jupiter, Io, Saturn, Titan, Uranus, Neptune, Triton), and have been investigated with the radio occultation technique pioneered by Lindal and colleagues (e.g.,Lindal et al. 1987;Lindal 1992;Tyler et al. 1989). The ionospheres of Venus and Mars have been probed by both the radio occultation technique and by in situ plasma instruments (Brace and Kliore 1991;Barth et al. 1992). Earth's ionosphere has been studied in great detail by in situ and ground-based radar techniques (Kelley 1989), but has only recently been probed in detail by radio occultations (Hajj et al. 1994). Here, I focus on the lower ionosphere of Neptune, although much of the chemistry should be applicable to the upper atmospheres of the giant planets in general. Each of the giant planets exhibits sharp, high density layers of electrons in its lower ionosphere (Atreya 1986). The absence of such layers in the ionospheres of the non-magnetic planets demonstrates the key role played by the magnetic field in layer formation. On Earth, these layers are known to consist primarily of metallic ions, produced during meteoroid ablation, and gathered together by wind shears in the presence of Earth's magnetic field (Kelley 1989). Substantial modeling of terrestrial sporadic-E has been performed (Kelley 1989), but only the influx of material from Io to Jupiter has been studied for the giant

planets (Chen 1981).

2. Voyager 2 radio occultation data

The radio occultation experiment at Neptune (Tyler et al. 1989) was performed as Voyager 2 passed behind the planet as seen from Earth. Propagation effects along tangents through Neptune's atmosphere induced variations in the phases of the S-band (2.3 GHz) and X-band (8.4 GHz) spacecraft carriers. For a frequency $\omega >> \omega_p$, the plasma frequency, the change in phase relative to a vacuum is (Fjeldbo et al. 1965) (G. Lindal is known as G. Fjeldbo in earlier publications)

$$\Delta\phi = -\frac{e^2}{2\epsilon_0 m_e \lambda \omega^2} \int_{path} N_e \, ds \qquad (1)$$

where e is the electron charge, m_e is the electron mass, ε_0 is the permitivity of free space, λ is the wavelength, and N_e is the electron number density. Contributions to $\Delta\phi$ come from all plasma along the ray path, including the solar wind and terrestrial ionosphere, but are principally from Neptune's ionosphere. Figure 1 shows the S-band $\Delta\phi$ (versus time) measured at the egress occultation point when Voyager 2 was about 76,000 km behind the limb of Neptune. The integration time for each phase point is 0.1024 seconds, which for a spacecraft velocity perpendicular to Neptune's limb of 12.8 km sec^{-1}, corresponds to a vertical resolution of $\approx$ 1.3 km. The size of the Fresnel zone, which characterizes the scale at which diffraction effects become important, is 3.1 km at S-band and 1.6 km at X-band for egress. The sharpest layers are 7 to 10 km in width, and are

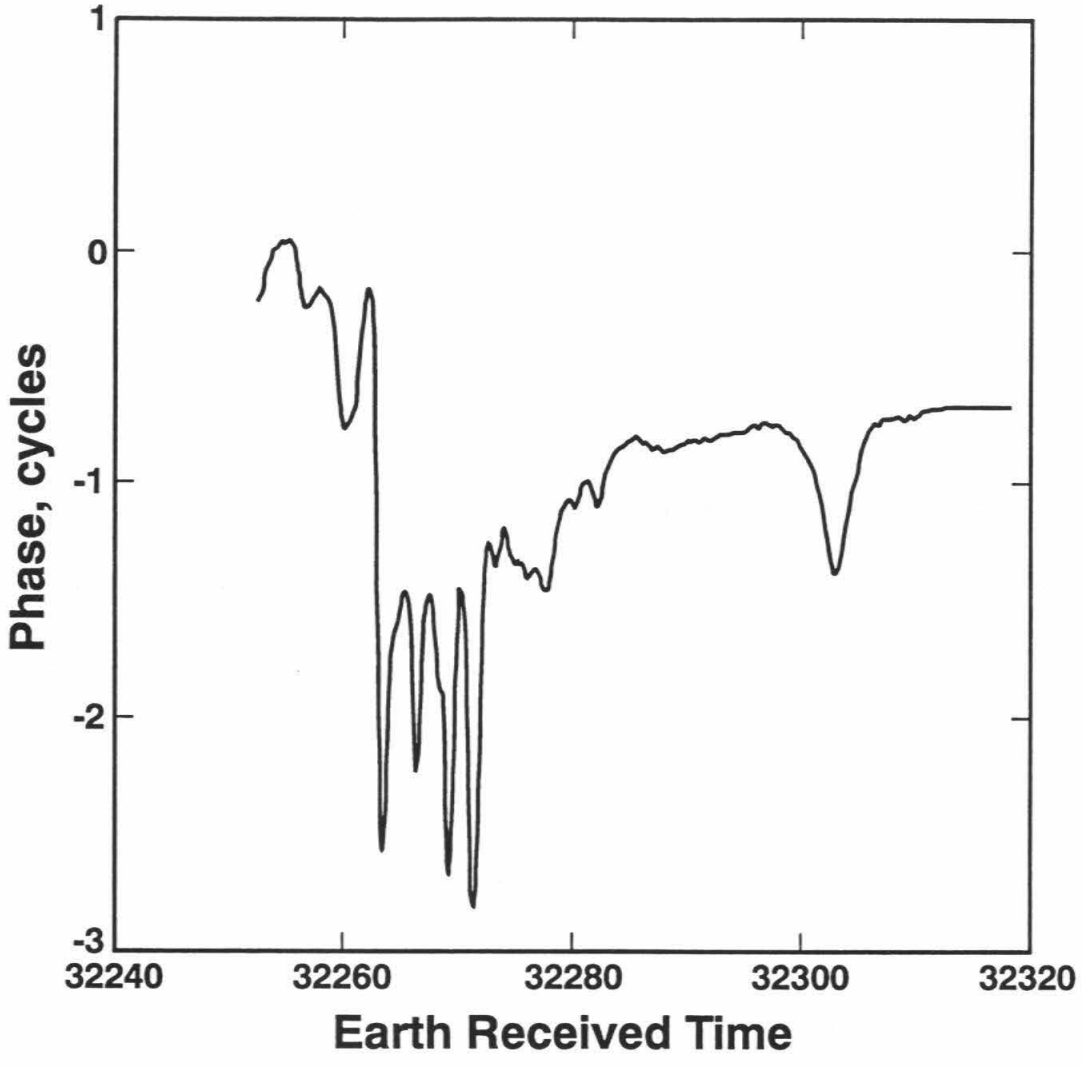

Fig. 1 Observed S-band phase perturbation due to passage of the spacecraft signal through Neptune's ionosphere at the egress occultation point. The phase, in cycles, is plotted against Earth received time in seconds past midnight (spm). The time scale can be converted to a distance scale by multiplying by the spacecraft velocity (perpendicular to the limb) of 12.8 km sec^{-1}. Note the four sharp layers between 32260 and 32280 spm.

therefore well sampled and not expected to produce significant diffraction.

Assuming local spheroidal symmetry in the horizontal distribution of electrons, Lindal (1992) inverted the phase data, obtaining the electron number density profiles for the ingress and egress locations. Figure 2 shows an expanded view of the lower ionosphere for egress; ingress data are shown in (Lindal 1992). The narrow structures seen in the phase (Fig. 1) correspond to the sharp layers seen in N_e at altitudes from ~ 650 to 750 km in Fig. 2. The high noise-level of the electron number density in the layer region is most likely due to deviations from local spheroidal symmetry of N_e (Lindal 1992). In addition, it is possible that the signal variations were not fully resolved (10). S-band spectra showed some broadening in the layer region; therefore, only X-band data were used for the approximately 20 second section of phase containing the sharp layers. These data were then converted to S-band and merged with the remaining S-band data. The net result is that the electron number densities of the four main layers are uncertain by as much as a factor of two, but the altitude of the layers is well determined.

Another potential source of error, multipath propagation, can be shown to be unimportant everywhere in the ionosphere. Sharp gradients in phase produce focussing and defocussing of rays, and can, if the gradients are sharp enough or the spacecraft far enough behind the planet, result in multipath propagation. The condition for multipath propagation is given by Fjeldbo (1965) in terms of the refractive gain, $G_r = -10\log_{10}|1 + D d\alpha/d\rho|$, where D is the distance from the limb to the spacecraft, α is the bending angle given by $\alpha = \lambda d\Delta\phi/d\rho$, and ρ is the height of the ray periapse relative to the center of the planet. At a caustic, rays cross, and in the geometric optics limit $G_r \rightarrow \infty$. Multipath

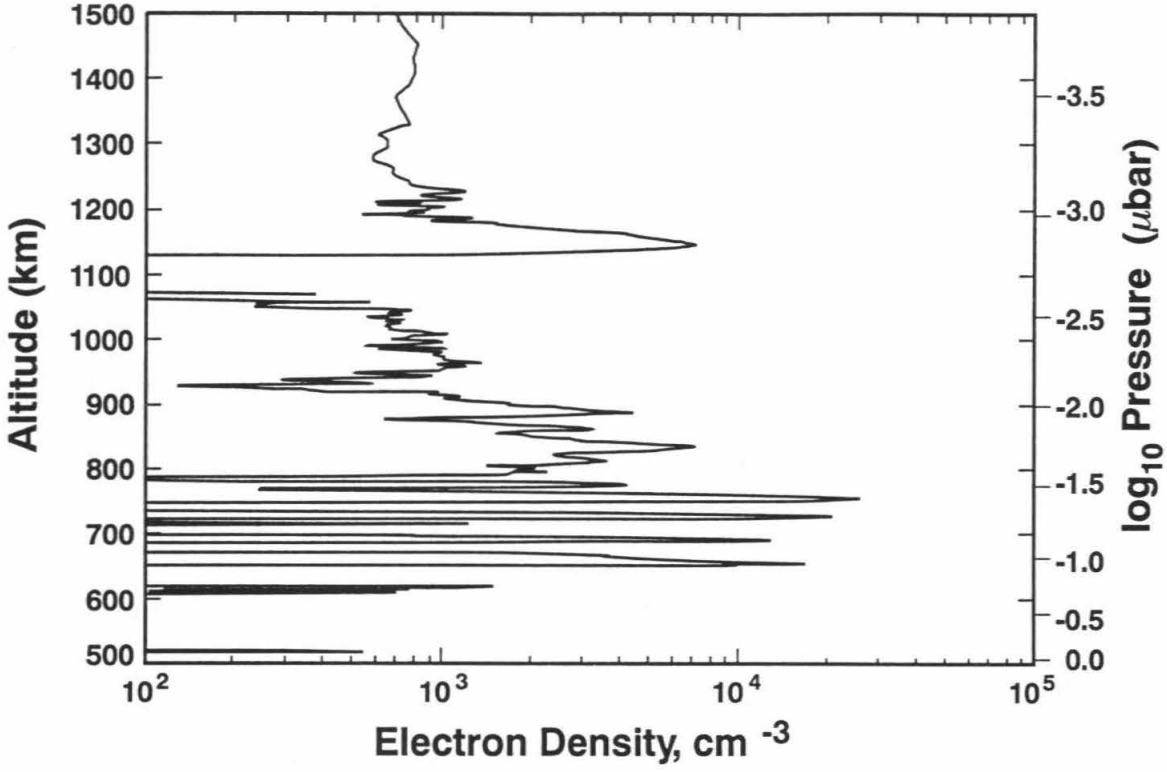

Fig. 2. Electron number density profile obtained (Lindal 1992) from inversion of the phase data in Fig. 1. The noise level above 1100 km is ~ 1000 cm^{-3}; below 1100 km, the noise level is significantly higher (~ 5000-10000 cm^{-3}). Although the uncertainty in the electron abundance is high in the lower ionosphere, the altitude of the layers is well determined from the phase.

propagation occurs when $D d\alpha/d\rho < -1$. From the phase variations (Fig. 1), it can be shown that this condition is not met at any time at either S or X-band. However, the layers produce detectable defocussing of ~ 2 db at S-band and ~ 0.2 db at X-band.

3. Interpretation of the radio data

The simplest assumption regarding the origin of the layers is that, by analogy with Earth, they are long-lived metallic ions caught in a horizontal wind with a vertical shear (see below). However, the terrestrial ionosphere has also revealed that a richness of plasma structures can exist, due both to particle precipitation and plasma instabilities. The latitude and longitude of the Neptune egress occultation point is 44°S, 229°W, which according to the magnetic model of Connerney et al. (1991) corresponds to a field magnitude of B = .65 gauss, an inclination (or dip) angle of I = 65°, and a declination angle of D = -65°. Because egress occurred near the auroral zone, particle precipitation must be considered. To form a layer at 700 km would require electrons with energy ~ 1 MeV, about 100 times more energetic than terrestrial auroral electrons; protons are incapable of reaching such depths before undergoing charge exchange or ionizing the background gas. Plasma instabilities (Kelley 1989) may contribute to the observed structure, but given that the topside ion densities are only ~ 1×10^3 cm^{-3}, instabilities probably are not responsible for the sharp layers in the lower ionosphere. Another potential source of plasma structure is plasma drift across the terminator. Because of the distance of Neptune, the occultation points are necessarily both near the (morning)

terminator; i.e., the solar zenith angle is nearly 90°. Although diurnal variation due to radiative recombination of atomic ions is negligible, the low electron densities observed suggest that a faster loss process may be occurring, so that plasma flow may important.

4. Chemical modeling of the lower ionosphere

To determine whether or not metallic ions could be responsible for the sharp layers observed in Neptune's lower ionosphere, a comprehensive one-dimensional model of Neptune's upper atmosphere was developed. The model extends from 1 mbar to 10^{-10} mbar, accounts for eddy and molecular diffusion (Allen et al. 1981), and includes ion and neutral chemistry of hydrocarbons, water and related species, and "metals" (i.e., non-CHON species). Metals are produced in the model by meteoroid ablation, with volume production rates as computed by Moses (1992) for Neptune. The meteoroids are assumed to be of cometary composition (Jessberger and Kissel 1991), with 30 % by mass water ice. The specific metal species considered are S, Si, Mg, Fe, and Na; in computing ablation production rates, no attempt was made to account for the differing volatilities of mineral grains that these species may occur in. The flux of meteorids was taken to be 10 times the Oort cloud particle flux defined by Moses (1992), which is roughly the geometric mean of the two fluxes considered in (Moses 1992). Ablation is assumed to occur between 10 and 0.1 microbar, midway between the pure water ice and pure silicate ablation profiles of Moses (1992). In the model, the eddy diffusion coefficient of Romani et al. (1994) was employed, with a CH_4 mixing ratio of 10^{-4} at 1 millibar.

Figure 3 shows the number density profiles predicted by the model for several neutral species, including four of the atomic metals. Neutral silicon, although comparable to Fe and Mg in cosmic abundance, is rapidly consumed in reactions with C_2H_4 and other hydrocarbons, and therefore does not accumulate in the atmosphere. The column production rate of Fe, Mg, and Si is 3.0×10^5 cm^{-2} sec^{-1}, with peak production occurring from 425 to 500 km. Loss is primarily by recondensation onto dust particles (Hunten et al. 1980), with a column rate of 2.7×10^5 cm^{-2} sec^{-1} from 300 to 400 km. The condensation timescale in the model is ~ 3×10^5 seconds at z ~ 400 km, corresponding to a haze particle number density of ~ 300 cm^{-3} for 3 nanometer particles (Moses 1992). At a rate about 10 times lower than condensation, loss of neutral metals also occurs by charge exchange with molecular ions. There have been very few laboratory studies of the kinetics of metal atom reactions with hydrocarbons. Defining 'M' as one of Mg, Fe, Si, Na, or S, it is possible that species such as MH and MCH_3 are produced during reactions of M with higher hydrocarbons. MH and MCH_3 are likely to react with H to yield M and H_2 or CH_4, thus returning atomic metals to the system. Bond strengths have been measured for some metal hydrides (CRC 1986), yielding values ~ 2 eV, so that reactions with H and CH_3 would indeed be exothermic for the metals considered here. Except for Si and S, reactions of M with hydrocarbons are not included in the model. The model column abundances of Mg and Fe are ~ 6×10^{11} cm^{-2}, and for Na the column density is ~ 3×10^{10} cm^{-2}. These column densities were not large enough to be detected by the Voyager spacecraft.

Ion profiles predicted by the model are shown in Fig. 4. The topside ionosphere

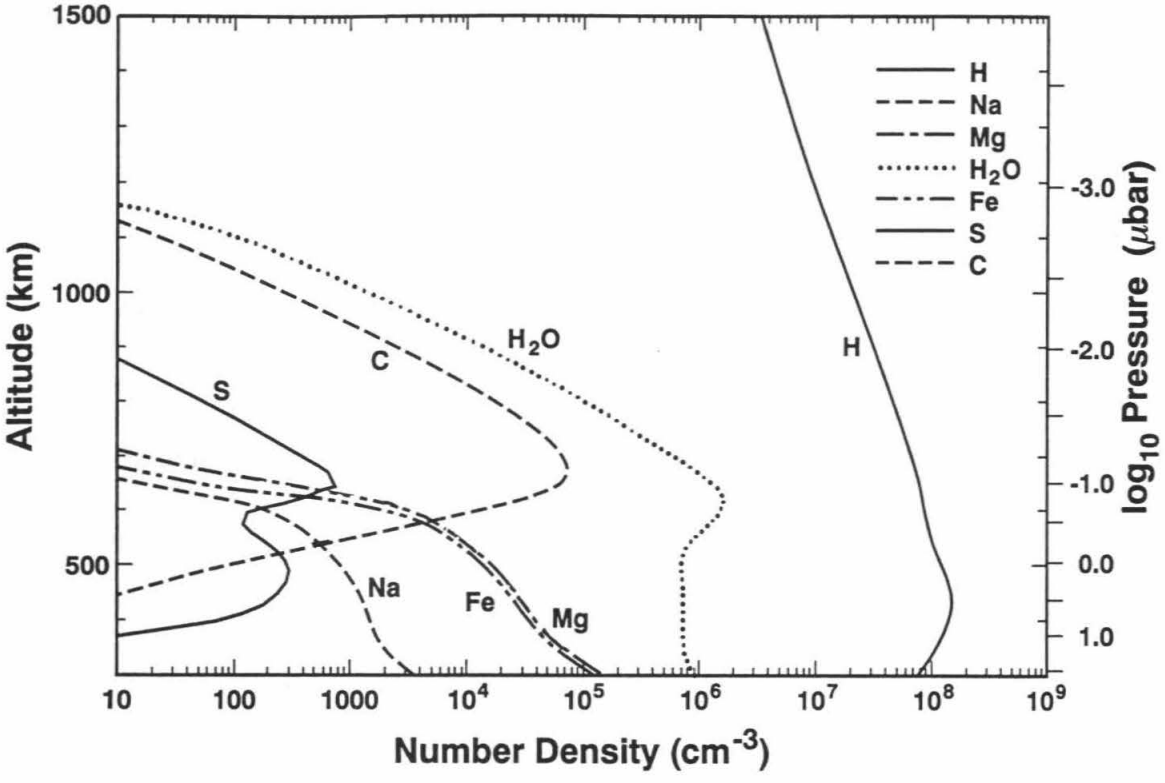

Fig. 3. Model number density profiles for several metal species, water, carbon and hydrogen. The calculations are for a meteoroid flux ~ ten times the Oort cloud particle flux at Neptune (Moses,1992). The meteoroid composition is assumed to be cometary with 30 % water ice by mass.

is dominated by H^+. Using recent measurements of the rate coefficient for dissociative recombination (Canosa et al. 1992), H_3^+ is more than an order of magnitude less abundant than H^+. Water produced during meteoroid ablation reacts with H^+ to eventually produce H_3O^+ by a sequence of reactions described previously (Connerney and Waite 1984;Atreya 1986). The model topside electron density is ~ 5 times larger than the observed electron density (Fig. 2). There are several possible reasons for the discrepancy, which have been discussed elsewhere (Strobel et al. 1991) but will only be listed here. They are as follows: 1) reaction of H^+ with $H_2(v\geq4)$ to form $H_2^+(v)$, which further reacts with molecular hydrogen; 2) influx of water at a high enough altitude to consume H^+; in the present model the topside density is reduced by almost a factor of two due to water influx, but larger reductions have been predicted; 3) transport of H^+ to the northern hemisphere by meridional winds; 4) vertical winds and/or enhanced escape of H^+.

The lower ionosphere is predicted to be dominated by the metallic ions Mg^+ and Na^+ (Fig. 4). Metal ions are formed primarily by charge exchange with hydrocarbon ions and H_3O^+; solar ionization of neutral metals contributes < 10 % to the metal ion production rate in the model. The formation of hydrocarbon ions is driven by solar ionization of CH_4 and C_2 hydrocarbons, and proceeds along a complex path (see e.g., Atreya 1986;Kim and Fox 1991) that leads to the formation of C_3 and C_4 hydrocarbon ions, here denoted as $C_3H_m^+$ and $C_4H_n^+$. The kinetics of hydrocarbon ion-molecule reactions have been well studied in the laboratory, with the result that most rate coefficients are known (Anicich 1993). The principal formation pathway for metal ions

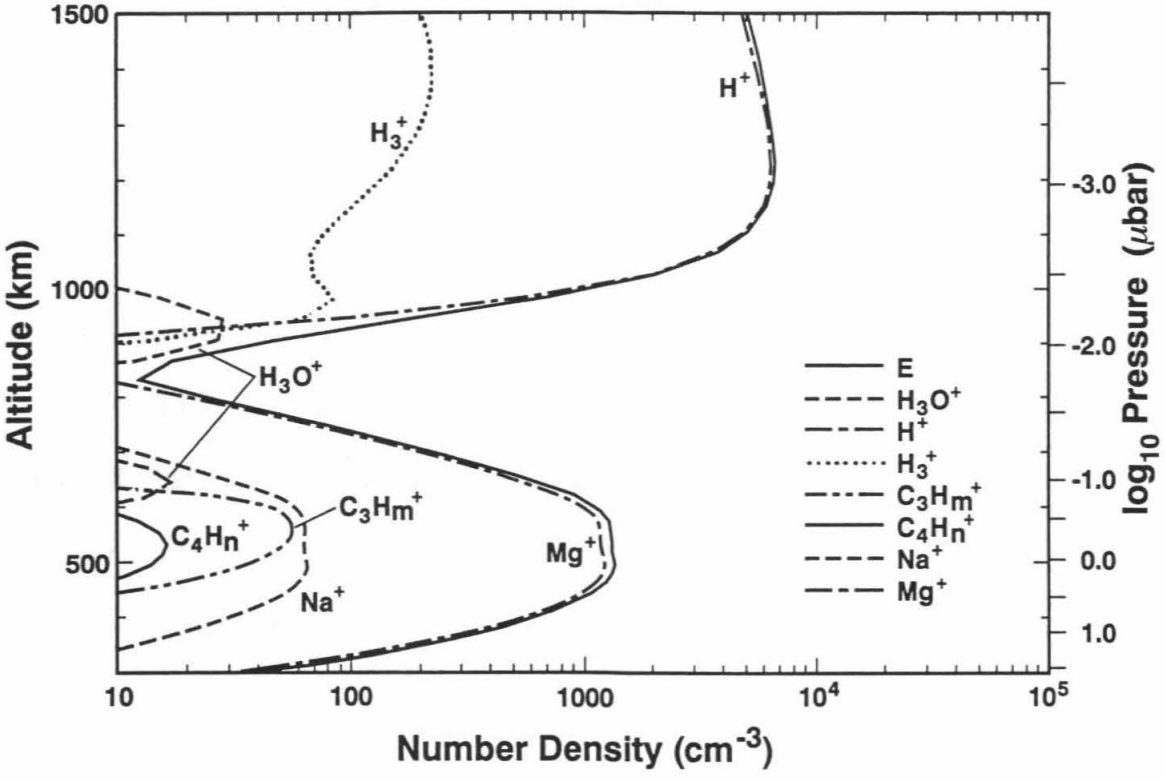

Fig. 4. Model ion profiles for the lower ionosphere of Neptune.

is

$$C_3H_m^+ + M \rightarrow M^+ + C_3H_m \qquad \text{(R1)}$$

The rate coefficient of this reaction is assumed to be 1×10^{-9} cm^3 sec^{-1}, by analogy with the reaction $CH_5^+ + Mg \rightarrow Mg^+ + CH_4 + H$ (Anicich 1993). Because most of the metal species have high proton affinity (Huntress 1977), species such as MH^+ are also likely products. The large abundance of H ensures that MH^+ will be converted to M^+ via the reaction

$$MH^+ + H \rightarrow M^+ + H_2 \qquad \text{(R2)}$$

analogous to the reaction $MO^+ + O \rightarrow M^+ + O_2$ in the terrestrial ionosphere (Ferguson and Fehsenfeld 1968). Theoretical estimates (Ohanessian and Goddard 1990; Bauschlicher and Langhoff 1990) of bond strengths in metal hydride ions shows that reaction R2 will be exothermic for the metals considered here. In the model, charge exchange to form M^+ is assumed to form MH^+ with equal probability, and the rate for R2 is assumed to be 1×10^{-10} cm^3 sec^{-1}. Fe^+, S^+, and C^+ are not present in Fig. 4 due to reactions with CH_4, C_2 hydrocarbons, and water. Similar reactions with C_3 and higher hydrocarbons may occur for Mg^+ and Na^+, but apparently these have not been studied in the laboratory.

5. Modeling of the sharp ionization layers

Clearly, the model lower ionosphere shown in Fig. 4 does not account for the observed electron layers. However, there is sufficient Mg^+ abundance predicted that the

magnesium ions could be compressed into sharp layers. The short chemical lifetime of molecular ions makes them unsuitable as candidates for layer formation. According to the mechanism proposed to explain sporadic E in the terrestrial ionosphere (Whitehead 1961), compression of ions into layers can result from a horizontal wind with a vertical shear acting on the ions in the presence of a magnetic field. Such wind shears are usually produced by atmospheric gravity waves and tides. The motions of ions and neutrals are coupled through ion-neutral collisions. However, in the presence of a magnetic field, ion motion is further influenced by the Lorentz force.

By balancing the Lorentz force with the rate of momentum exchange due to collisions with neutrals, an expression may be derived for the vertical ion velocity, w_i, in terms of the neutral wind components. The ratio of the ion-neutral collision frequency to ion gyro frequency, $\eta_i=\nu_{in}/\Omega_i$, characterizes the dominant influence on ion motion. Expressions for these two frequencies are given by Atreya (1986), and are $\nu_{in}=2\pi(\alpha_{in}e^2/\mu_{in})^{½}n$ and $\Omega_i=eB/m_i$. Following earlier work (e.g., Kirkwood and Collis 1989; Bristow and Watkins 1991), balancing the Lorentz force and the rate of ion-neutral collisions, $e\mathbf{v}_i\times\mathbf{B}=m_i\nu_{in}(\mathbf{v}_i-\mathbf{v}_n)$, where $\mathbf{v}_i$ and $\mathbf{v}_n$ are the ion and neutral velocity vectors. Solving for the vertical component of ion velocity yields $w_i=u\cos I\cos D/\eta_i$ for $u>>v,w$, the meridional and vertical components of the neutral wind, and for $\eta_i>>1$. Thus, at an altitude for which $\eta_i>>1$ (valid for $z < 800$ km), and assuming the zonal wind, u, is the dominant neutral wind component, $w_i \propto u/\eta_i$, demonstrating that changes in the horizontal neutral wind are translated into changes in the vertical ion velocity.

Compression of the ions requires a convergent vertical ion wind, $\partial w_i/\partial z < 0$, where

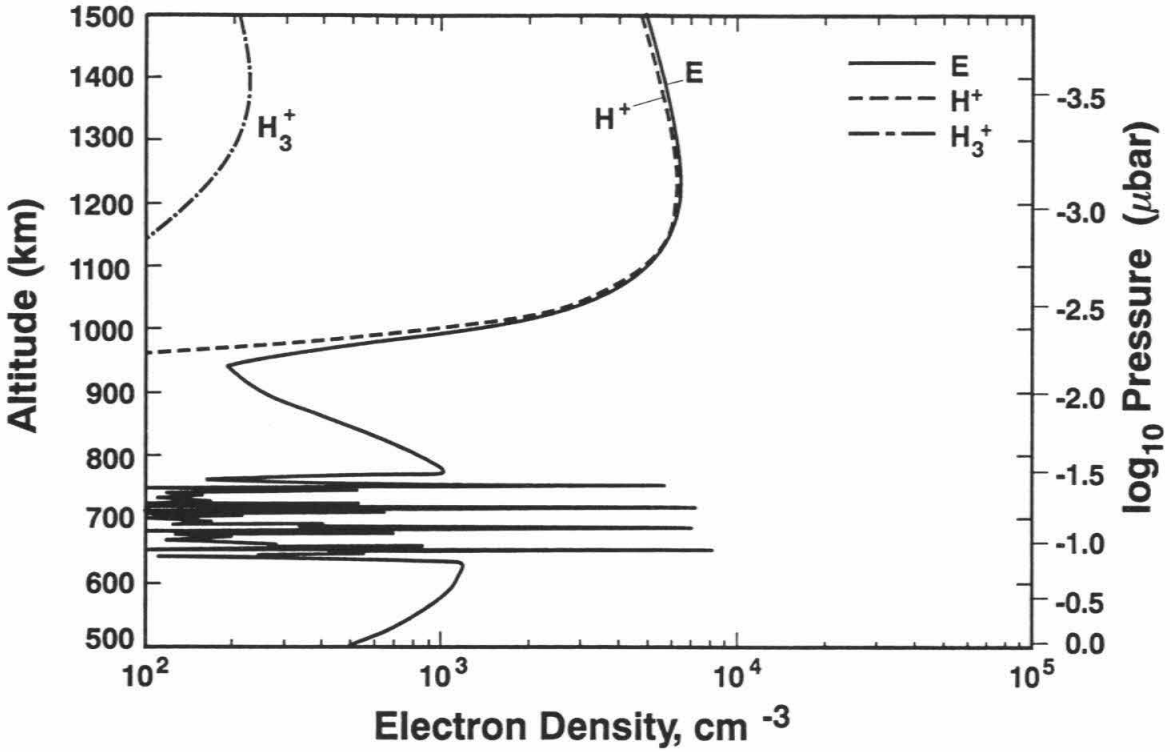

Fig. 5. Magnesium ions in the lower ionosphere are compressed into sharp layers by a sinusoidal vertical ion wind. The wind was applied from 630 to 770 km for a total of 5000 seconds, in steps of 500 seconds. The vertical resolution of the model has been enhanced to 2 km over this altitude range; elsewhere the resolution is one third of a scale height. Note that the lower ionosphere was first raised ~ 150 km by an upward ion wind of 1 m sec^{-1}, applied from 400 to 1000 km for ~ 10^5 seconds. The upward wind is assumed to result from E×B drift, and requires an electric field ~ 0.1 mV/m.

z is the altitude. Differentiation of w_i with respect to z yields the expression $\partial w_i/\partial z = \cos I \cos D(\partial u/\partial z + u/H_n)/\eta_i$, relating the divergence of the vertical ion wind to the vertical shear in the zonal neutral wind. Figure 5 shows the result of applying an alternately convergent and divergent ion wind to the lower ionosphere shown in Fig. 4. The lower ionosphere was first raised ~ 150 km, bringing the model profile into better agreement with the observations. The upward wind is usually (e.g., Majeed and McConnell 1991) attributed to $\mathbf{E} \times \mathbf{B}$ drift; in this case, the magnitude of the electric field component perpendicular to B and z is $E_\perp \approx w_i B/\cos I = 0.1$ millivolt m^{-1}. Such an electric field may be generated by a dynamo associated with upper atmospheric winds driven by Triton or solar tides. The prescribed wind was a sinusoid, $w_i = w' \sin[m(z-z_0)]$, where $m=2\pi/d$ for a layer spacing $d \approx 33$ km, $z_0=633$ km, and $w'=3$ m sec^{-1}. This form of w_i results in the four layers seen in the lower portion of Fig. 5. The maximum vertical gradient of the ion wind is $\partial w_i/\partial z \approx 0.6$ m sec^{-1} km^{-1}, which at an altitude ~ 700 km corresponds to a maximum $\partial u/\partial z$ ~ 30 m sec^{-1} km^{-1}, a substantial but not implausible wind shear.

The choice of a sinusoidal ion wind field was motivated both by the occurrence of multiple ion layers in the lower ionosphere and by the likelihood of vertically stratified zones of wind shear associated with atmospheric gravity waves. Earth-based stellar occultation data (Sicardy et al. 1992; Roques et al. 1994) of Neptune's upper atmosphere suggest the presence of convectively unstable waves at pressures as low as 0.1 to 0.03 microbar, with vertical wavelengths comparable to the ion layer spacing (~20 to 30 km). Assuming waves with m >> k (horizontal wavenumber), the time required for a wave to propagate h, one ionospheric layer height, is $h/v_g \sim hm^2/Nk$. For m/k ~ 10 , the buoyancy

frequency N ~ 7×10^{-3} s^{-1}, and a layer vertical thickness h ~ 10 km, h/v_g ~ 3000 to 3×10^4 seconds. Thus, the wave can form a single layer before significant smearing of the layer occurs, consistent with the results shown in Fig. 5. The value of the wave vertical velocity perturbation, w', given above corresponds to a temperature perturbation of $T' \sim (mw'/kc_s)(\gamma-1)^{1/2}T_0 \sim 5$ K for m/k ~ 10, consistent with the occultation data of Roques et al. (1994). Calculations of viscous dissipation of gravity waves with m >> k suggests that the waves must have m/k << 100 if they are to have significant amplitudes at pressures ~ 10^{-2} μbar. A detailed discussion of gravity waves, including chemical calculations with a time-dependent (i.e., propagating) wind field, will be given elsewhere.

Laboratory data on the kinetics of neutral and ionized atomic metals, particularly Mg, in two-body, three-body and cluster reactions with hydrocarbons and H_2 are crucial to a more complete understanding of the lower ionospheres of Neptune and the other giant planets. The detection (Noll et al. 1994) of abundant Mg and Mg^+ at the impact site of the G fragment of Comet Shoemaker Levy 9 makes clear the need for further study of metals in reducing environments.

Acknowledgements

Discussions with G. Lindal, J. Connerney, Y. Yung, W. Goddard, T. Rebold, and S. Asmar, are gratefully acknowledged. G. Lindal provided the electron number density profile. This work was supported by NASA grants NAGW-2362 and NAGW-1509.

References

Allen, M., Y. L. Yung, J. W. Waters 1981. Vertical transport and photochemistry in the terrestrial mesosphere and lower thermosphere. *J. Geophys. Res.* 86, 3617-3627.

Anicich, V. G. 1993. Evaluated bimolecular ion-molecule gas phase kinetics of positive ions for use in modeling planetary atmospheres, cometary comae, and interstellar clouds. *J. Phys. Chem. Ref. Data* 22, 1469-1569.

Atreya, S. K. 1986. *Atmospheres and Ionospheres of the Outer Planets and their Satellites*, Springer-Verlag (Berlin).

Barth, C. A., A. I. F. Stewart, S. W. Bougher, D. M. Hunten, S. J. Bauer, A. F. Nagy 1992. Aeronomy of the current Martian atmosphere, in *Mars*, H. Kieffer et al. (eds.), University of Arizona Press (Tucson).

Bauer, S. J. 1973. *Physics of Planetary Ionospheres*, Springer-Verlag (New York).

Bauschlicher, C. W., Jr., and S. R. Langhoff 1990. Theoretical study of the bonding in molecular transition-metal cations. *Int. Rev. Phys. Chem.* 9, 149-185.

Brace, L. H., and A. J. Kliore 1991. The structure of the Venus ionosphere. *Space Sci. Rev.* 55, 81-163.

Bristow, W. A., and B. J. Watkins 1991. Numerical simulation of the formation of thin ionization layers at high latitudes. *Geophys. Res. Lett.* 18, 404-407.

Canosa, A. et al. 1992. Further measurements of the H_3^+(v=0,1,2) dissociative recombination rate coefficient. *J. Chem. Phys.* 97, 1028-1030.

Chen, R. H. 1981. Studies of Jupiter's lower ionospheric layers. *J. Geophys. Res.* 86,

7792-7794.

Connerney, J. E. P., and J. H. Waite 1984. New model of Saturn's ionosphere with an influx of water from the rings. *Nature* 312, 136-138.

Connerney, J. E. P., M. H. Acuna, N. F. Ness 1991. The magnetic field of Neptune. *J. Geophys. Res.* 96, 19,023-19042.

CRC Handbook of Chemistry and Physics, 67th ed. 1986. (Weast et al., eds.), CRC Press, Inc. (Boca Raton).

Ferguson, E. E., and F. C. Fehsenfeld 1968. Some aspects of the metal ion chemistry of the Earth's atmosphere. *J. Geophys. Res.* 73, 6215-6223.

Fjeldbo, G., V. R. Eshleman, O. K. Garriott, F. L. Smith,III 1965. The two-frequency bistatic radar-occultation method for the study of planetary ionospheres. *J. Geophys. Res.* 70, 3701-3710.

Hajj, G. A., R. Ibañez-Meier, E. R. Kursinski, L. J. Romans 1994. Imaging the ionosphere with the Global Positioning System. submitted to *Int. J. Imaging Sys. Tech.*

Holton, J. R. 1992. *An Introduction to Dynamic Meteorology*, 3rd ed., chap. 9, Academic Press (San Diego).

Hunten, D. M., R. P. Turco, O. B. Toon 1980. Smoke and dust particles of meteoric origin in the mesosphere and stratosphere. *J. Atmos. Sci.* 37, 1342-1357.

Huntress, W. T., Jr. 1977. Laboratory studies of bimolecular reactions of positive ions in interstellarclouds, in comets, and in planetary atmospheres of reducing composition. *Astrophys. J. Suppl.* 33, 495-514.

Jessberger, E. K., and J. Kissel. 1991. Chemical properties of cometary dust and a note

on carbon isotopes, in *Comets in the Post-Halley Era* (R. L. Newburn et al. eds.), Kluwer Academic Publishers (Netherlands), 1075-1092.

Kelley, M. C. 1989. *The Earth's Ionosphere*, Academic Press (San Diego).

Kim, Y. H., and J. L. Fox 1991. The Jovian ionospheric E region. *Geophys. Res. Lett.* 18, 123-126.

Kirkwood, S., and P. N. Collis 1989. Gravity wave generation of simultaneous auroral sporadic-E layers and sudden neutral sodium layers. *J. Atmos. Terr. Phys.* 51, 259-269.

Lindal, G. F., J. R. Lyons, D. N. Sweetnam, V. R. Eshleman, D. P. Hinson, G. L. Tyler 1987. The atmosphere of Uranus: results of radio occultation measurements with Voyager 2. *J. Geophys. Res.* 92, 14987-15001.

Lindal, G. F. 1992. The atmosphere of Neptune: An analysis of radio occultation data acquired with Voyager 2. *Astron. J.* 103, 967-982.

Majeed, T., and J. C. McConnell 1991. The upper ionospheres of Jupiter and Saturn. *Planet. Space Sci.* 39, 1715-1732.

McElroy, M. B. 1973. The ionospheres of the major planets. *Space Sci. Rev.* 14, 460-473.

Moses, J. I. 1992. Meteoroid ablation in Neptune's atmosphere. *Icarus* 99, 368-383.

Noll, K. and the Hubble Space Telescope Team. 1994. *IAU Circular No. 6038.*

Ohanessian, G., and W. A. Goddard III 1990. Valence-bond concepts in transition metals: metal hydride diatomic cations. *Acc. Chem. Res.* 23, 386-392.

Romani, P. N., J. Bishop, B. Bezard, S. Atreya 1994. Methane photochemistry on Neptune: Ethane and acetylene mixing ratios and haze production. *Icarus* 106,

442-463.

Roques, F., B. Sicardy, R. G. French, W. B. Hubbard et al. 1994. Neptune upper-stratosphere, 1983-1990 - ground-based stellar occultation observations. 3. Temperature profiles. *Astron. Astrophys.* 288, 985-1011.

Shinagawa, H., and J. H. Waite 1989. The ionosphere of Neptune. *Geophys. Res. Lett.* 16, 945-948.

Sicardy, B., P. Goldreich, F. Roques 1992. Constraints on gravity waves in upper planetary atmospheres from occultation observations. *Bull. Am. Astron. Soc.* 24, 963.

Stone, E. C., and E. D. Miner 1989. The Voyager 2 encounter with the Neptune system. *Science* 246, 1417-1421.

Strobel, D. F., R. V. Yelle, D. E. Shemansky, S. K. Atreya. 1991. The upper atmosphere of Uranus, in *Uranus*, (Bergstralh, Miner, Matthews, eds.), Univ. of Arizona Press (Tucson).

Tyler, G. L., D. N. Sweetnam, J. D. Anderson, S. E. Borutzki et al. 1989. Voyager radio science observations of Neptune and Triton. *Science* 246, 1466-1473.

Whitehead, J. D. 1961. The formation of the sporadic-E layer in the temperate zone. *J. Atmos. Terr. Phys.* 20, 49-58.

PAPER III

Constraints on meteoroidal influx into the upper atmospheres of Uranus and Neptune

James R. Lyons

Division of Geological and Planetary Sciences

California Institute of Technology

Pasadena, California 91125

submitted to Geophysical Research Letters

Abstract

Results from a recent analysis of meteoroid ablation rates in the atmosphere of Neptune have been coupled with photochemical models of the upper atmospheres of Neptune and Uranus to yield estimates of stratospheric water profiles as a function of meteoroid influx. Because water has never been detected in the upper atmospheres of the giant planets, the tangential column opacities of the model water profiles were compared with ultraviolet absorption measurements made by Voyager to determine maximum water influxes. For Uranus an upper limit of 4×10^{6} water molecules cm^{-2} sec^{-1} is obtained. For a Triton-like meteoroid composition (30% water ice by mass), this flux is consistent with an Oort-family particle population, but is not consistent with a large population of planet-family dust particles. For Neptune the model water profile is strongly dependent on the still uncertain eddy diffusion coefficient, making it difficult to rule out a large planet-family population of IDP's. However, an IDP population sufficiently large to account for the CO observed in Neptune's atmosphere can be ruled out.

1. Introduction

Little is known about the abundance and composition of interplanetary dust particles (IDP's) in the outer solar system. In situ spacecraft measurements made by Pioneer 10 and 11 (Humes 1980) suggested a constant spatial particle density from 1 to 18 AU for particles in the mass range of 10^{-8} to 10^{-9} g. The flux of IDP's is believed to be a key factor in determining the lifetime of ring systems (Cuzzi and Durisen 1990) and in producing dust (Burns et al. 1980) and other ring features (Goertz and Morfill 1983). Meteoroidal and ring particle influx have been proposed as the principal sources of oxygen species to the upper atmospheres of Jupiter (Prather et al. 1978), Saturn (Connerney and Waite 1984) and Titan (Ip 1990), and it has been suggested (Moses 1992) that meteoroidal deposition of water could be the source of CO recently observed (Rosenqvist et al. 1992, Marten et al. 1993) in Neptune's stratosphere. High yield excavation of ring particles and satellite surfaces by meteoroidal impact has been proposed as the source of dust in portions of the Uranian and Neptunian ring systems (Smith et al. 1989, Smith et al. 1986), and in the magnetosphere of Neptune (Gurnett et al. 1991).

On the basis of orbital characteristics, two families of projectiles are defined in the outer solar system (Cuzzi and Durisen 1990). The Oort cloud family consists of particles with large eccentricities and random inclinations, generated by volatile emission from Oort cloud objects. The planet family IDP's have low eccentricities and small inclinations, and are thought to be derived from collisions among Kuiper belt objects.

These two comet families will produce IDP's with very different velocity distributions in the outer solar system. The result is a significant difference in the gravitational focusing of particles by the planet, with the planet-family particles being slower and therefore more focused. At Neptune and Uranus the focusing factors differ by about a factor of 20 for the two populations (Moses 1992), suggesting the possibility of large atmospheric meteoroid fluxes associated with planet-family IDP's. However, the spatial density of IDP's at the orbits of Uranus and Neptune is unknown. Smith et al (1989) claim that an impact flux ~ 100 times that at Jupiter and Saturn is needed to explain the dustiness of Neptune's rings. Cratering rates of the Uranian and Neptunian satellites may require a large number of planet family impactors (Smith et al. 1989). Given that collisions among Kuiper belt objects should occur infrequently (compared to objects in the asteroid belt), it seems reasonable to expect low IDP abundances in the outer solar system. Recent estimates (Flynn 1994) of the rate of dust production, P, due collisions in the Kuiper belt yield values of P ~ 10^4 to 10^8 g/sec. This corresponds to a mass flux at the orbit of Neptune ~ aP/V, where a ≈ 30 AU is the distance to Neptune's orbit, and V is the volume of the dust production region in the Kuiper belt. Assuming that the dust production region is a torus extending from 30 to 40 AU, 2 AU in thickness, the mass flux corresponding to the maximum estimated dust production rate is 3×10^{-21} g cm^{-2} sec^{-1}, more than three orders of magnitude smaller than the estimated Oort-family IDP flux at Neptune (see below). Such estimates are, of course, extremely uncertain, both in terms of the dust production rate and the volume of the torus. Photochemical considerations can provide another constraint on the flux of particles coming from the Kuiper belt.

2. Meteoroid ablation and photochemical model

Recently, a thorough analysis of meteor ablation in the atmosphere of Neptune was performed by Moses (1992). Ablation rate profiles were computed for water ice and silicate meteoroids for possible Oort and Neptune families of projectiles. Here, the ablation rate profiles computed by Moses (1992) are coupled with a comprehensive photochemical model of Neptune's upper atmosphere with the objective of computing water vapor profiles. Ultraviolet absorption due to the water is then estimated from the profiles and can be compared with solar occultation experiments performed with the Voyager utraviolet spectrometer (UVS) (Broadfoot et al. 1989). Because water has never been detected in the upper atmospheres of the giant planets, only upper limits to the water profiles, and hence water influx, can be inferred. The photochemical model assumes (following Moses (1992)) a Triton-like composition for the meteoroids (Smith et al. 1989), with a water ice mass fraction of 30% and the rest as silicates; this corresponds to a dust to gas ratio of 2.3. The model is one dimensional, extends from 100 mbar to 10^{-10} mbar and includes vertical transport by eddy and molecular diffusion (Allen et al. 1981). The chemical species solved for include H_2O, OH, O and $O(^1D)$, in addition to CH_4 and other hydrocarbons (Moses et al. 1992). Temperature, eddy coefficient, and (measured) hydrocarbon and H_2 profiles are from Yelle et. al. (1993). The photochemical model has several hundred reactions (including ion-molecule), a list of which is available from the author. Key reactions involving water and its photodissociation products are given in Table 1. The solar flux model is for near solar maximum conditions at Neptune

(Mount and Rottman 1983, Torr and Torr 1985, Woods and Rottman 1983) and solar minimum at Uranus, where the latter flux model is derived from the Solar Mesospheric Explorer data of 4 December 1985. The LISM flux measured at Neptune is included for both the Uranus and Neptune models.

The model H_2O number density profiles computed for Neptune are very dependent on the assumed eddy diffusion coefficient, K. Two eddy diffusion coefficients have been suggested for Neptune. The Yelle et al. (1993)/Moses (1992) eddy coefficient, K_{YM}, increases monotonically, while the Romani et al. (1994) eddy coefficient, K_R, rises very sharply in the stratosphere and decreases slightly at lower pressures. In the present work, the assumed methane mixing ratios at the tropopause are 10^{-3} and 10^{-4}, respectively, for K_{YM} and K_R, respectively.

Water profiles were computed for possible Oort and Neptune families of meteoroids as defined by Moses (1992). The Oort population is estimated by assuming a constant spatial density of IDP's from 1 to 30 AU. Because the velocity of the Oort cloud projectiles is proportional to the inverse square root of the heliocentric distance, the flux at 30 AU is decreased by a factor of $1/\sqrt{30}$ relative to the flux at 1 AU. This corresponds to a mass flux of 7.4×10^{-18} g cm^{-2} sec^{-1} at 30 AU. The mass flux of IDP's at 1 AU is taken from Grün et al. (1985). Moses (1992) computed the Neptune-family mass flux of IDP's by assuming that the gravitationally focused flux of IDP's at the inner edge of the Neptune ring system is ~ 100 times the corresponding flux at Saturn, as suggested by Voyager measurements (Smith et al. 1989). This corresponds to an unfocused mass flux at 30 AU of 8.1×10^{-17} g cm^{-2} sec^{-1}, or about twice the flux at 1 AU.

Gravitational focusing enhances these fluxes in the vicinity of Neptune by the factor $(1+v^2_{esc}/u^2)$, where the escape velocity is 22.9 km sec^{-1} and u is the velocity relative to Neptune. For the Oort cloud projectiles Moses (1992) assumes a monochromatic velocity distribution of u = 7.7 km sec^{-1}, the escape velocity at Neptune's orbit, which corresponds to an enhancement factor of 10. For the Neptune-family population the relative velocity of the projectiles is ≈ 30 % or less of Neptune's orbital velocity, or u ~ 1.6 km sec^{-1}, which corresponds to an enhancement factor of about 200. The mass fluxes of the two projectile populations therefore differ by ~ 200. For pure water ice most of the ablation occurs in the 10^{-2} to 1 microbar region, whereas for pure silicate the ablation rate is a maximum from 1 to 10^2 microbars. The total column ablation rates for water ice meteoroids are 7×10^5 and 2×10^8 cm^{-2} sec^{-1} for Oort and Neptune family populations, whereas for silicates the corresponding fluxes are 3×10^5 and 5×10^7 cm^{-2} sec^{-1}, respectively (Moses 1992). The H_2O production rate profile for ablation of particles of Triton-like composition is assumed to have the same altitude dependence as for the pure water ice meteoroids considered by Moses (1992).

3. Results - Neptune

Computed water profiles are shown in Fig. 1 for K_{YM} for both Oort and Neptune families of meteoroids. The agreement between modeled and measured abundances of CH_4 and H is good, whereas C_2H_6 and C_2H_2 are too high, the latter by an order of magnitude. The water profile for the Neptune-family projectiles has a peak density of

Reaction	Rate Constant	Reference
R1 $H_2O + h\nu \rightarrow OH + H$	7.3×10^{-9}	Slanger and Black (1982)
$\rightarrow O + 2H$	7.5×10^{-10}	Stief et al. (1975)
$\rightarrow O(^1D) + H_2$	6.4×10^{-10}	Haddad and Samson (1986)
R2 $OH + H_2 \rightarrow H_2O + H$	$7.7 \times 10^{-12}\ e^{-2100/T}$	Atkinson et al. (1989)
R3 $O + H_2 \rightarrow OH + H$	$8.5 \times 10^{-20}\ T^{2.7}\ e^{-3160/T}$	Baulch et al. (1992)
R4 $O(^1D) + H_2 \rightarrow OH + H$	1.1×10^{-10}	Atkinson et al. (1992)
R5 $OH + C_2H_4 \rightarrow$ prod	$2.2 \times 10^{-12}\ e^{+411/T}$	Atkinson (1986)
R6 $O + CH_3 \rightarrow CH_2O + H$	1.4×10^{-10}	Atkinson et al. (1992)

Table 1. Selected list of reactions involving water and its dissociation products in a hydrogen atmosphere. The units for rate coefficients are sec^{-1} and $cm^3\ sec^{-1}$ for photodissociation and two-body reactions, respectively. The photodissociation coefficients are for globally averaged values of solar flux at 30 AU and during solar maximum conditions at 30 AU.

1.5×10^9 cm^{-3} at 300 km. Below the peak water vapor is lost by condensation, which is assumed to occur with a time constant of 10^7 seconds, sufficiently fast to prevent supersaturation. The Oort-family water profile has a peak density of 6×10^6 cm^{-3} at 300 km. Water is photodissociated yielding primarily OH, but also O and O(^{1}D). The hydroxyl radical reacts with H_2 in the reaction (Table 1)

$$OH + H_2 \rightarrow H_2O + H \qquad \text{R2}$$

which is the key pathway in reforming the water molecule. O(^{1}D) reacts rapidly with H_2 to produce OH, while O also forms OH with H_2 but much more slowly. OH and O also react with hydrocarbons to produce species that are precursors to CO (Prather et al. 1978, Ip 1990). For the results shown in Fig. 1 the principal pathway leading to CO formation is

$$OH + C_2H_4 \rightarrow product \qquad \text{R5}$$

where the product is assumed to be a precursor species to CO. However, only about 10 % of OH contributes to CO formation; the majority proceeds by R2 with the resulting water then being lost by condensation. To first order, the column abundance of CO in Neptune's atmosphere is related to the water influx by the expression (Strobel and Yung 1979)

$$N_{CO} \approx \frac{4\varepsilon\phi_0 H_a^2}{K_0} \qquad (1)$$

where ε is the efficiency of conversion of H_2O to CO, ϕ_0 is the downward flux of water,

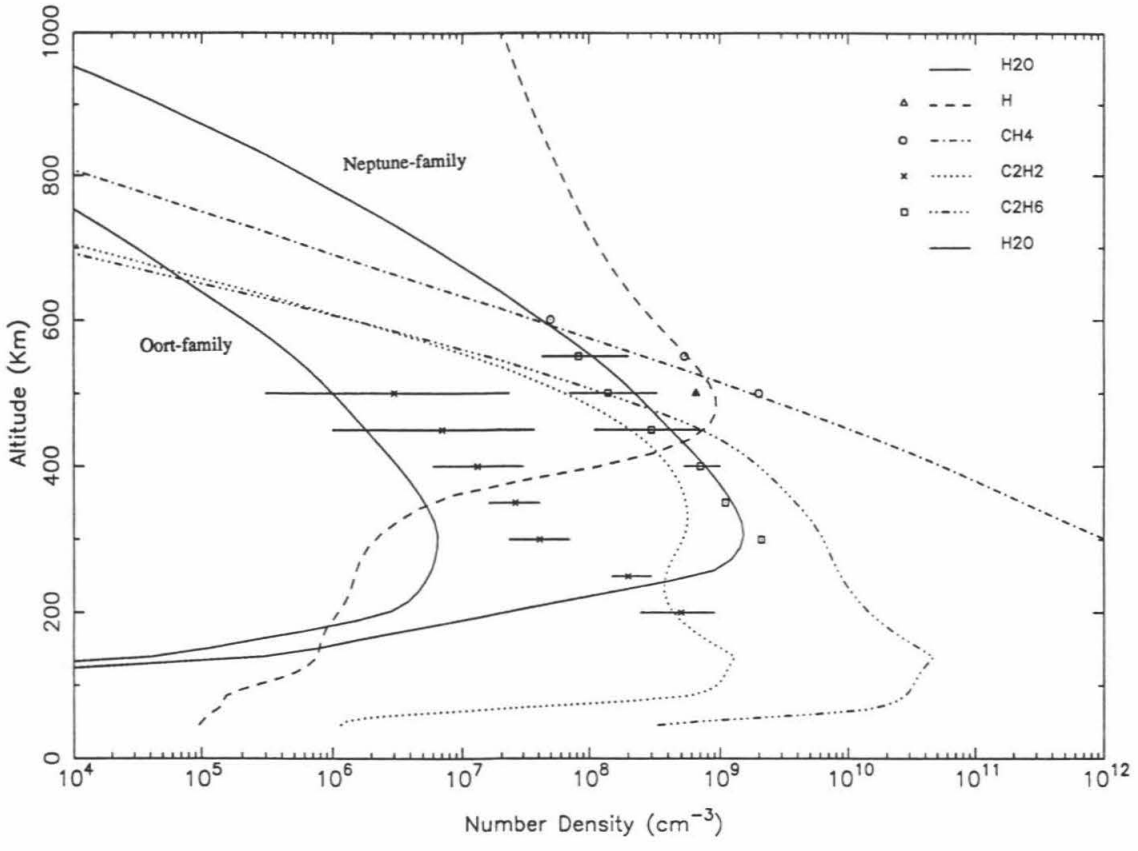

Figure 1. Model number density profiles of the key ultraviolet absorbers in the upper atmosphere of Neptune for the Yelle-Moses eddy coefficient (see text). Observed values are indicated by data points for H_2, CH_4 and C_2H_6 (Yelle et al. (1993)), and for H (Broadfoot et al. (1989)). Computed water profiles for both the Oort-family and Neptune-family of meteoroids are shown. The model hydrocarbon and H profiles are shown for the Oort-family of meteoroids, but do not differ greatly for the two meteoroid families.

H_a is the scale height of the background atmosphere, and K_0 is the eddy diffusivity at the tropopause. For $K_0 = 10^3$ cm^2 sec^{-1} (Moses et al. 1992), $H_a = 17$ km and ε=0.1, the resulting CO column abundance is 2×10^{17} cm^{-2}. Therefore, the flux of Neptune-family meteoroids with the Yelle-Moses eddy profile is about a factor of 100 too small to account for the observed abundance (Rosenqvist et al. 1992, Marten et al. 1993) of CO of 1.7×10^{19} cm^{-2} on Neptune. However, it must be noted that K_0 is not known, and could be $<< 10^3$ cm^2 sec^{-1}.

The corresponding water profiles for the Romani eddy profile are shown in Fig. 2. Although the model overestimates CH_4 and underestimates H, the C_2H_2 and C_2H_6 abundances are in much better agreement than for the K_{YM} profile. The H_2O abundances are reduced from the Yelle-Moses case by about two orders of magnitude at 300 km, illustrating the dramatic effect the eddy profile has on the water profiles. The conversion efficiency for ablated H_2O to form CO is again about 10%. The peaks in the water profiles below 200 km result correspond to supersaturated H_2O, due to the condensation time scale exceeding the diffusion time scale. The supersaturation can be removed by decreasing the condensation timescale to ~ 10^5 seconds.

The UVS solar occultation experiment (Broadfoot et al. 1989) measured absorption from 500 to 1650 Å and was sensitive down to the 5 to 10 % level (Yelle et al. 1993). The tangential column opacity of the computed water profiles at a given altitude and wavelength is given by $\tau(\lambda,z) = \sigma(\lambda)N(z)$, where σ is the absorption cross section and N is the tangential column number density of water molecules. Cross section data for the hydrocarbons (Atreya 1986) and for water (Slanger and Black 1982, Stief et al. 1975,

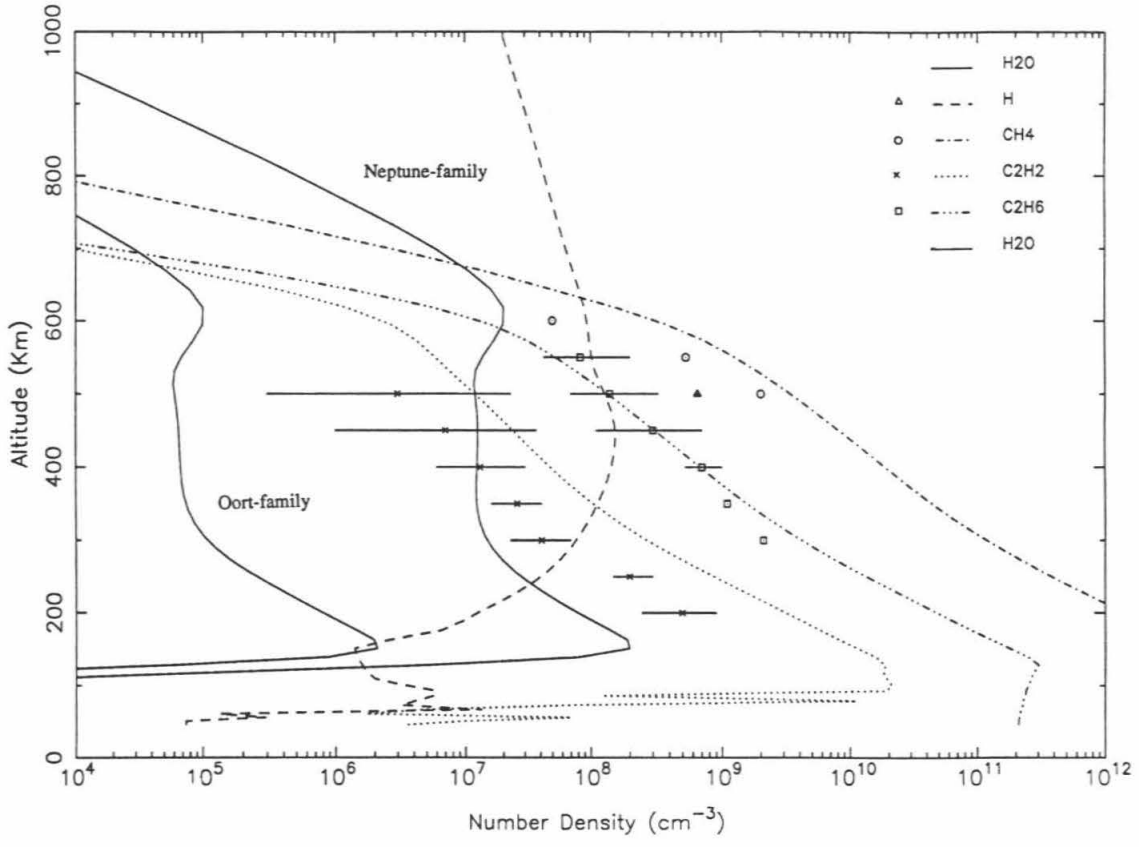

Figure 2. Same as Figure 1 except for the Romani eddy coefficient.

Haddad and Samson 1986) are readily available. Observed opacities were calculated from the extinction coefficients, k_λ, given in Yelle et al. (1993) by integrating along the tangential path,

$$\tau_\lambda(z) = 2\int_z^\infty \frac{k_\lambda(z')\ (z'+R_p)}{((z'+R_p)^2-(z+R_p)^2)^{1/2}}\ dz' \qquad (2)$$

where R_p is the planet radius at the 1 bar level. At 1600 Å, the extinction coefficient was approximated by the expression

$$k_{1600\text{Å}} = 0.060\, e^{-\frac{z}{39.1}} \qquad (3)$$

where z is in kilometers. Equation (3) is accurate for a wavelength range of 1585-1620 Å and from about 160 to 300 km (Yelle et al., 1993), but was assumed to be valid at all altitudes for the present calculations. Results of these calculations are shown in Fig. 3.

Short wavelength (<1000 Å) absorption is dominated by H_2. At 1350 Å absorption by methane is the principal source of opacity. At 1450 Å C_2H_6 is the dominant absorber and will mask the presence of H_2O. By 1550 Å the Neptune-family water profile of Fig. 1 would be detectable (i.e., opacity ≥ 0.1) from below 300 km to about 500 km. According to the profiles of Yelle et. al. (1993), the opacities due to C_2H_2, C_2H_4 and C_2H_6 are less than 0.1 above 300 km at 1550 Å. At 1600 Å water would be detectable to nearly 550 km, as shown in Fig. 3. Yelle et al. (1993) reported that from 1550 to 1600 Å weak absorption was detected below 250 km, but that no absorption was detected above 300 km. This clearly demonstrates that the number density of the water profile resulting from the Neptune-family meteoroids for the K_{YM} profile is at least a factor of 10 too high from

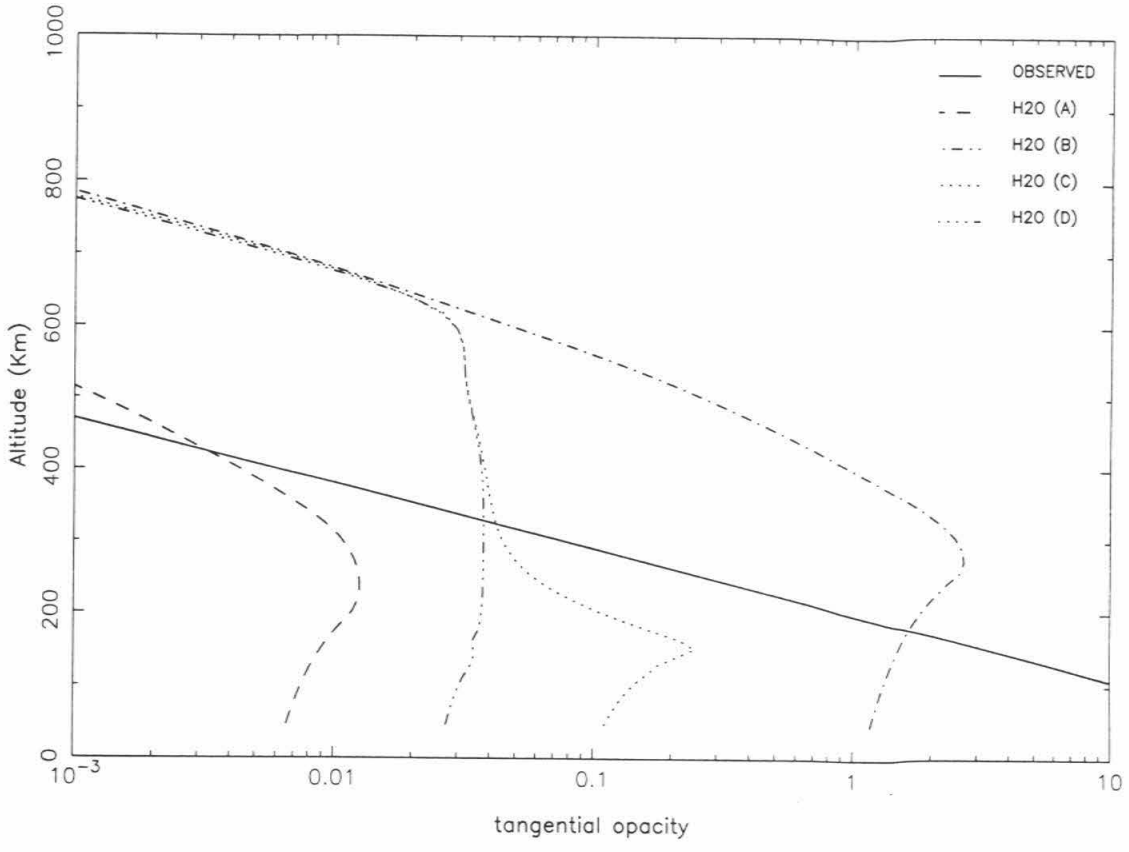

Figure 3. Model tangential column opacities at a wavelength of 1600 Å for several water profiles and the observed opacity as determined by integration of the ~ 1600 Å extinction coefficient of Yelle et al (1993). The water opacity profiles include the Oort and Neptune family meteoroid influx models for the Yelle-Moses eddy coefficient, labelled H_2O A and B, respectively, and the Neptune family meteoroid model for the Romani eddy coefficient for two rates of water condensation. H_2O curve C is for a condensation time of 10^7 seconds and results in a supersaturated water profile, and curve D is for a condensation time of 10^5 seconds, fast enough to prevent supersaturation. The Voyager UVS detection limit is ~ .05 to .10, so only curve A corresponds to a detectable level of water opacity.

300 to 500 km, and suggests that the influx of water can be no more than 2×10^7 molecules cm^{-2} $sec^{-1}$for this eddy profile. This is an order of magnitude smaller than for the Neptune-family flux assumed by Moses (1992). Also shown in Fig. 3, the Neptune-family flux of meteoroids does not produce detectable levels of water for the Romani eddy profile.

Because the altitude range at which ablation occurs and the exact species produced by ablation are uncertain, several sensitivity tests were performed with the photochemical model. As discussed by Moses (1992), actual meteoroids will be a mixture of ice and rock components, so it may be reasonable to expect the bulk of ice ablation to occur at pressures between that of pure water ice and pure silicate meteoroids. Alternatively, a fluffy aggregate composition (density $<<$ 1 g cm^{-3}) could result in ablation of ices at altitudes higher than for icy meteoroids with densities $\approx$ 1 g cm^{-3}. Photochemical model runs were therefore made with the ablation production rate curves used to generate Figures 1 and 2 (arbitrarily) shifted to pressures 10 times higher and 3 times lower. While not significantly affecting the water and hydrocarbon profiles, varying the altitude of H_2O injection modified the ionosphere, reducing the peak ion density by a factor of 2 for the case of high-altitude ablation. The effect of water on giant planet ionospheres has been described previously (Connerney and Waite 1984, Shinagawa and Waite 1989, Majeed and McConnell, Waite and Cravens 1987).

Dissociation of ablated H_2O molecules will result in a change in the oxygen-bearing species injected into the atmosphere. H_2O molecules traveling at the velocity of a meteoroid in Neptune's atmosphere (about 23 km sec^{-1}) have a kinetic energy of 50 eV

relative to the thermal background gas, enough to dissociate and ionize H_2. In the frame of a just-ablated H_2O molecule, background H_2 molecules and He atoms have kinetic energies of 5.4 and 10.9 eV, respectively, enough to dissociate H_2O and OH molecules but not enough to directly ionize them. Unfortunately laboratory data in which H_2O is the projectile and H_2 is the target are not available for these energies. Model runs were therefore made in which the ablated species were assumed to be dissociated to H and OH, and 2H and O instead of remaining as H_2O; $O(^1D)$ was not considered because it rapidly forms OH. Detailed results of these runs will not be given here. The key point, however, is that significant conversion of the oxygen-bearing ablation species to CO only occurs for oxygen atoms, with near total conversion occurring at higher pressures (lower temperatures). The large activation energy of R3 (Table 1) inhibits formation of H_2O from O, allowing O to react with hydrocarbons, principally via (Strobel and Yung 1979)

$$O + CH_3 \rightarrow H_2CO + H \qquad \text{R6}$$

Furthermore, the inhibition of R3 at low temperatures results in a reduction of the water profile to number densities that are just below detectable levels. Increasing the ablation rate by a factor of 10 yields a CO production rate comparable to that required to explain the observations (Rosenqvist et al. 1992, Marten et al. 1993), but also results in detectable levels of H_2O. This does illustrate, however, that penetrative meteoroids producing primarily free oxygen at relatively low temperatures can yield significant quantities of CO, while simultaneously generating undetectable levels of H_2O.

4. Results - Uranus

The photochemical model of Neptune's upper atmosphere was adapted to Uranus and water profiles due to meteoroid ablation were computed. The principal difference between the upper atmospheres of Uranus and Neptune is the extent of vertical mixing, with the former having an eddy diffusivity of only 10^3 to 10^4 cm^2 sec^{-1} at the homopause (Summers and Strobel 1989, Herbert et al. 1987, Bishop et al. 1990) versus the latter's 10^7 to 10^8 cm^2 sec^{-1} (Moses 1992, Yelle et al. 1993, Romani et al. 1994). This results in the ablation region on Uranus being nearly free of hydrocarbons, thus allowing a stronger constraint to be placed on the water influx, and reducing the conversion efficiency of H_2O to CO. Hydrocarbon and water number density profiles for Uranus are shown in Fig. 4 for an Oort-family flux (scaled to Uranus) and for 10 times an Oort flux. The temperature profile corresponding to a thermospheric heat source at ~ 10^{-5} microbar was employed (Stevens et al. 1993), although similar water profiles are obtained for the temperature profile of Herbert et al. (1987). Sensitivity tests of the type described above for Neptune produce profiles that do not differ significantly from the profiles in Fig. 4. The efficiency of conversion of H_2O and OH to CO is < 10 %, while for O influx in the 0.1 to 10 microbar range the efficiency is < 20%. The profiles in Fig. 4 imply a maximum water influx at Uranus of 4×10^6 $cm^{-2}sec^{-1}$, corresponding to two times the Oort influx. Shinagawa and Waite (1989) suggested an upper limit of 10^6 cm^{-2} sec^{-1} , although they did not relate this to the meteoroid influx. At 1600 Å, hydrocarbon absorption and Rayleigh scattering are not important above 300 km.

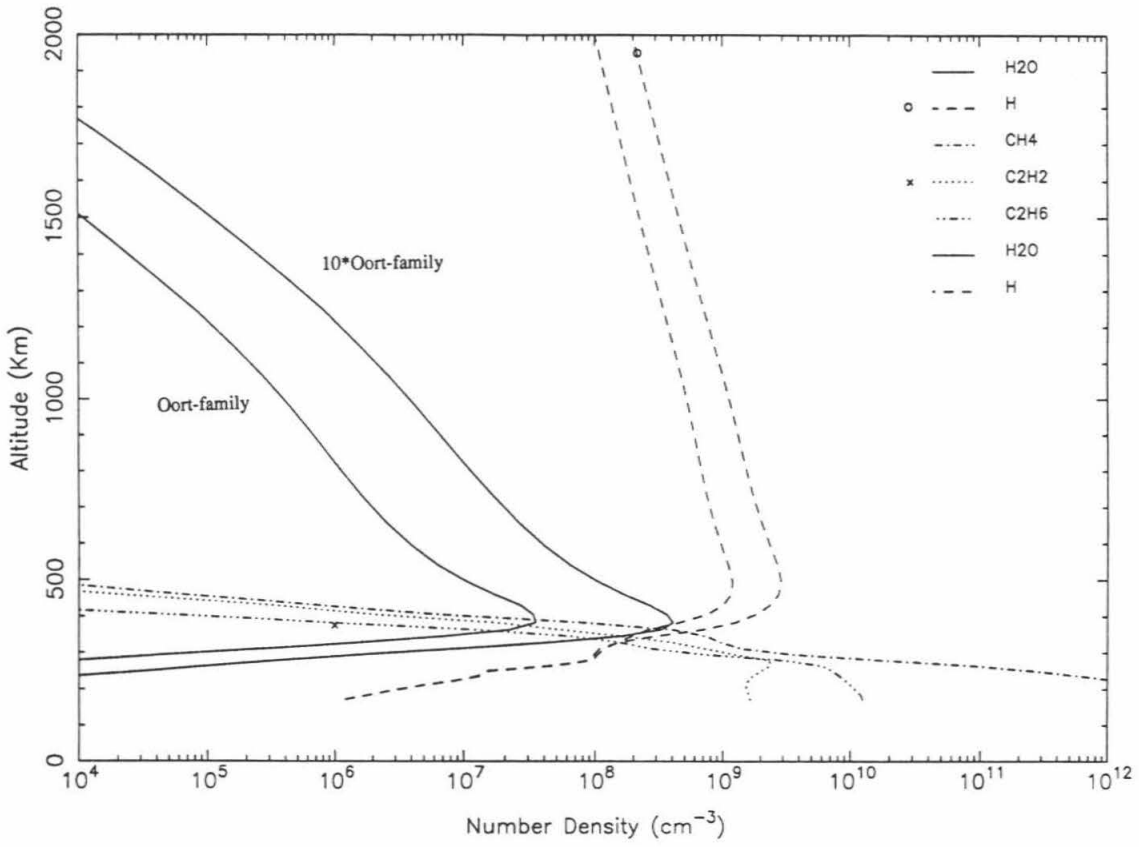

Figure 4. Same as Fig. 1 except for the upper atmosphere of Uranus. Observed values are from Herbert et al. (1987). The meteoroid ablation rates have been scaled (by a factor of 1.5) to Uranus from the values computed for Neptune (Moses 1992). The water profiles were computed for an Oort-family of meteoroids and for a meteoroid flux a factor of 10 higher than the Oort case.

The weak eddy mixing on Uranus renders the water profile sensitive to vertical advection velocities > D/H, where D is the molecular diffusion coefficient and H the scale height for H_2O. At the peak in the water profiles (380 km), the chemical loss and diffusion time constants are ~ 2×10^7 sec, and D/H~.03 cm sec^{-1}. Vertical advection velocities > .03 cm sec^{-1} may not be unreasonable to expect above the hydrocarbon homopause on Uranus. Advective control of the water profile in Earth's mesosphere has been proposed by Bevilacqua et al. (1990).

The extended exosphere of Uranus limits the lifetime of dust in the inner rings and leads to a significant flux of material to the upper atmosphere of Uranus (Esposito and Colwell 1989). Because the ultraviolet solar occultation measurements were made near the equator, the expected region of greatest ring particle influx, it may be possible to constrain the H_2O abundance of the dust-sized ring particles. Esposito and Colwell (1989) estimate a mass influx of 6×10^{11} g yr^{-1} due to erosion of ring particles and subsequent atmospheric gas drag. Rizk and Hunten (1990) assume the ring particles enter the atmosphere in an equatorial strip of width L ~ 1000 km. The mass influx in this strip is then 1×10^{-14} g cm^{-2} sec^{-1}. The column production rate of H_2O is to first order given by $f_w\phi/\mu$, where f_w is the volume fraction of water in the ring particles, ϕ is the particle mass influx, and μ is the mean molecular mass of an ablated molecule. An upper limit to f_w can be determined from the H_2O production rate due to ablation, and the lack of water detection by the Voyager UVS. The latter places an upper limit on the H_2O number density of n_{max} ~ 10^8 cm^{-3}. The constraint on f_w is then

$$f_w < \frac{n_{\max} H_w \mu K_h}{\phi L^2} \qquad (4)$$

where K_h is the horizontal eddy diffusion coefficient, and H_w is the scale height of water. For $K_h \sim 10^{10}$ cm^2 sec^{-1} (Rizk and Hunten 1990), $H_w \approx 30$ km, and $\mu \approx 30$ amu, equation (3) yields $f_w < 1$, implying that even if the ring particles were pure water ice, the resulting water profile would not have been detected. As the albedo of the Uranian ring particles is known to be very low (Smith et al. 1986), most likely $f_w << 1$, making the detection of water even less likely.

5. Summary and Conclusions

At present it is difficult to constrain the influx of water into Neptune's atmosphere due to the uncertainty in the eddy diffusion coefficient. The eddy coefficient of Romani et al. (1994) yields the best overall agreement between model and observed hydrocarbons, and predicts rapid transport of water out of the ablation region to lower altitudes where condensation occurs. As a result the water abundance is too low to result in an observable opacity even for the Neptune family of meteoroids defined by Moses (1992). Larger planet-family populations, sufficient to account for the observed CO, result in detectable levels of H_2O, and can therefore be ruled out. These results imply that the stratospheric CO seen on Neptune (Rosenqvist et al. 1992, Marten et al. 1993) is not from an extraplanetary source, but instead is mixed upward from the troposphere, as suggested previously (Atreya et al. 1992, Lodders and Fegley 1993). If the ablated H_2O is

dissociated to ground state O relatively deep (pressure > 10 microbar) in the atmosphere, larger influxes of IDP's are allowed.

The Yelle-Moses eddy profile yields stronger constraints on the IDP influx. Except for the case of ablation occurring at higher pressures and the water being dissociated to O, the model results for the Yelle-Moses eddy profile require that the influx of water to Neptune be $\leq 2 \times 10^{7}$ cm^{-2} sec^{-1} to be consistent with the non-detection of H_2O by Voyager. This value corresponds to a mass flux into Neptune's atmosphere of 2×10^{-15} g cm^{-2} sec^{-1} for meteoroids that are 30% water ice. The upper-limit to the unfocused Oort-family meteoroid flux at 30 AU (for the velocity distribution described above) is therefore 2×10^{-16} g cm^{-2} sec^{-1}. The Oort-family flux assumed here and by Moses (1992) is always less than this value. The upper limit to the unfocused Neptune-family projectile flux is 1×10^{-17} g cm^{-2} sec^{-1} for particles with mean velocity equal to 30% of Neptune's orbital velocity. Therefore, the Neptune-family flux defined by Moses (1992) must be reduced by decreasing the spatial density at 30 AU by an order of magnitude if the Yelle-Moses eddy profile is correct. This upper limit is more than 10^3 times the dust mass flux estimated above due to collisions among Kuiper belt objects, suggesting that an accurate assessment of dust production in the Kuiper belt may provide a much stronger constraint on the dust flux at Neptune than the photochemical constraint presented here.

The upper limit to the Uranian water influx of 4×10^{6} molecules cm^{-2} sec^{-1} implies maximum unfocused mass fluxes of 8×10^{-17} and 4×10^{-18} g cm^{-2} sec^{-1} for the Oort and Uranus-family meteoroids, respectively, at the orbit of Uranus, consistent with an Oort-family of IDP's but not with a large population of Uranus-family particles. The ring

particle influx at Uranus, for the conditions outlined by Rizk and Hunten (1990), will not produce a detectable abundance of H_2O, even for the assumption of pure water ice particles. The IDP results for both Uranus and Neptune assume IDP's of cometary or Triton-like composition, and are not consistent with an influx of meteoroids that are significantly depleted in water ice (<< 30 % by mass).

It is interesting to note that models of water influx to Jupiter (Prather et al. 1978) have invoked high values of meteoroidal influx (depending on the assumed eddy diffusion coefficient) in an effort to explain what was then believed to be stratospheric CO. Later measurements (Noll et al. 1988) have shown that the CO is actually in the troposphere, strongly implying that the CO is not the result of a present day extraplanetary source of water, but rather is from the interior of the planet. Similarly, the oxygen ion source invoked by Strobel and Yung (1979) must be reduced, or its resulting chemistry modified appropriately, so as to not result in detectable levels of stratospheric CO in their model of Jupiter's stratosphere.

Acknowledgements

Numerous discussions with J. Moses are gratefully acknowledged. J. Cuzzi, A. Ingersoll, J. Moses and Y. Yung provided helpful comments on an earlier draft of this paper. Partial support was provided by the Neptune Data Analysis Program, NASA grant # NAGW-2362 (to Y. L. Yung).

References

Allen, M., Y. L. Yung, J. W. Waters 1981. Vertical transport and photochemistry in the terrestrial mesosphere and lower thermosphere. *J. Geophys. Res.* 86, 3617-3627.

Atkinson, R. 1986. Kinetics and mechanisms of gas-phase reactions of the hydroxyl radical with organic compounds under atmospheric conditions. *Chem. Rev.* 86, 69.

Atkinson, R., D. L. Baulch, R. A. Cox, R. F. Hampson, Jr., J. A. Kerr, J. Troe 1989. Evaluated kinetic data for atmospheric chemistry. Supplement III, *J. Phys. Chem. Ref. Data* 18, 881-1097.

Atkinson, R., D. L. Baulch, R. A. Cox, R. F. Hampson, Jr., J. A. Kerr, J. Troe 1992. Evaluated kinetic and photochemical data for atmospheric chemistry, Supplement IV. *J. Phys. Chem. Ref. Data* 21, 1125-1568.

Atreya, S. K. 1986. *Atmospheres and Ionospheres of the Outer Planets and their Satellites.* (Springer-Verlag, Berlin).

Atreya, S. K., T. C. Owen, D. Gautier, A. Marten 1992. HCN and CO on Neptune: and intrinsic origin. *Bull. Am. Astron. Soc.* 24, 972.

Baulch, D. L., C. J. Cobos, R. A. Cox, C. Esser, P. Frank, Th. Just, J. A. Kerr, M. J. Pilling, J. Troe, R. W. Walker, J. Warnatz 1992. Evaluated kinetic data for combustion modeling. *J. Phys. Chem. Ref. Data* 21, 411-429.

Bevilacqua, R. M., D. F. Strobel, M. E. Summers, J. J. Olivero, M. Allen 1990. The seasonal variation of water vapor and ozone in the upper mesosphere: implications for vertical transport and ozone photochemistry. *J. Geophys. Res.* 95, 883-893.

Bishop, J., S. K. Atreya, F. Herbert, P. Romani 1990. Reanalysis of Voyager 2 UVS occultations at Uranus: hydrocarbon mixing ratios in the equatorial stratosphere. *Icarus* 88, 448-464.

Broadfoot, A. L. et al. 1989. Ultraviolet spectrometer observations of Neptune and Triton. *Science* 246, 1459-1466.

Burns, J. A., M. R. Showalter, J. N. Cuzzi, J. B. Pollack 1980. Physical processes in Jupiter's ring: clues to its origin by Jove!. *Icarus* 44, 339-360.

Connerney, J. E. P. and J. H. Waite 1984. New model of Saturn's ionosphere with an influx of water from rings. *Nature* 312, 136-138.

Cuzzi, J. N. and R. H. Durisen 1990. Bombardment of planetary rings by meteoroids: general formulation and effects of Oort cloud projectiles. *Icarus* 84, 467-501.

Esposito, L. W. and J. E. Colwell 1989. Creation of the Uranus rings and dust bands. *Nature* 339, 605-607.

Flynn, G. J. 1994. Does the Kuiper belt contribute significantly to the zodiacal cloud and the stratospheric interplanetary dust? *Lunar Planet. Science Conf. Abstracts*, 399-400.

Goertz, C. K. and G. E. Morfill 1983. A model for the formation of spokes in Saturn's ring. *Icarus* 53, 219-229.

Grün, E., H. A. Zook, H. Fechtig, R. H. Giese 1985. Collisional balance of the meteoritic complex, *Icarus* 62, 244-272.

Gurnett, D. A., W. S. Kurth, L. J. Granroth, S. C. Allendorf, R. L. Poynter 1991. Micron-sized particles detected near Neptune by the Voyager 2 plasma wave instrument.

J. Geophys. Res. 96, 19177-19186.

Haddad, G. N. and J. A. R. Samson 1986. Total absorption and ionization cross sections of water vapor between 100 and 1000 Å. *J. Chem. Phys.* 84, 6623-6626.

Herbert, F., B. R. Sandel, R. V. Yelle, J. B. Holberg, A. L. Broadfoot, D. E. Shemansky, S. K. Atreya, P. N. Romani 1987. The upper atmosphere of Uranus: EUV occultations observed by Voyager 2. *J. Geophys. Res.* 92, 15093-15109.

Humes, D. H. 1980. Results of Pioneer 10 and 11 meteoroids experiments: interplanetary and near-Saturn. *J. Geophys. Res.* 85, 5841-5852.

Ip, W.-H. 1990. Meteoroid ablation processes in Titan's atmosphere. *Nature* 345, 511-512.

Lodders, K. and B Fegley 1993. The origin of carbon monoxide in Neptune's atmosphere. *Bull. Am. Astron. Soc.* 25, 1080.

Majeed, T. and J. C. McConnell 1991. The upper ionospheres of Jupiter and Saturn, *Planet. Space Sci.* 39, 1715-1732.

Marten, A., D. Gautier, T. Owen, D. Sanders, H. E. Matthews, S. K. Atreya, R. J. P. Tilanus, J. Deane 1993. First observations of CO and HCN on Neptune and Uranus at millimeter wavelenths and their implications for atmospheric chemistry. *Astrophys. J.* 406, 285-297.

Moses, J. I. 1992. Meteoroid ablation in Neptune's atmosphere. *Icarus* 99, 368-383.

Moses, J. I., Y. L. Yung, M. Allen 1992. Hydrocarbon nucleation and aerosol formation in Neptune's atmosphere. *Icarus* 99, 318-346.

Mount, G. H. and G. J. Rottman 1983. The solar absolute spectral irradiance 1150-3173 Å: May 17, 1982. *J. Geophys. Res.* 88, 5403-5410.

Noll, K. S., R. F. Knacke, T. R. Geballe, A. T. Tokunaga 1988. The origin and vertical distribution of carbon monoxide in Jupiter. *Astrophys. J.* 324, 1210-1218.

Prather, M. J., J. A. Logan, M. B. McElroy 1978. Carbon monoxide in Jupiter's upper atmosphere: an extraplanetary source. *Astrophys. J.* 223, 1072-1081.

Rizk, B. and D. M. Hunten 1990. Solar heating of the Uranian mesopause by dust of ring origin. *Icarus* 88, 429-447.

Romani, P. N., J. Bishop, B. Bézard, S. Atreya 1994. Methane photochemistry on Neptune: ethane and acetylene mixing ratios and haze production. *Icarus* 106, 442-463.

Rosenqvist, J. E., E. Lellouch, P. N. Romani, G. Paubert 1992. Millimeter-wave observations of Saturn, Uranus, and Neptune: CO and HCN on Neptune. *Astrophys. J. Lett.* 392, L99-L102.

Shinagawa, H. and J. H. Waite 1989. The ionosphere of Neptune. *Geophys. Res. Lett.* 16, 945-948.

Slanger, T. G. and G. Black 1982. Photodissociative channels at 1216 Å for H_2O, NH_3, and CH_4, *J. Chem. Phys.* 77, 2432-2437.

Smith, B. A. et al. 1986. Voyager 2 in the Uranian system: imaging science results. *Science* 233, 43-64.

Smith, B. A. et al. 1989. Voyager 2 at Neptune: imaging science results. *Science* 246, 1422-1449.

Stevens, M. H., D. F. Strobel, F. Herbert 1993. An analysis of the Voyager 2 ultraviolet spectrometer occultation data at Uranus: inferring heat sources and model

atmospheres. *Icarus* 100, 45-63.

Stief, L. J., W. A. Payne, R. B. Klemm 1975. A flash photolysis-resonance flourescence study of the formation of $O(^1D)$ in the photolysis of water and the reaction of $O(^1D)$ with H_2, Ar, and He. *J. Chem. Phys.* 62, 4000-4008.

Strobel, D. F. and Y. L. Yung 1979. The Galilean satellites as a source of CO in the Jovian upper atmosphere. *Icarus* 37, 256-263.

Summers, M. E. and D. F. Strobel 1989. Photochemistry of the atmosphere of Uranus. *Astrophys. J.* 346, 495-508.

Torr, M. R. and D. G. Torr 1985. Ionization frequencies for solar cycle 21: revised. *J. Geophys. Res.* 90, 6675.

Yelle, R. V., F. Herbert, B. R. Sandel, R. J. Vervack, Jr., T. M. Wentzel 1993. The distribution of hydrocarbons in Neptune's upper atmosphere. *Icarus* 104, 38- 59.

Waite, J. H. and T. E. Cravens 1987. Current review of the Jupiter, Saturn, and Uranus ionospheres. *Adv. Space Res.* 12, 119-134.

Woods, T. N. and G. J. Rottman 1990. Solar EUV irradiance derived from a sounding rocket experiment on Novenber 10, 1988. *J. Geophys. Res.* 95, 6227-6236.

PAPER IV

A Chemical Kinetics Model for Analysis of the Comet Shoemaker-Levy 9 Impacts with Jupiter

James R. Lyons

Division of Geological and Planetary Sciences

and

Anuraag Kansal

Division of Chemistry and Chemical Engineering

California Institute of Technology

Pasadena, California 91125

Submitted to Icarus

September, 1995

Abstract

A chemical kinetic model is developed for gas phase species containing the elements H,C,N,O,S and Si which is valid at high temperatures and for H-dominated compositions. The kinetic model is tested by running it to steady state equilibrium and then comparing the results with species abundances as determined from a thermochemical model for a range of temperatures (1000 to 4000 K) and pressures (1 μbar to 1 bar). By such comparison, incorrect reaction rate coefficients, missing species, and missing chemical pathways were identified and corrected in the kinetic model. Fairly good agreement between kinetics and thermochemistry was obtained for species comprised of H,C,N,O but agreement was less satisfactory for species containing S and Si, due to a lack of rate coefficient data. Some species, such as S_2, were noted to undergo a significant transient overshoot in abundance, particularly at low pressures. Such overshoot may have contributed to the large observed abundances of some of these species.

The kinetic model was run for pressure-temperature (P-T) histories likely to be relevant to the Comet Shoemaker-Levy 9 impacts on Jupiter. Model runs were made for a variety of fireball and plume reentry temperatures, and for two compositions (C>O and C<O). For C>O, S_2 and CS_2 are favored by low plume temperatures (~1500 K), whereas CS is produced in plumes with temperature > 2500 K. Atomic Si is abundant in hot plumes (~3500 K). NH_3 >> HCN is favored for lower fireball temperatures (~2000 K), as is CO ~ 10×H_2O. C>O requires a greater than 50:1 mix of Jupiter gas to vaporized comet, or Jovian gas from pressures < several bars (assuming C<O below the Jovian water

cloud). For C<O, CO and H_2O dominate the carbon and oxygen species, and species such as SO, NO and SiO became significant; S_2 remained abundant. The results suggest that the observed atomic and molecular species were produced over a range of temperatures. When run with similar P-T histories, our model and the model of Zahnle et al. (1995) yield different results for sulfur species. However, we do confirm the importance of disequilibrium chemistry during plume reentry. A brief consideration of atomic metals suggests that thermal emission up to ~ 1 hour after a given impact may be due to reentry of a non-visible, high velocity plume component. Metal ion number densities may have been high enough to yield a significant local enhancement in the Pedersen conductivity, particularly if the ions are at pressures < 0.1 μbar.

1. Introduction

The impact of the fragments of Comet Shoemaker-Levy 9 with Jupiter resulted in a wealth of observable physical and chemical processes. A wide variety of chemical species were observed, many not previously detected in giant planet atmospheres. In addition, an extensive and dark impact debris formed massive scars on Jupiter. The composition and origin of this impact debris is as yet unknown. In this paper we focus on a kinetic description of the high temperature chemistry of gases of Jovian and mixed, Jovian and cometary, composition. Our main goal is to explain the origin of the various spectroscopically detected gas phase species. However, we also consider plausible compositions and formation mechanisms for the impact debris.

Impact-generated molecules were observed with several different instruments. Noll et al. (1995) reported UV observations made with the Hubble Space Telescope (HST) Faint Object Spectrograph (FOS) at the G/S impact sites a few hours and a few days after impact. HST detected several sulfur species (S_2, CS_2, H_2S) in absorption, and CS and several neutral and ionic atomic metals in emission. Additionally, upper limits were placed on H_2O, SO, SO_2 and SiO. In the visible, metal lines were detected for Na, Ca, Mg, Fe, K, and Li by Roos-Serote et al. (1995) and Fitzsimmons et al. (1995). Many spectroscopic observations were made in the near-infrared. Crisp and Meadows (1995) reported seeing CO and H_2O evolve over timescales of tens of minutes at the R impact site. Encrenaz et al. (1995) reported detection of CH_4, H_3^+, and H_2. In the submillimeter wavelength range, Marten et al. (1995) detected HCN. At millimeter wavelengths

Lellouch et al. (1995) reported observing CO, OCS and CS at various times from 10 hours after a given impact to several days later for several individual and complex impact sites. Finally, the composition of the impact debris is constrained by two observations. First, the imaginary component of the index of refraction of the debris particles has been determined from HST observations made at multiple phase angles and at wavelengths from the near IR to the near UV. Second, the detection of propagating waves at several of the impact sites (Hammel et al. 1995) places a constraint on either the volatility or the "stickiness" of the debris particles.

Initial modeling of the high temperature sulfur chemistry of the impacts has been performed by Zahnle et al. (1995). They demonstrated the importance of kinetic (i.e., disequilibrium) processes in the formation of S_2 and other sulfur species. However, they did not compare their chemical kinetics model against thermodynamic predictions by running the kinetics to equilibrium. It is, therefore, difficult to evaluate the accuracy of their model. On the other hand, they did use a 2-D hydrodynamic code (MacLow and Zahnle 1994) to compute the total mass of atmosphere that experienced a given temperature-pressure history. We have not done this here, choosing instead to focus on the high temperature chemistry. Our results are therefore not directly comparable to the spectroscopic observations, except qualitatively.

2. Comparison of Kinetics with Equilibrium Thermodynamics

The high temperatures associated with the entry of Comet SL9 into Jupiter's

atmosphere suggest that chemical equilibrium will be achieved for some portions of the impact, particularly the fireball phase. However, lower temperature regions, and the low temperatures associated with plume reentry (Zahnle et al. 1995), will cool before reaching chemical equilibrium. Hence, kinetics effects are likely to be important. Compilations exist for gas phase kinetic rate coefficients at high temperatures (Baulch et al. 1981), with specific application to combustion chemistry. The literature is fairly complete with regard to H-C-O-N systems, but is lacking in rate coefficient data for sulfur, silicon, and metals, especially under reducing conditions. In order to provide some constraint on the kinetics of an H-C-O-N-S-Si system, we have made detailed comparisons of our kinetics code, run to equilibrium at a specific temperature and pressure, with thermodynamic values predicted by a standard thermochemistry code. The tedious task of adjusting the kinetics to obtain agreement with the thermodynamics is perhaps the best way to ensure accurate kinetic behavior when experimental data are lacking.

The kinetics code we used is the one-dimensional photochemical code developed by Allen et al. (1981), adapted to run as a zero-dimensional box model. At present, the kinetics model has over 210 species and 1700 reactions. The species and reactions will not be listed here, but are available upon request from the authors. A reduced set of species and reactions is shown in Appendix 1, however, this reaction set has not yet been fully tested against the full set. Thermodynamic calculations were performed with a code developed at the University of Chicago and provided by S. Yoneda (Yoneda and Grossman 1994). Results of the equilibrium comparison are shown in Figures 1a-d for an H-C-O-N-S system at a pressure of 1 bar. The chemical system is dominated by H, with

trace species mixing ratios (relative to H_2) of 2×10^{-3}, 1×10^{-3}, 3×10^{-4}, and 1×10^{-4} for C, O, N, and S respectively. The values for C and N are for Jovian CH_4 and NH_3 (Atreya,1986); S is an estimate for Jovian gas below the NH_4SH cloud. The amount of O is that expected for a mixture of Jovian gas and cometary material in a ratio of about 200 to 1 by number, or from Jovian gas at a pressure of $\approx$ 2 bars. A significantly higher cometary fraction (< 50 to 1) results in O>C, assuming a solar ratio of O/C for the bulk comet, and results in a vastly different set of chemical species at equilibrium; equilibrium results for this case are not presented. The parent species in the kinetics code were H_2, CH_4, NH_3, H_2S and H_2O. Agreement between the kinetics and thermodynamics codes is considered to be acceptable if the mixing ratios of the resulting species are within an order of magnitude of each other over the full range of temperatures (1000 to 4000 K) considered. Thus, the hydrocarbons, nitrogen species, and oxygen species shown in Figures 1a-c exhibit reasonably good agreement. (Discrepancies arise at 1000 K for some species due to difficulty in attaining equilibrium with the kinetics code.) The sulfur species, Figure 1d, show considerable error at 1500 K and 2000 K. The sulfur kinetics suffers not only from unknown rate coefficients, but probably also from missing reaction pathways; clearly more work needs to be done on sulfur. Although not shown, agreement between kinetics and thermodynamics improves as the pressure is decreased.

Figure 2 shows the equilibrium time, τ_{eq}, defined here as the time required for a species to attain one-half of its equilibrium value, for CH_4 as a function of temperature and pressure. At 1000 K negligible change occurred in CH_4, so a value for the equilibrium time is not defined. Loss of CH_4 occurs primarily by thermal dissociation and

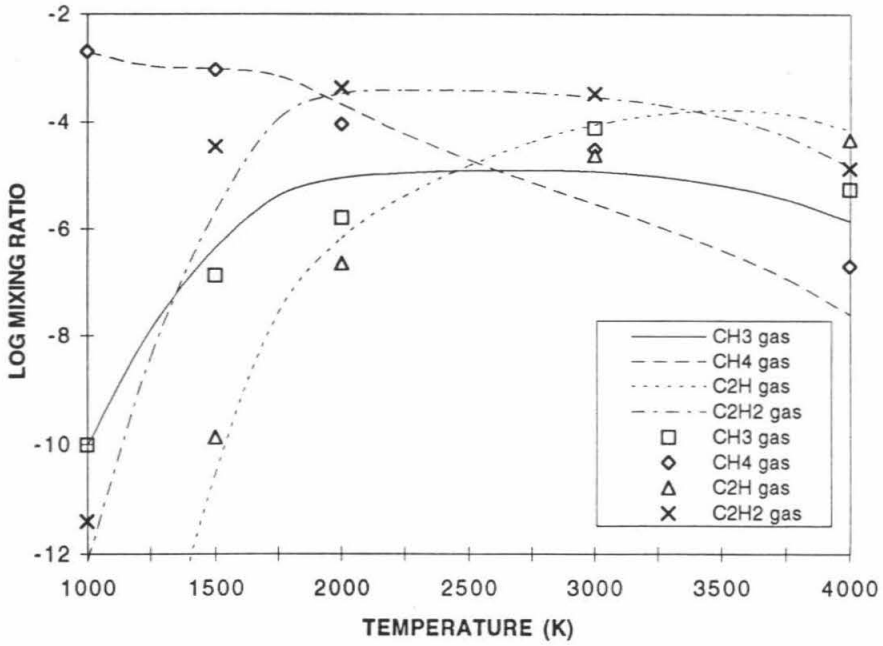

Fig. 1a. Comparison of kinetics code, run to steady state equilibrium (symbols), with thermochemical equilibrium values (curves) for several hydrocarbon species.

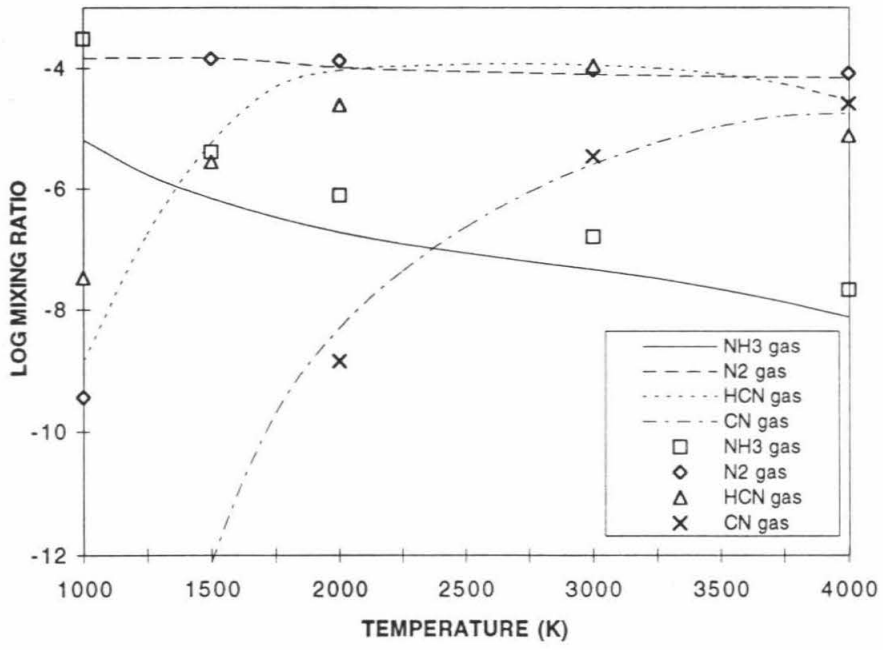

Fig. 1b. Same as Fig. 1a but for several nitrogen species.

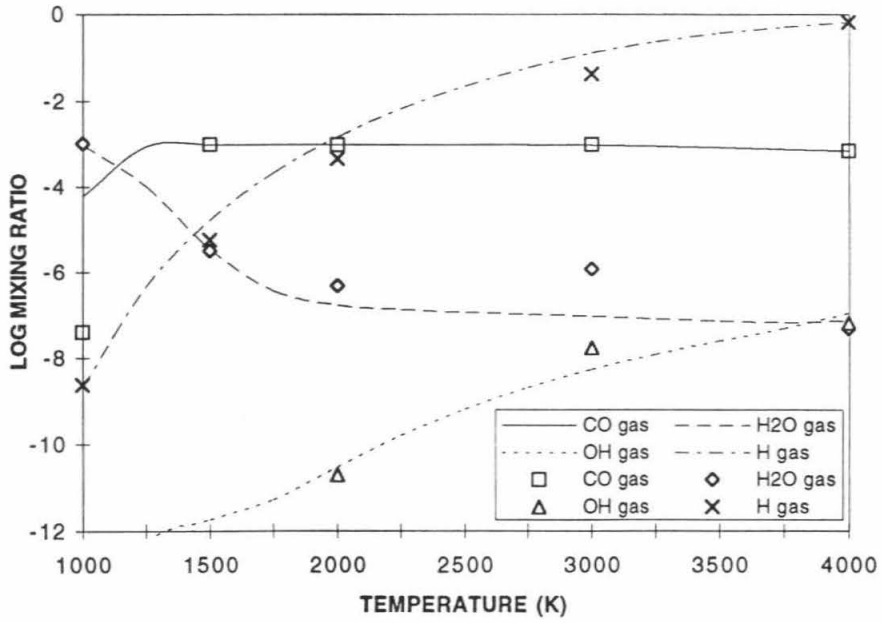

Fig. 1c. Same as Fig. 1a, but for several oxygen species and atomic hydrogen.

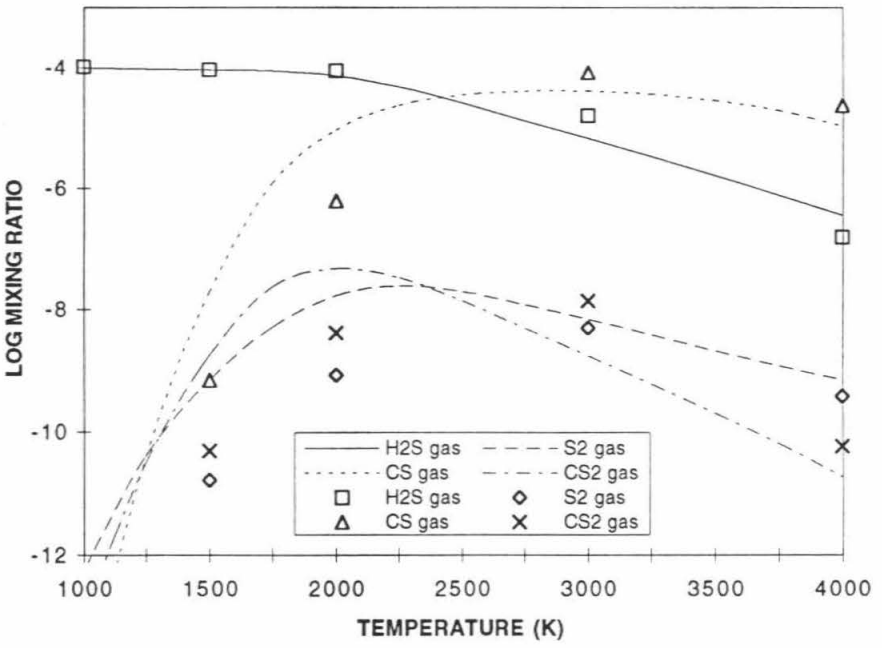

Fig. 1d. Same as Fig. 1a, but for several sulfur species.

by reaction with hydrogen atoms. The values of τ_{eq} at low pressures greatly exceed cooling timescales (see below), and clearly demonstrate that disequilibrium processes are inevitible during plume reentry (Zahnle et al. 1995). Although not shown here, the equilibrium time is, in general, different for different species, illustrating the fact that a single quench temperature is not applicable to most chemical systems.

The parent species, CH_4, NH_3, H_2S, and H_2O, decrease monotonically with time, allowing a well-defined value of τ_{eq} to be determined. Secondary species often exhibit overshoot or other complex behavior, as shown by S_2 in Figure 3. The figure shows the S_2 abundance versus time as determined by the kinetics code for a temperature of 3000 K. At 1μbar a difference of five orders of magnitude exists between the peak S_2 mixing ratio and the equilibrium value. This kind of overshoot behavior may have contributed to the high S_2 abundances seen by HST (Noll et al. 1995).

3. Impact Kinetics Results

By specifying a pressure-temperature history for the kinetics code (with zero space dimensions), an estimate can be made of the chemical evolution of a given parcel of gas during the course of an impact. Following Zahnle et al. (1995), the time history of the impact is broken into three stages: 1) rising fireball phase undergoing adiabatic expansion, 2) plume phase travelling along a ballistic trajectory, and 3) plume reentry and subsequent radiative cooling. Two earlier phases also exist, but are neglected here: 1) entry phase in which very high temperatures ($>10^4$ K) result in ionization of Jovian gas and cometary

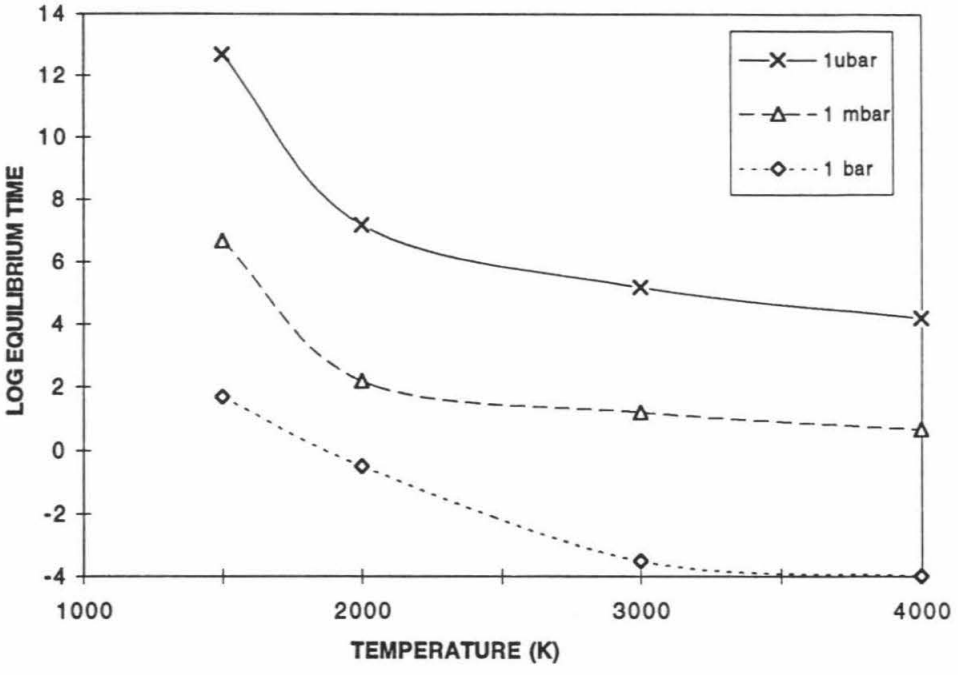

Fig. 2. Equilibrium times for CH_4 as determined from the kinetics model at various pressures and temperatures. Methane, a parent species, displays a fairly regular behavior.

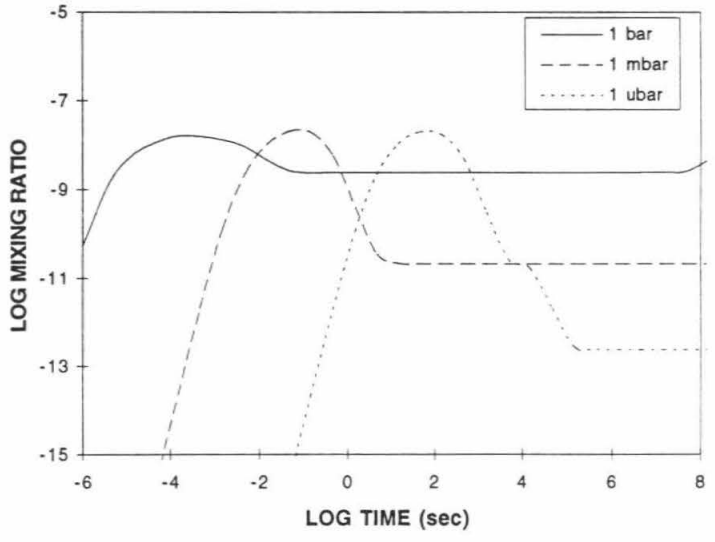

Fig. 3. Mixing ratio of S_2 versus time as determined from the kinetics code at 3000 K. Note the overshoot past the steady state value, particularly at low pressures.

material, and 2) expansion phase in which the fireball expands until achieving ambient pressure. Bounces of the reentering plume are also not considered.

A typical P-T history is shown in Figure 4. The pressure of the rising fireball phase is given by

$$P(t) = P_0 e^{-vt/H} \quad (1)$$

where P_0 is the initial fireball pressure, v is the fireball velocity assumed to be constant at 3 km sec^{-1}, t is time in seconds, and H is the atmospheric scale height assumed to be constant at 20 km. Temperature is determined from the adiabatic relation, $T=T_0(P/P_0)^{(\gamma 1)/\gamma}$, where T_0 is the initial fireball temperature and γ is the ratio of specific heats. γ is assumed to be 1.4, but in reality will decrease below 1.4 as additional vibrational degrees of freedom contribute to the molecular heat capacities at higher temperatures, and will increase above 1.4 at still higher temperatures as H_2 dissociation occurs. Additionally, H is not constant and v is not likely to be constant with altitude. Incorporating more exact representations of v, H, and γ is a simple matter, but has not been done since we are only trying to illustrate the range of possible chemical kinetic behavior; properly done, the kinetics would be computed along a set of P-T histories determined from detailed hydrodynamic codes (e.g., Boslough et al. 1994; MacLow and Zahnle 1994; Takata et al. 1994).

During the ballistic phase of the plume, the temperature is assumed to decrease to a minimum of 200 K, and the pressure decreases to a minimum of 10^{-2} μbar. Several processes have been neglected, including expansion of the plume due to divergent gas/particle trajectories, photochemical processing of the plume material, and condensation

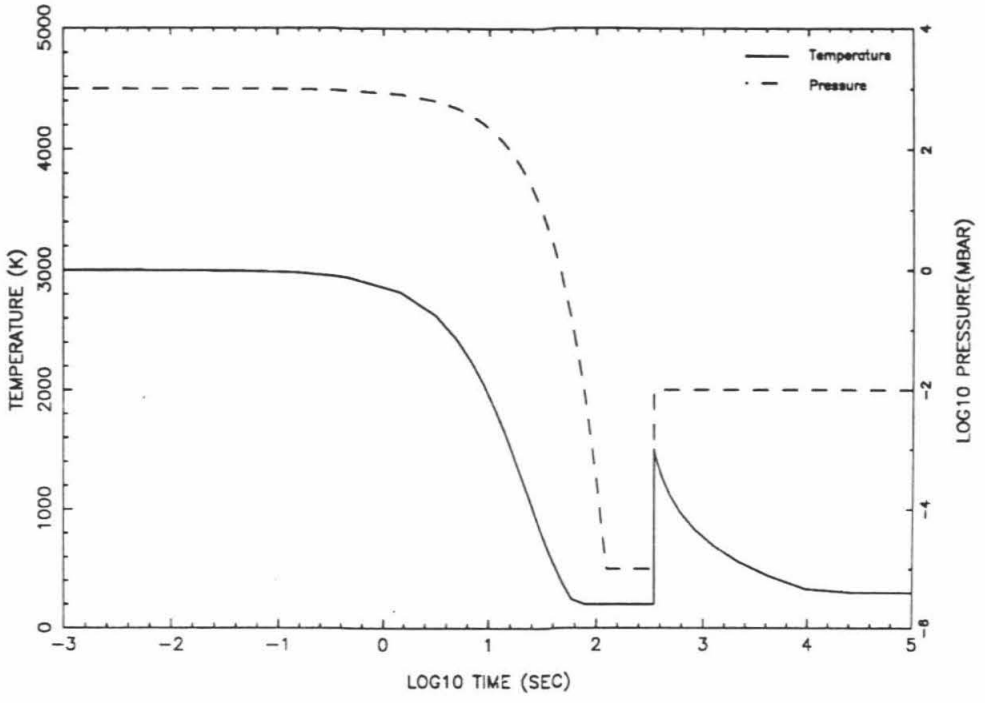

Fig. 4. Sample temperature-pressure history, assuming adiabatic expansion during the fireball phase. Plume reentry is at 10 μbar. Initial fireball temperature is 3000 K, plume shock temperature is 1500 K, and plume reentry occurs at 350 seconds.

of supersaturated plume constituents. Since the plume is aloft for only ~10^3 seconds, photochemical processing is negligible (Moses et al. 1995). Similarly, many plume condensates may be sufficiently volatile that they reevaporate during plume reentry. Neglecting the divergence of the plume results in a plume reentry event in which the incoming gas is more concentrated than is realistic. The plume reentry event is modeled as a single shock event at a pressure of 10 μbar, and for which no dilution occurs due to mixing with Jovian gas. The latter is certainly not true, hence the kinetics model overpredicts the mixing ratios of computed species. The value of 10 μbar is determined by assuming the reentering plume penetrates the Jovian atmosphere to a pressure level at which the column mass density of Jovian atmosphere and plume are comparable. That is, $P \sim gM_p/L_p$, where the mass of the plume is assumed to be $M_p \sim 10^{16}$ g, and the horizontal extent at the time of reentry is $L_p \sim 20{,}000$ km.

Again, following Zahnle et al. (1995), the shocked plume is assumed to cool radiatively. An expression for the timescale for radiative cooling by a blackbody is easily determined from the equation of heat transfer (Chamberlain and Hunten 1987)

$$\frac{\partial T}{\partial t} = -\beta T^4 \qquad (2)$$

where $\beta=(\varepsilon\sigma g/C_pP)$, ε is the emissivity of the hot plume, σ is the Stefan-Boltzman constant, and g is the acceleration of gravity on Jupiter. Based on the form of the solution of this equation for β assumed to be constant with time and temperature, we specify the

temperature to vary with time as

$$T = T_1\left(\frac{\tau}{\tau+(t-t_1)}\right)^{1/3} \quad (3)$$

where T_1 is the peak shock temperature of the plume during reentry, t_1 is the time at which plume reentry occurs, and $\tau^{-1} = 3\beta T_1^3$ is a parameter determined from fitting to observed impact lightcurves. From the R impact lightcurve of Nicholson et al. (1995), we estimate $\tau \sim 50$ sec using the ratio of the flux at the peak to the flux at four minutes past the peak (ratio ≈ 0.10), and assuming ε constant. The reentered plume gas is allowed to cool to a minimum temperature of 300 K.

Results of a kinetics calculation along the P-T history of Figure 4 are shown in Figures 5a-e for a system with H>>C>O>N>S>Si. The Si mixing ratio was chosen to 1×10^{-5}; the mixing ratios of the other species are as given above. This Si abundance corresponds to depletion by a factor of ~5 to 10 compared to solar. The choice of Si depletion factor is arbitrary, but represents incomplete vaporization of Si relative to more volatile cometary elements. Figure 5a shows the evolution of hydrogen atoms and several hydrocarbons. These species all reach equilibrium during the fireball phase. C_2H_2 and CH_4 are only moderately affected by adiabatic cooling and subsequent plume reentry. C_2H_4 increase during adiabatic cooling, whereas H and CH_3 decrease. The relatively low abundance of hydrogen atoms has important implications for several other species. At 10^4 seconds after impact, CH_4, C_2H_2, and C_2H_4 are all present in significant quantities. Figure 5b shows the conversion of H_2O to CO and NH_3 to N_2 and HCN; all five of these species are unaffected by the relatively low temperature plume reentry.

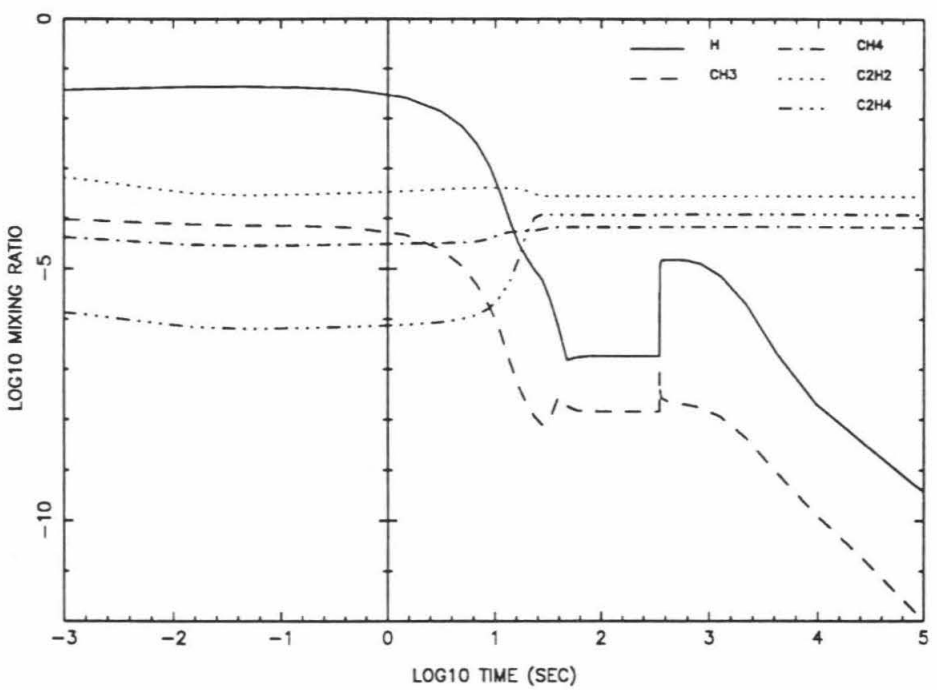

Fig. 5a. Time history of mixing ratios of selected species as determined from the kinetics model using the pressure-temperature history shown if Fig. 4. Several hydrocarbon species are shown.

Several sulfur species are shown in Figure 5c. The sulfur is assumed to be Jovian, all initially in H_2S. Rapid production of S_2, by the reaction

$$S + SH \rightarrow S_2 + H \qquad \text{(R1)}$$

occurs during adiabatic cooling of the fireball; growth by another order of magnitude occurs during cooling after plume reentry. H_2S remains the most abundant sulfur species at 10^4 seconds. According to Moses et al. (1995), the photochemical lifetime of H_2S is ~ 2×10^5 seconds at the 10 μbar level of Jupiter's atmosphere. Figure 5d shows several carbon-containing sulfur molecules. CS_2, produced in the reaction

$$CS + SH \rightarrow CS_2 + H \qquad \text{(R2)}$$

during fireball cooling, dominates these species; CS abundance drops with time due to the same reaction. Neither OCS nor H_2CS are principal sulfur species, but the detection of OCS (Lellouch et al. 1995) suggests that perhaps thioformaldehyde is also detectable. Si species are shown in Figure 5e. Si, SiS, and SiO dominate the fireball phase, but cooling favors conversion of SiS to SiS_2 by reaction of SiS with SH; condensation of these will occur but has been neglected. By 10^4 seconds, Si is entirely negligible, suggesting that a different scenario must be responsible for the Si seen by the HST FOS (Noll et al. 1995). Similarly, S_2 and CS_2 were observed to be more abundant than H_2S by HST (Yelle and McGrath 1995).

Different gas parcels will, of course, experience different P-T histories, depending on proximity to the path of the impactor. To determine the sensitivity to temperature, we

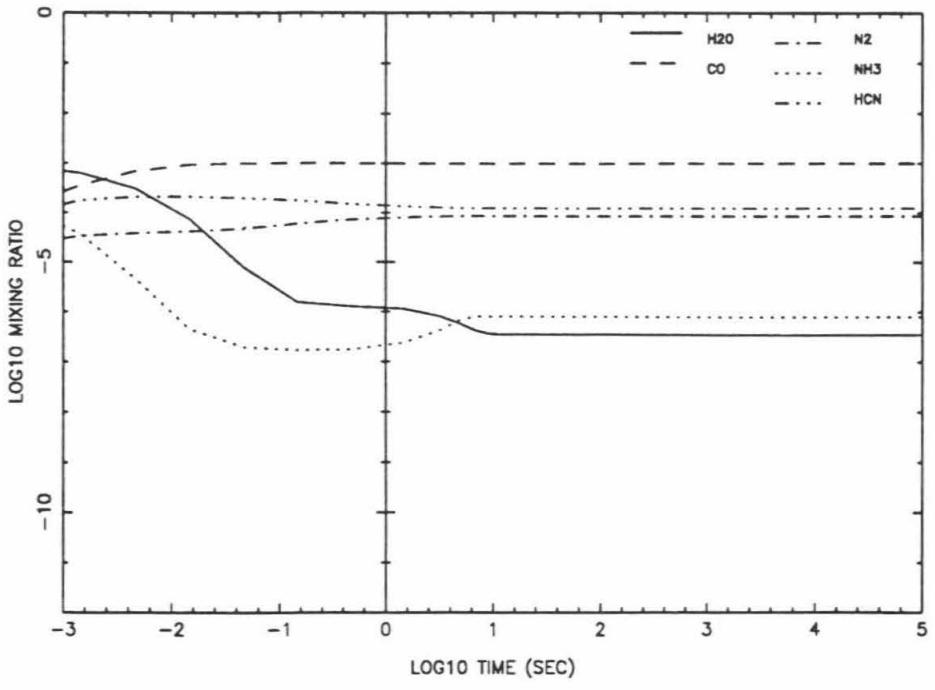

Fig. 5b. Same as Fig. 5a, but for several oxygen and nitrogen species.

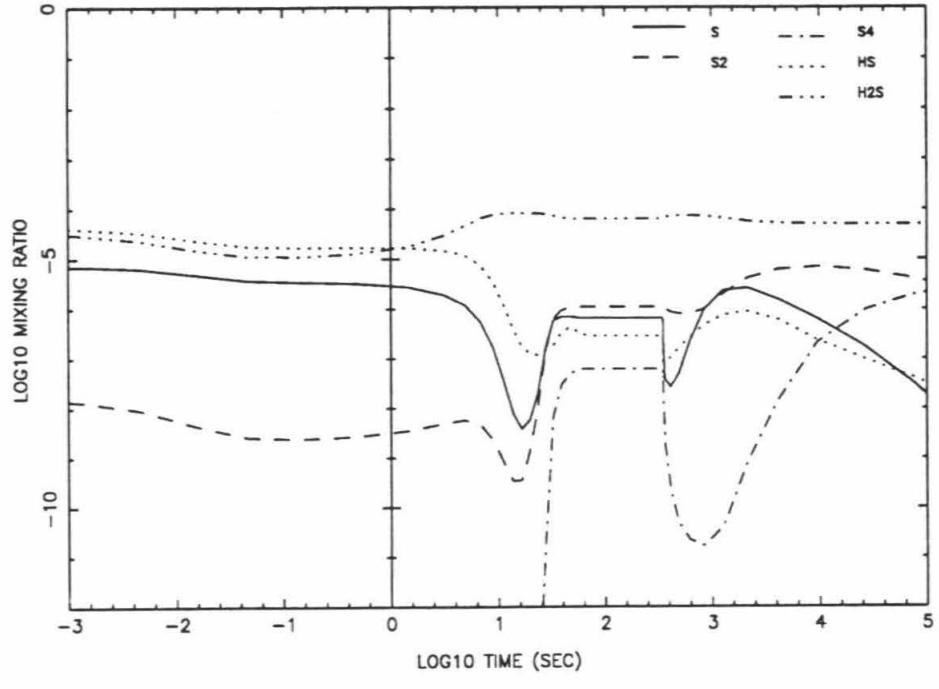

Fig. 5c. Same as Fig. 5a, but for several sulfur species.

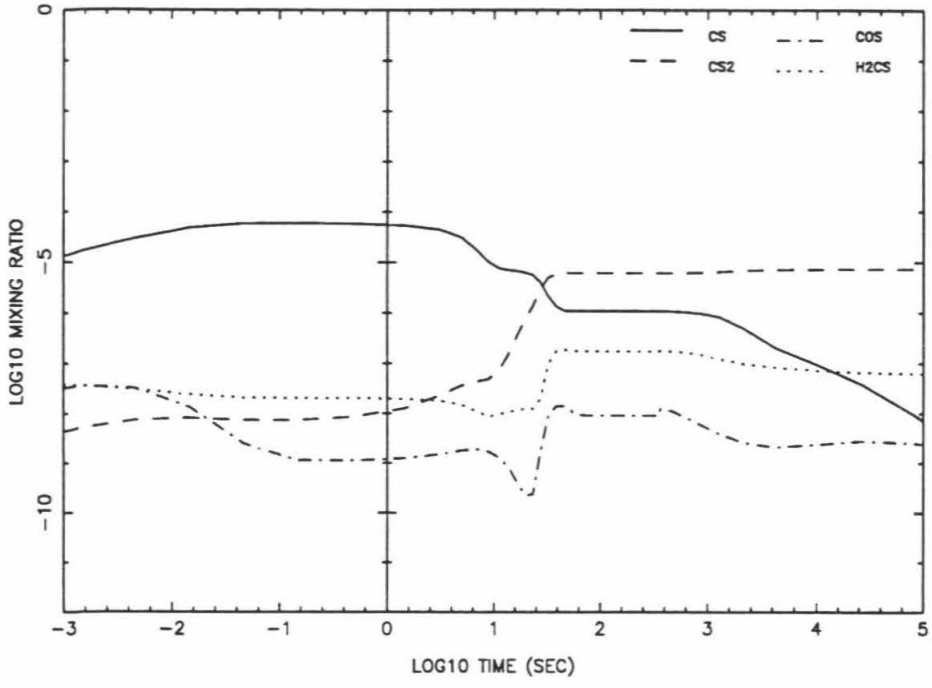

Fig. 5d. Same as Fig. 5a, but for several sulfur and carbon containing species.

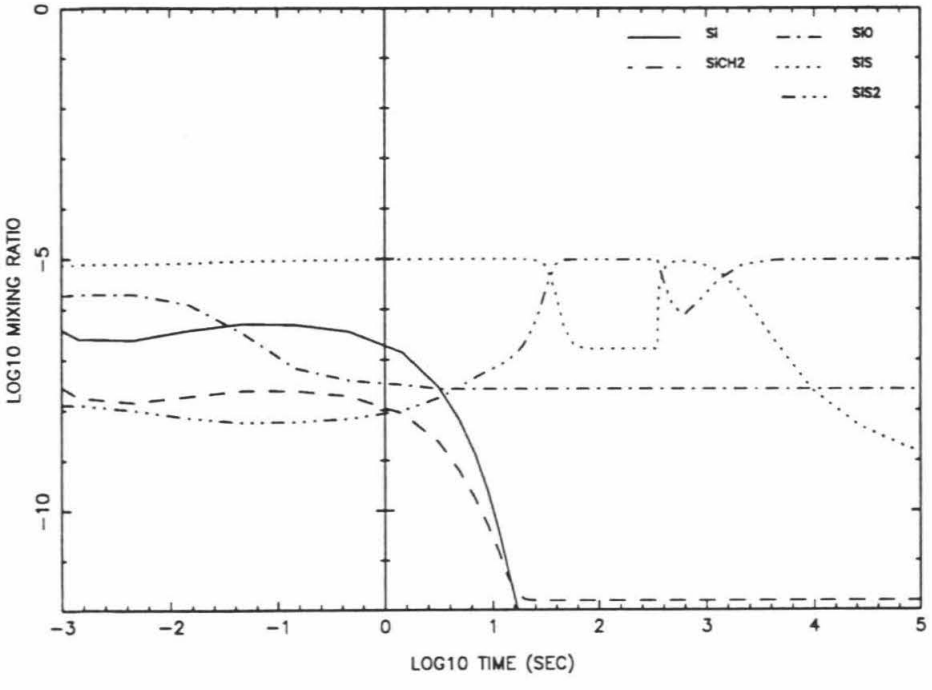

Fig. 5e. Same as Fig. 5a, but for several silicon species.

have run the kinetics code for various fireball/plume temperature pairs; in all runs the initial fireball pressure was 1 bar, and the plume pressure during reentry was 10 μbar. For the sake of convenience, the fireball velocity was held constant, regardless of the assumed temperatures; since T_1 is proportional to the square of the reentry velocity, this assumption cannot be correct for a ballistic plume with a distribution of velocities. The results, for the same composition as for Figs. 5, and at 10^4 seconds, are summarized in Table 1. The table reveals that several types of solutions exist depending on temperature, but that some species are more dependent on the fireball temperature, while others depend more on the plume reentry temperature. Hydrogen atoms, which drive much of the chemistry, decrease with time after plume reentry for the 1500 K initial plume temperature. The loss of H occurs by abstraction of a hydrogen atom from H_2S,

$$H_2S + H \rightarrow SH + H_2 \qquad \text{(R3)}$$

For $T_1 \geq 2500$ K, H retains a high value throughout plume reentry, regardless of fireball temperature.

Methane is readily converted to C_2H_2. Acetylene abundances are high for all values of T_1, except for the case when T_0 = 1000 K, which is too cold for significant processing of CH_4 to occur in the fireball. Ethylene is abundant except at higher plume temperatures. At these mixing ratios, higher hydrocarbons (e.g., C_4H_2, benzene) are formed but not in significant quantities.

As is readily seen from Table 1, the hydrogen atom abundance has important implications for sulfur chemistry. The mixing ratios of SH and H_2S differ by many orders

of magnitude between the high H (high T_1) and low H (low T_1) cases, due to hydrogen atom abstraction by H from SH and H_2S. A high abundance of SH leads to $CS_2 > CS$ via reaction R2; low SH implies $CS > CS_2$. Similarly, S_2 abundance is enhanced by high SH by reaction R1. However, S_4 is more dramatically affected, due to the hypothetical reaction

$$S_4 + H \rightarrow S_2 + HS_2 \qquad \text{R4}$$

Hence, conversion of S_2 to solid sulfur via condensation of S_8 may be inhibited by a high abundance of hydrogen atoms. This assumes three-body recombination of S_4 is the principal pathway forming S_8. The relatively high values of S_4 predicted to occur at 10^4 seconds for T_1 = 1500 K suggest that placing an observational upper limit on S_4 may be useful. OCS and H_2CS are both favored by low H, but neither is predicted to be abundant. For high values of T_1, sulfur is primarily in S and CS at 10^4 seconds.

Unlike hydrocarbons and sulfur species, nitrogen and oxygen species abundances are determined primarily by T_0 for a gas composition with C>O for plume temperatures $\leq$ 2500 K. This is especially true for destruction of H_2O and NH_3 and production of CO. Production of N_2 and HCN is certainly favored by higher T_0, but also occurs for moderate plume reentry temperature. At the highest plume temperature considered, NH_3 and H_2O are completely consumed, regardless of T_0. Substantial production of NO is predicted for T_0 = 2000 K, suggesting that an observational upper limit on this species could be useful.

Results for silicon species are also included in Table 1. Si, the only observed silicon species, occurs in substantial abundance only for the highest value of T_1. For T_1 = 1500 K, SiS_2 predominates, followed by SiS and SiO. At T_1 = 2500 K, the same

Species	T_o, T_1 (Kelvin)						
	1000 , 1500	2000 , 1500	2000 , 2500	2000, 3500	3000 , 1500	3000 , 2500	4000, 3500
H	2.4E-09	1.7E-07	3.0E-03	4.80E-01	2.0E-08	2.5E-03	4.80E-01
CH4	2.0E-03	2.7E-04	4.2E-07	2.80E-10	6.6E-05	4.2E-07	2.90E-10
C2H2	1.7E-08	2.8E-04	8.5E-04	3.30E-04	2.8E-04	4.0E-04	3.50E-04
C2H4	2.5E-06	4.9E-04	9.7E-06	5.20E-09	1.2E-04	5.3E-06	5.50E-09
H2O	1.0E-03	8.3E-04	8.2E-04	3.80E-17	3.5E-07	3.5E-07	3.50E-17
CO	9.2E-11	1.7E-04	1.8E-04	1.00E-03	9.9E-04	9.9E-04	1.00E-03
CO2	6.9E-18	1.2E-15	9.1E-09	2.10E-19	5.7E-14	1.5E-11	2.00E-19
N2	1.1E-12	1.5E-06	5.3E-05	1.10E-04	8.5E-05	8.5E-05	1.20E-04
NO	2.6E-10	1.6E-07	1.6E-08	9.20E-25	1.9E-16	1.6E-14	1.50E-24
NH3	3.0E-04	3.0E-04	1.6E-04	2.80E-18	8.0E-07	5.5E-07	3.00E-18
HCN	5.2E-11	4.3E-07	3.7E-05	8.00E-05	1.2E-04	1.2E-04	6.60E-05
S	2.0E-07	1.7E-06	5.2E-05	2.40E-06	6.2E-07	3.3E-05	2.50E-06
SO	3.2E-11	2.5E-10	2.8E-10	4.60E-23	8.4E-16	2.3E-14	3.60E-23
S2	2.1E-06	2.4E-05	5.8E-07	1.60E-13	6.9E-06	3.5E-07	1.70E-13
S4	1.9E-08	2.6E-06	2.7E-13	5.00E-25	2.1E-07	1.2E-13	9.10E-26
SO2	1.3E-14	3.3E-10	3.2E-11	1.10E-24	1.5E-15	1.1E-15	6.80E-25
HS	1.5E-07	3.2E-07	2.0E-11	1.80E-13	2.3E-07	9.1E-12	1.90E-13
H2S	8.7E-05	1.8E-05	4.8E-13	1.90E-16	5.0E-05	2.7E-13	2.00E-16
CS	3.1E-09	1.7E-08	2.8E-05	9.70E-05	9.8E-08	4.1E-05	9.70E-05
CS2	8.5E-08	1.4E-06	4.8E-06	3.10E-12	7.2E-06	7.0E-06	3.30E-12
OCS	5.9E-12	2.9E-09	1.6E-10	8.90E-16	2.3E-09	5.2E-12	9.40E-16
H2CS	1.4E-07	5.3E-08	3.8E-10	3.50E-15	7.2E-08	2.2E-10	3.80E-15
Si	4.6E-13	4.3E-20	6.6E-08	9.50E-06	3.5E-20	2.5E-09	9.60E-06
SiCH2	6.2E-06	1.5E-12	8.1E-07	1.80E-08	1.5E-12	4.3E-08	1.80E-08
SiC2	6.9E-16	1.9E-16	5.9E-09	2.40E-07	1.9E-16	9.8E-11	2.50E-07
SiN	1.7E-11	1.6E-15	1.3E-08	9.00E-15	2.3E-17	2.7E-12	9.80E-15
SiO	3.9E-10	5.1E-07	5.3E-07	1.90E-22	2.6E-08	2.6E-08	1.80E-22
SiS	4.8E-09	1.0E-07	8.3E-06	2.40E-11	2.5E-08	2.5E-08	2.40E-11
SiS2	3.6E-06	9.2E-06	6.9E-13	5.40E-23	9.5E-06	9.5E-06	5.60E-23

Table 1. Mixing ratios of major species at 10^4 seconds after impact. At later times, photochemical processes cannot be neglected. T_0 is the initial fireball temperature. T_1 is the shock temperature for plume reentry. Elemental mixing ratios in the model are identical to those of Fig. 1, with a Si mixing ratio of 1×10^{-5}; gas mixture has C>O.

principal species exist, in different proportions, and $SiCH_2$ is also significant. At 3500 K, Si atoms are the principal silicon species from the time of reentry to ~ 10^4 seconds. A comparison of kinetics and thermodynamics for silicon species is still in progress, so the silicon kinetics results in Table 1 should be considered preliminary.

Table 2 shows kinetics results for the same conditions as for Table 2, except that C<O. This qualitatively represents the case of a mixture of cometary material with Jovian gas in a proportion > 1:50, comet to Jupiter. To be quantitatively consistent with such a mixture, the elemental abundances of C,N,S, and Si would be slightly different from the case considered in Table 1, but we consider here only the affect of an enhanced abundance of O. Several differences from the C>O solutions are immediately obvious. At T_0 = 3000 K, nearly all C is converted to CO; the next most abundant C species is OCS, five orders of magnitude less abundant. At T_0 = 2000 K, C chemistry is still far from equilibrium, and C_2H_2 and CO are of comparable abundance. In fact, the solutions for T_0 = 2000 K are qualitatively similar for C>O and C<O. This may simply be a result of specifying the initial oxygen as H_2O rather than as O, thus slowing the rate of CO formation (see below).

Table 2 indicates that at T_0 = 3000 K, substantial amounts of SO and SiO are produced. Since neither of these species was observed (although a feature in the HST FOS spectrum (Noll et al. 1995) lies very close to a SiO line at 2993.2 Å), and because of the low CS_2 and HCN abundances predicted, this scenario could not have been the principal source of many of the species observed at the impact sites.

At the high entry velocity of the comet fragments, substantial dissociation and

Species	T_o, T_1 (Kelvin)						
	1000 , 1500	2000 , 1500	2000 , 2500	2000, 3500	3000 , 1500	3000 , 2500	4000, 3500
H	2.40E-09	2.70E-07	3.10E-03	4.80E-01	8.50E-08	2.40E-03	4.80E-01
CH4	2.00E-03	2.90E-04	3.40E-07	4.90E-22	4.80E-11	8.20E-14	6.60E-22
C2H2	1.70E-08	2.20E-04	7.20E-04	7.20E-19	6.70E-15	1.40E-14	3.40E-20
C2H4	2.50E-06	4.10E-04	8.30E-06	7.60E-24	6.30E-15	2.10E-16	9.50E-24
H2O	3.00E-03	2.60E-03	2.50E-03	8.70E-04	1.00E-03	1.00E-03	8.40E-04
CO	2.70E-10	4.30E-04	4.60E-04	2.00E-03	2.00E-03	2.00E-03	2.00E-03
CO2	5.70E-17	7.60E-10	7.00E-08	6.90E-06	8.70E-10	6.60E-08	6.80E-06
N2	1.80E-12	3.60E-06	6.00E-05	1.50E-04	1.50E-04	1.50E-04	1.50E-04
NO	7.00E-10	2.60E-07	8.10E-08	4.00E-06	4.50E-09	7.20E-09	9.60E-08
NH3	3.00E-04	2.90E-04	1.50E-04	3.70E-17	6.10E-08	5.80E-08	1.00E-18
HCN	1.10E-10	1.00E-06	3.30E-05	3.30E-11	5.80E-09	5.80E-09	3.30E-13
S	2.00E-07	1.40E-06	5.80E-05	2.80E-05	1.70E-06	7.30E-05	2.90E-05
SO	9.50E-11	8.80E-10	1.10E-09	5.70E-06	1.00E-07	1.60E-06	5.90E-06
S2	2.10E-06	2.50E-05	9.00E-07	1.20E-09	2.90E-05	1.10E-05	1.40E-09
S4	1.90E-08	2.90E-06	6.50E-13	8.60E-22	4.00E-06	1.10E-10	1.10E-21
SO2	1.20E-13	2.80E-09	6.00E-10	6.60E-05	3.00E-08	5.80E-08	6.30E-05
HS	1.50E-07	4.40E-07	2.70E-11	2.00E-12	2.00E-07	5.60E-12	2.10E-12
H2S	8.70E-05	1.50E-05	6.50E-13	2.20E-15	1.70E-05	1.40E-12	2.40E-15
CS	3.10E-09	1.60E-08	2.10E-05	1.70E-17	2.60E-13	1.50E-12	1.90E-19
CS2	8.50E-08	1.70E-06	5.20E-06	2.80E-21	3.50E-11	5.30E-12	3.50E-24
OCS	1.80E-11	4.60E-09	5.10E-10	2.00E-14	2.90E-08	3.80E-11	2.20E-14
H2CS	1.40E-07	3.90E-08	3.30E-10	1.60E-26	6.70E-15	1.20E-17	1.50E-26
Si	4.60E-13	4.20E-20	5.90E-08	4.50E-21	9.00E-23	1.50E-15	5.60E-23
SiCH2	6.20E-06	1.20E-12	5.90E-07	1.40E-23	6.10E-23	1.50E-19	2.00E-23
SiC2	6.90E-16	1.50E-16	4.30E-09	2.40E-37	3.90E-30	2.70E-27	4.20E-38
SiN	1.60E-11	1.30E-15	8.10E-09	6.10E-27	2.60E-20	1.40E-17	3.40E-29
SiO	1.10E-09	1.30E-06	1.50E-06	9.40E-06	9.20E-06	9.20E-06	9.90E-06
SiS	4.80E-09	1.10E-07	7.70E-06	4.70E-07	7.20E-09	6.50E-07	7.00E-08
SiS2	3.60E-06	8.20E-06	8.40E-13	1.20E-17	6.20E-07	1.80E-14	1.90E-18

Table 2. Mixing ratios of major species at 10^4 seconds after impact. Same conditions as in Table 1, but oxygen mixing ratio is increased to 3×10^{-3} , resulting in O>C in the gas mixture.

ionization of ablated cometary material are to be expected. In order to determine the affect of dissociation of cometary material on the kinetic chemistry, computer runs were made for an initial composition consisting of Jovian gas (H_2, CH_4, NH_3, H_2S), with the mixing ratios given above but with no H_2O , and with atomic species in solar abundance except for H. The elements included were H, O, C, N, S, and Si with the mixing ratios 0.55, 0.25, .15, .015, .0063, and .012, respectively (Krankowsky and Eberhardt 1990); Mg, Fe, and perhaps other less abundant elements will be included at a later date. Defining the mixing of dry Jovian gas and cometary material by

$$x = \frac{f_{CH4}}{f_O - f_C + f_{CH4}} \tag{4}$$

where f_i is the volume mixing ratio for either molecule i in the Jovian atmosphere or element i in the dissociated comet. Runs were made for x = .01, corresponding to C_{tot}/O_{tot} = 1.4, and x = .04, corresponding to C_{tot}/O_{tot} = 0.80, where the subscript refers to the total elemental abundance from Jupiter plus comet. Results for the higher temperature fireball (T_0 > 3000 K) indicate that no qualitative difference exists between these runs and those which have a purely molecular starting composition and the same pressure and temperature history. For T_0 = 2000 K and T_1 = 1500 K, CO, HCN and N_2 form more rapidly due to the presence of the atomics. For T_0 = 1000 K, very large differences in the final HCN, N_2 ,CS_2, and OCS abundances occur (all are several orders of magnitude higher); however, it seems unlikely that significant dissociation would be accompanied by such low fireball temperatures. More reasonable is to expect very high fireball temperatures and partial (if not complete) ionization of vaporized cometary material and

adjacent Jovian gas.

4. Discussion

On comparison of our results in Fig. 5 with observations, one immediately sees a significant discrepancy in the order of magnitude of the mixing ratios of various species. For example, C_2H_2 has a mixing ratio in the reentering plume of 1×10^{-3} for most model runs with C>O, whereas the observed value is ~ 3×10^{-7} according to HST observations at the G impact site (Yelle and McGrath 1995). There are several possible reasons for this large difference, a factor of 3000 for acetylene. First, the reentering plume may penetrate to deeper than a pressure equivalent to its column mass density, resulting in dilution of the plume gas with Jovian gas. Additionally, horizontal expansion of heated atmosphere would distribute the plume material over a wider area than the plume occupied during reentry. Second, probably only a fraction of the plume contains a given species, even after reentry. A given species would then be further diluted by mixing within the plume and with Jovian gas during reentry. Third, plume species capable of polymerization may have contributed to the formation of the impact debris. Determining which of these mechanisms is most significant requires detailed knowledge of the pressure-temperature histories of the plume reentry event.

A comparison of the results in Table 1 for T_0 = 3000 K and T_1 = 2500 K with Fig. 2 of Zahnle et al. (1995) suggests that differences exist. In particular, at 10^4 seconds for shocked dry Jovian gas Zahnle et al. (1995) obtain $S_2 > CS_2 > CS >> H_2S$, whereas we

obtain CS > CS_2 > S_2 >> H_2S for similar conditions. Part of the difference may be that Zahnle et al. (1995) assumed about twice as much sulfur to be in the Jovian atmosphere than did we, but it is also likely that differences in chemistry contribute to the disparity. Our results at T_0 = 2000 and T_1 = 1500 K yield S_2 ~ H_2S > CS_2 > CS; at T_0 = 3000 K and T_1 = 1500 K, we obtain H_2S > S_2 ~ CS_2 > CS. We have not yet obtained a solution in which S_2 > CS_2 > CS >> H_2S. Since we know that our own sulfur results at 1 bar are not correct (see Fig. 1d), we cannot claim that Zahnle et al. (1995) are in error with regard to sulfur species. A more detailed comparison of the chemical models may help to resolve the differences.

Since we have not computed the actual mass of the various species produced during shock chemistry, quantitative comparison with observations is not possible at this time. However, qualititative comparisons are still useful, and are presented below. We plan to obtain pressure/temperature/mixing histories from the Eulerian hydrodynamic code of Boslough et al. (1994)/Crawford et al. (1995) run with tracer particles in order to properly model the chemistry of the impacts.

Data analysis of observations of sulfur species is still ongoing. The most recent analysis of the HST FOS data (Yelle and McGrath 1995) suggests that CS_2 is found at lower pressures than is H_2S; the latter may result from slow convective uplift of tropospheric air into the stratosphere. An upper limit on H_2S above 0.1 mbar was not given by Yelle and McGrath (1995). Atreya et al. (1995) did not detect H_2S in their analysis of the HST FOS data. Earlier reports of extremely high S_2 abundances at the G impact site (Noll et al. 1995) are under revision. Lellouch et al. (1995) reported the

detection of OCS at the K+W impact site several hours after the W impact. None of the model runs reported here produce significant quantities of OCS. One low temperature run with Jovian gas and dissociated cometary vapor for x = 0.04 (see above) yielded a OCS mixing ratio of 10^{-6}. Lellouch et al. (1995) also reported ~ 10^3 times as much CS as did Noll et al. (1995). Even with the larger aperture size of the mm-wave telescope used by Lellouch, there is still a discrepancy in observed CS. This may be consistent with our higher shock temperature runs (T_1 = 2500 K).

The principal oxygen-containing species observed at the impact sites were CO and H_2O. Using the KAO, Bjoraker et al. (1995) observed hot H_2O (T~1000-1200 K) during the G and K plume reentry events. At 7.7 μm they detected an H_2O column ~ 1×10^{18} cm^{-2}, and a comparable column of CH_4. With the HIFOGS on the KAO, Sprague et al. (1995) observed 5.7×10^{10} g and 2.2×10^{10}g of water at R+12 min and W+10 min, respectively. Lellouch et al. (1995) observed CO to be ~ 10^{14} g at G+10 hours. Since the mass of H_2O < the mass of CO at the G impact site, we may infer that C>O in the plume, according to Table 2, at least for the C/O ratio represented by these calculations. (The model results for O-containing species at ~ 10^3 seconds are similar to those at 10^4 seconds.) Model runs also need to be made for other C to O ratios. If the O is derived from the G fragment, then the cometary O is mixed with at least 50 times its mass in dry Jovian atmosphere, yielding a minimum plume mass of 3×10^{15} g. Alternatively, if the O is derived from Jupiter, it would have to be from Jovian gas for which $CH_4 > H_2O$, which will be true for pressures < 3 bars, assuming a solar (or greater) abundance of O on Jupiter. It may be possible to use the observed H_2O abundance at the G impact site to distinguish between

these two scenarios, since cometary O is likely to have been heated to much higher temperatures than is entrained Jovian air before either entered the plume. However, this requires knowing the P-T history of Jovian air entrained in the fireball. For example, Table 2 indicates that a fireball temperature between 2000 and 3000 K will yield CO ~ 10 times H_2O at 1 bar for a gas of Jovian composition. The observed CO and H_2O may, of course, be derived from a mixture of Jovian and cometary oxygen.

The only nitrogen species observed were NH_3 and HCN. Noll et al. (1995) detected NH_3 at the G site in the UV; Yelle and McGrath (1995) determined a mixing ratio of ~ 1×10^{-7} at pressures > 5 mbar; Atreya et al. (1995) obtained a value of ~ 1×10^{16} cm^{-2}. NH_3 was also detected in the IR by Orton et al (1995), who detected > 50 times enhancement in stratospheric ammonia, and by Griffith et al. (1995), who observed 2×10^{13} g NH_3 at the K impact site. HCN was observed at millimeter wavelengths by Marten et al. (1995) and by Bezard et al. (1995) in the IR; the former determined a value of 6×10^{11} g at G+21 hours, corresponding to a mixing ratio of 5×10^{-8} at < 0.5 mbar pressure level; the latter observed a column density of ~ 10^{16} cm^{-2} at E+2.6 hours, corresponding to three times the amount seen at the G site by Marten et al. (1995). The key point of these observations is that NH_3 exceeds HCN by 1-2 orders of magnitude. In addition, the HCN may be at lower pressures that the NH_3. According to Table 1, these results are consistent with the observed ammonia having remained at fireball temperatures < 3000 K. Given the relatively high pressure location of the NH_3, it was probably part of a low-velocity plume component that formed a parcel sufficiently dense to settle back to ~ 10 mbar, or that simply underwent slow upwelling from the troposphere as suggested by Yelle and

McGrath (1995). The HCN is probably from Jovain ammonia heated in the higher temperature portion of the fireball. However, according to Tables 1 and 2, significant HCN is also produced at relatively low fireball temperatures (2000 K) for both C>O and C<O Jovian compositions.

Metal species were seen both by HST FOS (Noll et al. 1995) (Mg, Mg^+, Fe, Fe^+, Si) and by ground based observers (Fitzsimmons et al. 1995; Roos-Serote et al. 1995), who saw Mn, Li, Na, K, Ca, Mg and Fe at visible wavelengths. We have only modeled Si here, but note that most of the other observed metals are much simpler chemically than Si. In particular, they form much weaker bonds with S and O, with the result that they occur as atomic species at lower temperatures than does Si. Our results for Si are in agreement with HST FOS, in that we predict significant quantities of Si to be present for ~ 10^4 seconds after impact, but only for a high plume temperature (3500 K). However, we have neglected the fact that Si reacts with C_2H_2 at room temperature, mainly because the products of this reaction are unkown. A reasonable assumption for this reaction is

$$Si + C_2H_2 \rightarrow SiC_2H + H \qquad \text{(R5)}$$

The assumed product (SiC_2H) of this reaction may be rapidly converted back to Si by reaction with H; alternatively, Si may be formed in a low-C environment during reentry. (Other products are possible in R5, such as SiC_2). A chemical loss timescale for Si of 45 minutes corresponds to C_2H_2 ~ 10^6 cm^{-3}. If, on the other hand, Si is scavenged by debris particles, the number of 0.15 micron particles (West et al. 1995) at 300 K is ~ 40 cm^{-3}, assuming unity sticking efficiency. It is also possible that the Si emission is not simply resonance scattering of solar Si lines, but instead is associated with relaxation of thermally

(or chemically) excited Si. Thermal excitation would be consistent with late reentry (relative to the observed plumes) of the plume material containing Si; in other words, a high-velocity component of the plume would have to exist. A 45 minute delay in reentry corresponds to a vertical velocity of about 35 km s^{-1} and a peak height of 24000 km above Jupiter; the visible plumes reported by Hammel et al. (1995) reached heights of only 3000 km. As an alternative to a high-velocity plume component, a slow upwelling of hot (T~1000 K) material to microbar levels may provide enough thermally excited metal atoms to account for the observed emission rate. A proper assessment of thermal emission from metal atoms requires considering the collisional deexcitation rate, which we will not attempt here.

Species such as Mg, Mg^+, Fe, and Fe^+ are much less reactive in a reducing environment than is Si (Lyons 1995), at least at room temperatures. As an example, Mg forms very weak bonds with S, H, C, and N. The ions are produced mainly during entry of the original fragment, and to a much lesser extent during reentry of plume material. It seems unlikely that the UV emission observed by the HST from these metals could be due to excited electronic states generated by exothermic chemical reactions long after impact has occurred. The bond strengths are not high enough (except for Si) to generate highly-populated excited electronic states capable of emitting UV photons, at least at temperatures ~ 300 K. If kinetic temperatures >> 300 K are somehow maintained for ~ 1 hour after impact, then electronic states will remain populated. If emission is not thermally or chemically generated, then it must be a result of either a high-velocity plume component or solar resonance scattering. Scavenging of these atomic metal species by

impact debris is probably their principal destruction pathway.

The ions may contribute to the generation of a motion-driven electric current (Hill and Dessler 1995) by enhancing the Pedersen conductivity of the lower ionosphere. The magnitude of this enhancement depends on the altitude distribution of the ions. For a mass 50 ion, we estimate that the ion-neutral collision frequency ~ ion cyclotron frequency at a pressure of ~ 0.1 microbar. If the column abundances reported by Noll et al. (1995) (derived assuming emission by solar flourescence) are distributed vertically over one atmospheric scale height (~50 km), then the peak ion number density is ~ 10^6 cm^{-3}. If the ions are located near 0.1 microbar, then they contribute ~ 3 mho to the integrated Pedersen conductivity. The equatorial conductivity is estimated to be 0.2 mho (Atreya 1986), so this may represent a substantial enhancement. If the ions are distributed much deeper in the atmosphere, say 10 microbar, then their conductivity would be negligible.

The impact debris raises several interesting questions, and although no attempts are made here to model it, it is likely that kinetic processes are crucial to debris formation. The key questions concerning the debris particles are what is the composition of the particles and from where do they come ? Since the particles clearly contain a substantial organic component (at the very least as a veneer) (West et al. 1995), and since they resemble the particles comprising Jupiter's polar hazes (Kim et al. 1991), it is reasonable to suspect that their organic component is from Jovian methane. Ion processes are thought to be responsible for Jupiter's polar haze (Pryor and Hord 1991), and could provide the principal pathway forming the impact debris. The polar haze is thought to be

formed by charged particle precipitation into Jupiter's auroral zones; ion chemistry then proceeds at relatively low temperatures (~ 300 K), favoring the formation of $C_{>3}$ hydrocarbon ions. These ions probably form clusters with neutral hydrocarbons, or recombine dissociatively with electrons forming condensible neutral hydrocarbons, initiating the formation of aerosols. In the case of an impact, a large number of ions are formed, but at the high temperatures associated with shock heating the chemical kinetics may not favor formation of $C_{>3}$ hydrocarbon ions. Instead, reactions with H_2 may predominate, at least until the temperatures have lowered substantially. Future kinetics work will include an assessment of such gas phase ion processes.

In addition to ion kinetics, several other mechanisms exist which could account for debris formation. The debris is clearly formed along the high temperature entry path of the fragments (Hammel et al. 1995). Polymerization of C_2H_2 with HCN, NH_3, and sulfur species could occur either in the gas phase or on the surfaces of very small (<< 1μm) silicate dust grains. The latter would be best studied experimentally (e.g., in a shock tube with suspended silicate dust), since little is known about heterogeneous chemistry involving hydrocarbons. These processes would not require cometary material (apart from dust grains). Other processes which do utilize cometary material can be envisioned. Ion chemistry may proceed with ions formed principally from the impactor. Alternatively, portions of the comet may have C>O, such as crustal material or portions for which H_2O was removed preferentially relative to C species during entry heating. In this case, C/H for the comet material could be >> 2×10^{-3}, the methane mixing ratio for Jupiter, with the result that many neutral higher hydrocarbons (e.g., $C_{>3}$) will form. Atreya et al. (1995)

constrained the column abundance of benzene (C_6H_6) to be < 3×10^{14} cm^{-2}. Combining this result with a combustion kinetics models (Cherchneff et al. 1992), and applying the acetylene dilution factor of 3000, we determine that C/H <= .01. Previous experimental work (Bar Nun et al. 1988; Khare and Sagan 1973) has simulated high C/H (~0.1) conditions in an effort to understand the color of Jovian clouds. Such experiments may be relevant to organic particle formation from vaporized (and dry) cometary material, but are not likely to be relevant to the case of a Jovian mixture of gases. Wilson and Sagan (1995) have pointed out that the Jovian impact debris has optical constants consistent with organic residue from Murchison, suggesting the possibility that the debris is from the comet. This may just suggest a similar formation process for the Murchison organics and the impact debris organics. Understanding whether the debris is derived from Jupiter or from the comet will likely have important implications for the quantity and composition of organic material transported to planetary surfaces (including early Earth) via comets, and may provide clues to the cause of Jupiter's coloration.

5. Summary and Conclusions

We have employed the technique of comparing a gas phase kinetics model, run to steady state equilibrium, with a thermodynamics code in an effort to ensure reasonable high temperature behavior of the kinetics. This was done for a system composed of the elements H,C,O,N,S and Si, and was found to be necessary because of the sparseness of rate coefficient data for S and Si species. Thermodynamics and kinetics were compared

over a range of temperatures from 1000 to 4000 K and a range of pressures from 1 μbar to 1 bar. Shock temperatures up to ~ 20000 K and shock pressures up to ~ 1 kbar were certainly achieved during the actual impact events but were not considered here; such high temperatures would lead to nearly complete dissociation and ionization and would require the addition of a large number of ion species to both the kinetics and thermochemical models. Not surprisingly, hydrocarbon species proved to be the most abundant group of compounds. Because of the substantial combustion kinetics literature, a fairly accurate and complete description of hydrocarbon kinetics is possible. Similarly, H-C-O and H-C-N compounds showed good agreement between steady state kinetics and thermodynamics. Sulfur and silicon compounds proved to be considerably more difficult; work still remains to be done on the H-C-Si system. The transient behavior of parent molecules and secondary products was seen to be very different. Parent species displayed a monotonic behavior during their approach to equilibrium, whereas some secondary species exhibited transient overshoots of several orders of magnitude. Such behavior may have contributed to the high S_2 abundances observed (Noll et al. 1995).

Model runs were made for a set of pressure-temperature histories thought to be relevant to the actual impact events. We simulated fireball rise and plume reentry, roughly following the approach of Zahnle et al. (1995). Initial fireball and plume reentry pressures of 1 bar and 10 μbar, respectively, were considered. The model was run for various pairs of fireball (T_0) and plume (T_1) shock temperatures. Direct comparison with Zahnle et al. (1995) for a particular P-T history showed that significant differences in sulfur species are obtained for the two models. For T_0 = 3000 K and T_1 = 2500 K, we obtained for dry

Jovian air (i.e., C>O) the relative abundances $CS>CS_2>S_2>>H_2S$, whereas Zahnle et al. (1995) obtained $S_2>CS_2>CS>>H_2S$. Such discrepancies must be resolved if we are to properly interpret the spectroscopic data taken at the impact sites.

Other results for gas compositions with C>O include the following: S_2 and CS_2 are favored by relatively by plume temperatures ~ 1500 K; CS is favored at higher values of T_1; at still higher plume temperatures, Si is produced, whereas at lower T_1 , $SiCH_2$ and SiS_2 are dominant; $NH_3>>HCN$, consistent with observations, results from relatively low fireball temperatures (T_0 ~ 2000 K); CO ~ $10\times H_2O$, as was observed at some impact sites, is also consistent with T_0 ~ 2000 K; C_2H_2 is the principal product of CH_4 pyrolysis. The description of species abundances as dependent on only T_0 or T_1 is , of course, only approximate. A C<O composition yields very different results: CO and H_2O dominate the carbon and oxygen species at all temperatures high enough to pyrolyse CH_4 (thereby producing CO); all other carbon containing species (C_2H_2, HCN, CS_2, CS) are present in negligble quantities; S_2 is often more abundant than in the C>O case due to the unavailability of C; SO, NO, SO_2, and SiO, all (apparantly) unobserved species, become significant in the model; at temperatures too low to completely pyrolyse CH_4, resulting abundances can be similar to the C>O case.

As discussed by Zahnle et al. (1995), we find that the observation of CS_2 and CS, but not SO and SO_2, is consistent with chemical processing of a gas of elemental composition C>O. Additionally, the observation of HCN, rather than NO, and Si rather than SiO, the apparant detection of C_2H_2, and perhaps even the production of the dark

impact debris are consistent with the same conclusion. For a mixture of dry Jovian gas with vaporized comet of comet Halley composition, C>O requires a mixture of at least 50 to 1, Jupiter to comet. Alternatively, if the O is all from Jupiter (which seems unlikely given the detection of metals), then the fireball must contain gas from a depth ~ few bars, but not ~ 20 bars, assuming O>C at the base of Jupiter's water cloud. The higher H_2O to CO ratios observed at the G and K impact sites would then be consistent with Jovian gas that had not undergone complete conversion of H_2O to CO. A low temperature entrainment of this type seems unlikely, but is best studied with a hydrodynamic model.

Several explanations for the observed metal lines are possible. The UV emissions from Mg and Mg^+ are probably just due to solar resonant scattering as suggested by Noll et al. (1995). Exothermic chemical reactions are an unlikely mechanism for exciting electronic states ~ 4 eV above the ground state in Mg and Mg^+ given the weak chemical bonds Mg and Mg^+ form with H,C,N and S species. On the other hand, if CO is formed, e.g. in the reaction $MgO + C \rightarrow Mg(^1P) + CO$, then the heat of the reaction is more than sufficient to yield $Mg(^1P)$; if MgO and C are in ground states, then CO must be in a triplet state to conserve spin. The chemical lifetimes of MgO and C in an H_2 atmosphere must be long enough to allow such a reaction to occur. The same is likely true for Fe and Fe^+, but not necessarily for Si. A high velocity plume component, such that plume material reenters up to ~ 1 hour after a given impact, could lead to thermal excitation of metals. A difficulty with this scenario is that the high velocity plume material would have to land in a location observed telescopically. Another way to produce emission well after an impact would be for a trail of dust particles to extend ~ 10^5 km behind (but not ahead

of) a given fragment. Regardless of the source of the emission, the metal ion abundances implied by the HST observations are sufficient to enhance the Pedersen conductivity locally by as much as an order of magnitude, assuming the ions are distributed at pressures < 0.1 μbar. This may have enhanced the amplitude of the current generated by the motion of ionized gas across magnetic field lines (Hill and Dessler 1995).

The chemical modeling results presented here are an exploration of a portion of the parameter space, namely fireball and plume temperatures, relevant to the Comet SL9 impacts on Jupiter. In the near future model runs will be made with pressure-temperature-mixing histories determined from the Sandia hydrodynamics code (Crawford et al. 1994; Boslough et al. 1994). Only by coupling the hydrodynamic and chemical models can a proper interpretation of the spectroscopic data be made.

Acknowledgements

Discussions with Y. L. Yung on how to modify the 1-D photochemical model for the present application are gratefully acknowledged. This work was supported by NASA grant NAGW-1509. This is contribution number 5597 from the Division of Geological and Planetary Sciences, California Institute of Technology.

References

Allen, M.,Y. L. Yung, and J. W. Waters 1981. Vertical transport and photochemistry in

the terrestrial mesosphere and lower thermosphere. *J. Geophys. Res.* 86, 3617-3627.

Atreya, S.K. 1986. *Atmospheres and Ionospheres of the Outer Planets and their Satellites.* Springer-Verlag, New York.

Atreya, S.K., S.G. Edginton, L.M. Trafton, J.J. Caldwell, K.S. Noll, and H.A. Weaver 1995. Abundances of ammonia and carbon disulfide in the Jovian stratosphere following the impact of comet Shoemaker-Levy 9. *Geophys. Res. Lett.* 22, 1625-1628.

Bar Nun, A., I. Kleinfeld, and E. Ganor 1988. Shape and properties of aerosols formed by photolysis of acetylene, ethylene and hydrogen cyanide. *J. Geophys. Res.* 93, 8383-8387.

Baulch, D.L., J. Duxbury, S.J. Grant, and D.C. Mantague 1981. Evaluated kinetic data for high temperature reactions, vol. 4, Homogeneous gas phase reactions of hydrogen and cyanide containing species. *J. Phys. Chem. Ref. Data* 10.

Bezard, B. C.A. Griffith, D. Kelly, J. Lacy, T. Greathouse, and G. Orton 1995. Mid-IR high-resolution spectroscopy of the SL9 impact sites: temperature and HCN retrievals. *IAU Colloquium 156: The Collision of comet P/Shoemaker-Levy 9 and Jupiter*, 9-12 May 1995, abstract book, 7.

Bjoraker, G.L., T. Herter, G. Gull, S. Stolovy, and B. Pirger 1994. Detection of water in the fireball of fragments G and K of comet Shoemaker-Levy 9. *Bull. Am. Astronom. Soc.* 26, 1578.

Boslough, M.B., D.A. Crawford, A.C. Robinson, and T.G. Trucano 1994. Mass and

penetration depth of Shoemaker-Levy 9 fragments from time-resolved photometry. *Geophys. Res. Lett.* 21, 1555.

Chamberlain, J.W. and D.M. Hunten 1987. *Theory of Planetary Atmospheres*, Academic Press, San Diego.

Cherchneff, I., J.R. Barker, A.G.G.M. Tielens 1992. Polycyclic aromatic hydrocarbon formation in carbon-rich stellar envelopes. *Astrophys. J.* 401, 269-287.

Crawford, D., M. Boslough, T. Trucano, and A. Robinson 1994. Numerical simulations of fireball growth and ejecta distribution during Shoemaker-Levy 9 impacts on Jupiter. *EOS* 75, 404.

Crisp, D., and V. Meadows 1995. Near-infrared imaging spectroscopy of the impacts of SL9 fragments C, D, G, K, N, R, V, and W with Jupiter. *IAU Colloquium 156: The Collision of comet P/Shoemaker-Levy 9 and Jupiter*, 9-12 May 1995, abstract book, 25.

Encrenaz, Th., R. Scuhlz, J.A. Stuwe, G. Wiedemann, P. Drossart, and J. Crovisier 1995. Near IR-spectroscopy of Jupiter at the time of comet Shoemaker-Levy 9 impacts: emissions of CH4, H3+, and H2. *Geophys. Res. Lett.* 22, 1577-1580.

Fitzsimmons, A., J.E. Little, P.J. Andrews, R. Catchpole, N. Walton, and I.P. Williams 1995. Optical spectroscopy of atomic emission from the L and Q1 impacts on Jupiter. *IAU Colloquium 156: The Collision of comet P/Shoemaker-Levy 9 and Jupiter,* 9-12 May 1995, abstract book, 37.

Griffith, C.A., B. Bezard, D. Kelly, J. Lacy, T. Greathouse, and G. Orton 1995. Mid-IR spectroscopy and NH3 and HCN images of K impact site. *IAU Colloquium 156:*

The Collision of comet P/Shoemaker-Levy 9 and Jupiter, 9-12 May 1995, abstract book, 42.

Hammel, H.B., R.F. Beebe, A.P. Ingersoll, G.S. Orton, J.R. Mills, A.A. Simon, P. Chodas, J.T. Clarke, E. De Jong, T.E. Dowling, J. Harrington, L.F. Huber, E. Karkoschka, C.M. Santori, A. Toigo, D. Yeomans, R.A. West 1995. HST imaging of atmospheric phenomena created by the impact of comet Shoemaker-Levy 9. *Science* 267, 1288-1296.

Hill, T.W., and A.J. Dessler 1995. Midlatitude Jovian aurora produced by the impact of comet Shoemaker-Levy 9. *Geophys. Res. Lett.* 22, 1817-1820.

Khare, B.N., and C. Sagan 1973. Red clouds in reducing atmospheres. *Icarus* 20, 311-321.

Kim, S.J., D. Goorvitch, P. Drossart, A. Moorwood, J. Caldwell, A. Moneti, J.P. Mailard, and J. Lecacheux 1991. The 2-μm polar haze of Jupiter. *Icarus* 91, 145-153.

Krankowsky, D., and P. Eberhardt 1990. Evidence for the composition of ices in the nucleus of comet Halley, *Comet Halley: Investigations, Results, Interpretations*, vol. 1, Ellis Howood Ltd.

Lellouch, E., G. Paubert, R. Moreno, M.C. Festou, B. Bezard, D. Bockelee-Morvan, P. Colom, J. Crovisier, T. Encrenaz, D. Gautier, A. Marten, D. Despois, D.F. Strobel and A. Sievers 1995. Chemical and thermal response of Jupiter to the impact of comet Shoemaker-Levy 9. *Nature* 373, 592-595.

Lyons, J.R. 1995. Metal ions in the atmosphere of Neptune. *Science* 267, 648-651.

Marten, A., D. Gautier, M.J. Griffin, H.E. Matthews, D.A. Naylor, G.R. Davis, T. Owens,

G. Orton, D. Bockelee-Morvan, P. Colom, J. Crovisier, E. Lellouch, I. de Pater, S. Atreya, D. Strobel, B. Han, and D.B. Sanders 1995. The collison of comet Shoemaker-Levy 9 with Jupiter: Detection and evolution of HCN in the stratosphere of the planet. *Geophys. Res. Lett.* 22, 1589-1592.

Moses, J.I., M. Allen, and G.R. Gladstone 1995. Post-SL9 sulfur photochemistry on Jupiter. *Geophys. Res. Lett.* 22, 1597-1600.

Nicholson, P.D., P.J. Gierasch, T.L. Hayward, C.A. McGhee, J.E. Moersh, S.W. Squyres, J. Van Cleve, K. Matthews, G. Neugubauer, D. Shupe, A. Weinberger, J.W. Miles and B.J. Conrath 1995. Palomar observations of the R impact of comet Shoemaker-Levy 9: I. Light Curves. *Geophys. Res. Lett.* 22, 1613-1616.

Noll, K.S., M.A. McGrath, L.M. Trafton, S.K. Atreya, J.J. Caldwell, H.A. Weaver, R.V. Yelle, C. Barnet, S. Edgington 1995. HST spectroscopic observations of Jupiter after the collision of comet Shoemaker-Levy 9. *Science* 267, 1307-1312.

Orton, G.S., M. A'Hearn, K. Baines, D. Demmig, T. Dowling, J. Goguen, C. Griffith, H. Hammel, W. Hoffman, D. Hunten, D. Jewitt, T. Kostiuk, S. Miller, K. Noll, K. Zahnle, N. Achilleos, A. Dayal, L. Deustch, F. Espenak, P. Esterle, J. Friedson, K. Fast, J. Harrington, J. Hora, R. Joseph, D. Kelly, R. Knacke, J. Lacy, C. Lisse, J. Rayner, A. Sprague, M. Shurea, K. Wells, P. Yanamandra-Fisher, D. Zipoy, G. Bjoraker, D. Buhl, W. Golisch, D. Griep, C. Kaminski, C. Arden, J. Goldstein, D. Gilmore, F. Fazio, T. Kanamori, H. Lam, T. Livengood, M.-M. Maclow, M. Marley, T. Momary, D. Robertson, P. Romani, J. Spitale, M. Sykes, J. Tennyson, D. Wellnitz, and S.-W. Ying 1995. Collision of comet Shoemaker-levy 9 with

Jupiter observed by the NASA Infrared Telescope Facility. *Science* 267, 1277-1281.

Pryor, W.R., and C.W. Hord 1991. A study of photopolarimeter system UV absorption data on Jupiter, Saturn, Uranus, and Neptune: implications for auroral haze formation. *Icarus* 91, 161-172.

Roos-Serote, M., A. Barussi, J. Crovisier, P. Drossart, M. Fulchignoni, J. Lecacheux, and F. Roques 1995. Metallic emission lines during the impacts L and Q1 of comet P/Shoemaker-Levy 9 in Jupiter. *Geophys. Res. Lett.* 22, 1621-1624.

Sprague, A.L., D.M. Hunten, F.C. Witteborn, R.W.H. Kozlowski, D.H. Wooden, and G. Bjoraker 1995. KAO observations of Jupiter during and following the impact of comet SL-9 fragments R and W using HIFOGS (4.9-9.4 and 9.3-14.5 μm). *Bull. Am. Astronom. Soc.* 26, 1579.

Takata, T., J.D. O'Keefe, T.J. Ahrens, and G.S. Orton 1994. Comet Shoemaker-Levy 9: Impact on Jupiter and plume evolution. *Icarus* 109, 3-19.

West, R.A., E. Karoschka, A.J. Friedson, M. Seymour, K.H. Baines and H.B. Hammel 1995. Impact debris particles in Jupiter's stratosphere. *Science* 267, 1296-1301.

Wilson, P.D. and C. Sagan 1995. Chemistry of the Shoemaker-Levy 9 Jovian impact blemishes: indigenous cometary vs. shock-synthesized organic matter. *IAU Colloquium 156: The Collision of comet P/Shoemaker-Levy 9 and Jupiter*, 9-12 May 1995, abstract book, 122.

Yelle, R. V., and M.A. McGrath 1995. Ultraviolet spectroscopy of the SL9 impact sites, I: The 175-230 nm region. Submitted to *Icarus*.

Yoneda, S., and L. Grossman, Calculated stability fields and compositions of non-ideal condensate liquids in a solar gas 1994. *Meteoritics* 29, 554-555.

Zahnle, K. and M.-M. MacLowe 1994. The collision of Jupiter and comet Shoemaker-Levy 9. *Icarus* 108, 1-17.

Zahnle, K., M.-M. MacLow, K. Lodders, B. Fegley Jr. 1995. Sulfur Chemistry in the wake of comet Shoemaker-Levy 9. *Geophys. Res. Lett.* 22, 1593-1596.

V. Summary and Future Work

This thesis has focussed on atmospheric chemistry for a variety of environments in the outer solar system, ranging from the unimaginably cold surface of Triton (38 K) to the enormously high temperatures (many 1000's of K) generated during the comet impact with Jupiter. It should be appreciated that such a range of temperatures is somewhat unusual in the arena of planetary atmospheric chemistry. Fate, of course, had a hand in this. What follows is a brief description of some of the salient features of the work presented here, along with thoughts on directions for future work.

Triton continues to pose many challenges. Within the context of this thesis, one of these puzzles is certainly the extent of magnetospheric electron precipitation. Until Lyons et al. (1992) identified the possible role of C^+ in Triton's ionosphere, electron precipitation was clearly the dominant form of energy input to the top of the atmosphere. The discovery of CO ice, and by inference CO gas, greatly strengthens the scenario of a C^+ ionosphere. Yet, other factors such as the temperature of the thermosphere and the abundance of nitrogen atoms seem to suggest that electron precipitation is still an important process. Key pieces of missing information are the rate coefficients for N_2^+ + C, and CO^+ + C, both forming C^+. Amazingly, not a single ion-molecule reaction has been studied in which C is a reactant. Another area of interest, and accessible to ground-based study, is the photochemistry of an oscillating atmosphere. Atmospheric collapse and subsequent rebirth are predicted to accompany surface temperature variations as Triton's orbital parameters evolve. The timescales for collapse can be very short, tens of years. For very low-opacity (in the uv) atmospheric states, surface photochemistry during the

collapsed state may be more relevant than atmospheric chemistry in determining issues such as surface coloration.

The ionosphere of Neptune is, as is true for the other giant planets, very poorly understood. Identifying the structures in Neptune's bottomside ionosphere as metal ions shaped by gravity waves is perhaps the most straightforward of the various problems. Understanding the topside density is more problematic. My best guess is that either a significant antisolar flow of protons exists, or enough water comes in to consume the protons. The latter is testable by the methods of Paper III. Failing either of these, the proton deficit may be due to reactions with $H_2(v \geq 4)$, suggesting that the observed deficit can be used to estimate the energy input to the topside ionosphere. This may give some clues to the energy cascade that leads to the high thermospheric temperatures observed observed on all of the giant planets. Finally, the raising and lowering of the ionosphere of Neptune by E×B drift generated in response to gravitational (Triton) and solar tides needs to be investigated quantitatively.

Information on the IDP population and velocity distribution at the distances of Uranus and Neptune is not likely to come soon. Careful observations of the vertical distribution of oxygen-bearing species (i.e., CO) will provide an important "boundary" condition on the photochemical models. A consideration only alluded to in Paper III is the rate of sputtering of water ice from IDP's. Obviously dry IDP's would contribute proportionally less water to an atmosphere. The same type of photochemical modeling needs to be performed for Titan, in this case coupling CO and CO_2, with H_2O from meteoroid ablation.

The high temperature kinetics model for an atmosphere of reducing composition presented in Paper IV still has a long way to go before it can be considered complete. In particular, ion chemistry needs to be added. In light of the sparse free-energy data available for ions, this is a big job. However, the immediate next step with the code is to run it with P-T histories as determined from hydrodynamics runs performed by colleagues at Sandia. Also, heavier hydrocarbons need to be added. This task is made possible by the wealth of data from the field of combustion chemistry. Unfortunately, the combustion chemists have made little progress in determining rate coefficients for heavier H-C-N and H-C-S compounds; it seems likely that such information will be necessary if kinetic modeling of the SL9 impact debris is ever to be complete. In the meantime, shock tube studies of mixtures of Jovian gases may be the only practical method for identifying the composition of the "brown stuff". If the impact debris can be shown to be derived from the comet, the consequences for terrestrial prebiotic chemistry could be profound.